AMERICAN UNIVERSITY OF BEIRUT

SOMATO-DENDRITIC MECHANISMS REGULATE THE FIRING BEHAVIORS OF "STUTTERING" NEURONS: A TWO-COMPARTMENT MODELING STUDY ON PREMOTOR RA-PROJECTING HVC NEURONS

by
MOUNIR FAWAZ ARAB

A thesis
submitted in partial fulfillment of the requirements
for the degree of Master of Science
to the Biomedical Engineering Program
of the Maroun Semaan Faculty of Engineering and Architecture
and Faculty of Medicine
at the American University of Beirut

Beirut, Lebanon
January 2023

AMERICAN UNIVERSITY OF BEIRUT

SOMATO-DENDRITIC MECHANISMS REGULATE THE FIRING BEHAVIORS OF "STUTTERING" NEURONS: A TWO-COMPARTMENT MODELING STUDY ON PREMOTOR RA-PROJECTING HVC NEURONS

by

MOUNIR FAWAZ ARAB

Approved by:

Signature 

Dr. Arij Daou — Advisor
Biomedical Engineering Program
Maroun Semaan Faculty of Engineering and Architecture

Signature 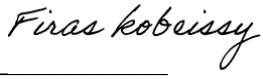

Dr. Firas Kobaissy — Co-Advisor
Department of Biochemistry and Molecular genetics
Faculty of Medicine

Signature 

Dr. Jason Amatoury — Member of Committee
Biomedical Engineering Program
Maroun Semaan Faculty of Engineering and Architecture

Signature 

Dr. Mazen Saghir — Member of Committee
Department of Electrical Engineering
Maroun Semaan Faculty of Engineering and Architecture

Date of thesis defense: January 17th, 2023

AMERICAN UNIVERSITY OF BEIRUT

THESIS RELEASE FORM

Student Name: _____ARAB_____MOUNIR_____FAWAZ_____
Last First Middle

I authorize the American University of Beirut, to: (a) reproduce hard or electronic copies of my thesis; (b) include such copies in the archives and digital repositories of the University; and (c) make freely available such copies to third parties for research or educational purposes:

☐ As of the date of submission

☒ One year from the date of submission of my thesis.

☐ Two years from the date of submission of my thesis.

☐ Three years from the date of submission of my thesis.

February 7th, 2022

_____

Signature Date

ACKNOWLEDGMENTS

I would like to express my sincere gratitude to my academic advisor Dr. Arij Daou. It is rare these days to find a great mentor with such an encouraging and positive spirit. My research journey was not easy, Dr. Daou ensured a smooth pass for my research route by providing me with the necessary expertise. I also would like to thank my colleague Sally Choker for assisting me and providing me with a smooth initial start on modeling work tasks.

I would like to thank Margoliash's laboratory in University of Chicago for providing us with voltage traces on which we built our analysis in this study. Moreover, I would like to acknowledge my committee members: Dr. Firas Kobaissy, Dr. Jason Amatoury and Dr. Mazen Saghir for their wise feedbacks and comments.

Finally, I would like to thank my family including Fawaz, Lina, Imad and Nour for being my backbone and support system throughout my 25 years of age. Not to forget to include our dog Zoe for being a good girl and my companion while working on my models.

A chapter in my AUB is towards the end, we close the curtains on my journey as a graduate student. I could not reach this far without you all. Here's to new beginnings. Cheers.

ABSTRACT
OF THE THESIS OF

Mounir Fawaz Arab for Master of Science
Major: Biomedical Engineering

Title: Somato-dendritic mechanisms regulate the firing behaviors of "stuttering" neurons: a two-compartment modeling study on premotor ra-projecting hvc neurons

The high vocal center (HVC) is the avian analogue of the premotor cortex in the songbird brain. It represents a central component of an interconnected circuit of brain nuclei known as 'the song system' and constitutes a critical neural site for song learning and production. HVC contains at least three neural populations: neurons that project to the RA (robust nucleus of arcopallium, or HVC_{RA}), neurons that project to Area X (basal ganglia), and interneurons. Recent intracellular whole-cell patch clamp recordings accompanied by neuropharmacological and histological manipulations have shown that HVC_{RA} neurons display a significant variability in their intrinsic firing patterns (Daou et al, in preparation). In particular, Daou et al showed that there exist three classes of HVC_{RA} neurons that are distinguished by their electrophysiological and morphological properties, a diversity that is orchestrated by a cocktail of ion channels that are expressed in these neurons. Despite the fundamental importance of this class of projecting premotor neurons during song learning and production, little is known about the ion channels orchestrating their intrinsic firing properties and their distribution inside the cells (i.e., soma and dendrites). In this work, we developed two-compartment HVC_{RA} conductance-based neuronal models that consist of somatic and dendritic compartments and fit the models to the electrophysiological data we collected in brain slices. Initially, the distribution of ion channels inside the cell membranes of HVC_{RA} followed a similar mammalian distribution of ion channels from neurons that exhibit the same ion channels and similar firing patterns. In the first part of the study, we reproduced the voltage traces exhibited by the three classes of HVC_{RA} neurons in brain slices in response to various current stimuli. Next, we focused on Class III HVC_{RA} neurons, a class of neurons that exhibit a stuttering or pausing firing behavior, reminiscent of the discharges that some classes of neurons in the somatosensory cortex, basolateral amygdala, dentate gyrus, visual cortex, and other areas of the brain exhibit. While some pharmacological manipulations have previously shed light on some of the ionic currents that govern these neurons' dynamics (not in the HVC), computationally there is yet no coherent mathematical model that provides a clear explanation and analysis of the parameters that orchestrate their intrinsic properties. The models we designed highlighted the importance of low-threshold voltage-gated D-type (I_D) and M-type (I_M) potassium currents in regulating the firing patterns of class I and class II HVC_{RA} neurons. The models as well highlighted a crucial interplay

between somatic I_M (M-type) and I_{SK} (calcium-dependent) potassium currents with dendritic I_D (D-type) and I_A (A-type) potassium currents in shaping the stuttering or pausing behaviors of class III HVC_{RA} neurons. In particular, somatic I_M was responsible for dampening their excitability, somatic I_{SK} regulates the number of bursts, while dendritic I_D and I_A control the inter-burst duration of the "stutters" in spike trains, the number of spikes in the corresponding epochs, and the delay to the onset of spiking in these neurons. Our models provide insight on the distribution and interactions between the distinct ion channels located on the surface membranes of the somatic and dendritic compartments of HVC_{RA} neurons, which we will be testing and verifying histologically. They also provide a solid mathematical framework that could be used to model other neurons in the brain that exhibit this distinctive firing pattern.

TABLE OF CONTENTS

ILLUSTRATIONS

Figure

TABLES

Table

CHAPTER I

INTRODUCTION

Acquiring and perfecting motor skills require the fine-tuning of sensorimotor circuit elements to eventually generate an accurate motor behavior (**Figure 1A**). Consequently, neurons in the premotor cortex should encode accurate sequences of neuronal activity (Shima, Isoda, Mushiake, & Tanji, 2007), which are determined by two components: the connectivity between neurons in the circuit and the intrinsic physiology of a neuron (**Figure 1A**). Although numerous studies have focused lately on understanding how synaptic weighted properties encode novel behaviors (Fiete, Senn, Wang, & Hahnloser, 2010; Gibb, Gentner, & Abarbanel, 2009a; Huang, Khaled, Kirschmann, Gobes, & Hahnloser, 2018; Solis & Perkel, 2005), a growing school of thought is considering the role of intrinsic properties –which are mediated by ion channels– in shaping neuronal activity and its correlation to ongoing behavior (Daou & Margoliash, 2020; Llinás, 2014). Moreover, ion channels are expressed in the axonic, somatic and dendritic compartments of biological neurons (**Figure 1B**), and the location and degree of expression of a particular ion channel in one compartment relative to another, affects the firing responses of neurons dramatically.

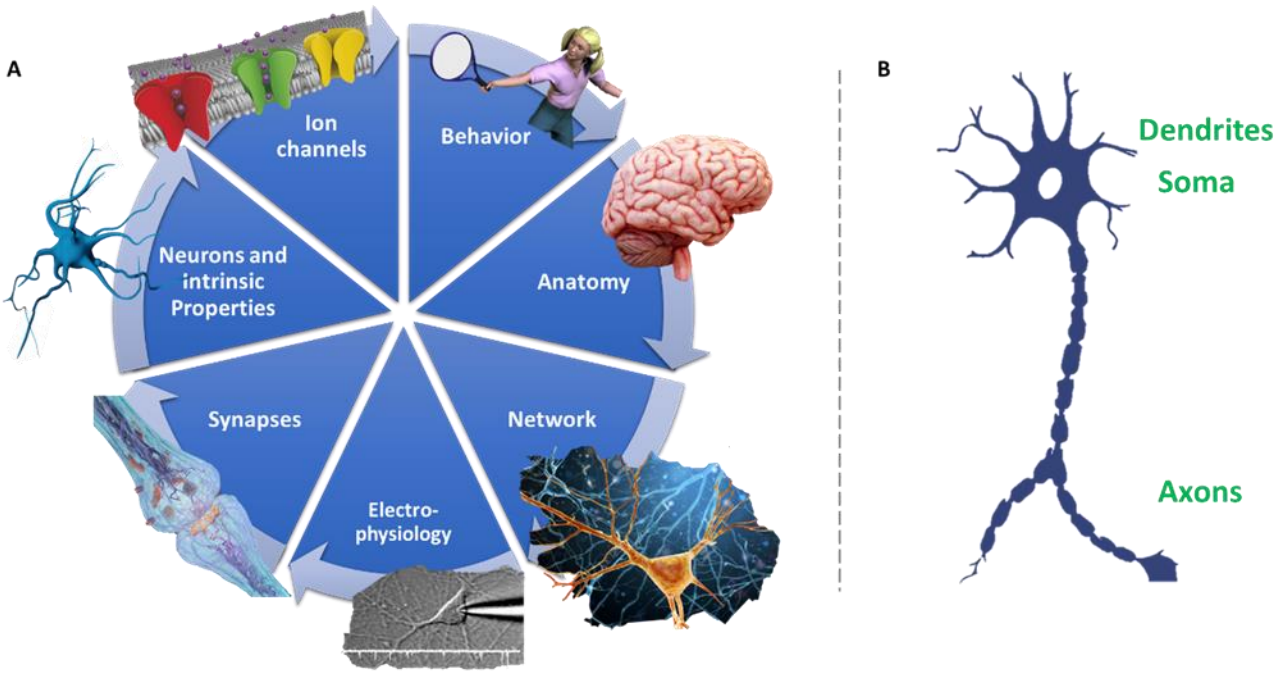

Figure 1: Breaking down the machinery behind motor behaviors. **A**) A certain behavior is dictated by brain anatomy which is formed by an ensemble of interconnected networks of brain cells that produce a sequential neural activity inside the corresponding brain nuclei. This activity results from either synaptic activity coming from surrounding neurons or from the intrinsic properties of the neuron itself. The latter properties originate from ion channels found inside the neurons. **B**) Anatomy of a neuron showing the localizations of soma, dendrites and axons.

In the present study we consider the case of vocal learning in oscine songbirds as model systems for studying the mechanisms of sensorimotor learning. Among these songbirds, male zebra finches are ones of the best-studied songbirds in terms of song learning, singing behavior and their underlying neural mechanisms. The song system comprises all the interconnected brain nuclei which ultimately mediate song learning and production. Among these neuronal nuclei, the telencephalic HVC nucleus (proper name) plays a central role as a junction of the auditory and song production pathways. Understanding the intrinsic properties of HVC neurons is critical to tackle the circuitry of the song system. These neurons are classified according to the projection of their axonal bouton

terminals: HVC_{INT} (non-projecting), HVC projecting to area X (HVC_X) and HVC projecting to the robust nucleus of archipallium (RA) (HVC_{RA}). In this thesis work, we only consider the case of HVC_{RA} neurons for technical reasons. These neurons were distinctively classified according to their firing pattern: type I (phasic), type II (tonic), and type III (stuttering). The firing pattern of an HVC_{RA} neuron and its response to inputs is mainly dictated by the densities and dynamics of ion channels inside the membrane of HVC_{RA} neurons. Although numerous studies previously recorded the voltage traces inside these cells, little is known about the ion channels orchestrating these intrinsic properties and their distribution inside the cell (i.e., soma and dendrites). To tackle this issue, biophysical models consisting of two compartments (i.e., somatic compartment and dendritic compartment) are built to investigate the mechanism behind the different firing patterns of HVC_{RA} neurons in the presence of somatic current supply.

Study objectives

In this study, we introduce the concept of duet compartmentalization of the membrane of HVC_{RA} neuron to make it hold two compartments: somatic and dendritic compartments. This concept would clarify the contribution of dendritic tree as a repertoire for the activities of ion channels that affect the overall intrinsic properties of HVC_{RA} neurons. To tackle this study, our efforts concentrate on examining the distribution of ion channels densities using biophysical modeling approaches. Hence, we aim in this study:

1- To expand the one compartment model of Choker and Daou. (2022) and build two-compartments model of HVC_{RA} neurons by fine tuning the densities of the

conductances of ion channels to fit the experimental traces recorded in HVC slices.

2- To explore the contribution of various ion channels in shaping the distinctive features of stuttering firing patterns.

CHAPTER II

LITERATURE REVIEW

Converting incoming inputs into action potentials (APs) is the ultimate principle underlying all neural cognitive events including the ones regulating song learning and production in songbirds. Hence, neurons engage their intricate molecular machinery to serve this principal objective. This process comprises the collective interplay of complex ion channels in their corresponding localizations inside the cell to elicit firing discharges and subthreshold responses in the presence of somatic current stimulus. Characterizing these electric phenotypes determining the passive and active characteristics of membrane potential are referred to as intrinsic properties of neurons. These electrophysiological properties dictate the excitability of a neuron, the shapes of individual APs, the firing rate of APs and their corresponding temporal patterns. Intrinsic properties are also quite unique, even if these neurons do hold the same molecular type or genetic composition (Edelman & Gally, 2001; Marder & Taylor, 2011). These realizations engender a desire to understand the roles of intrinsic ion channels and their interactions with one and another inside the membrane of neocortical neurons –HVC_{RA} neurons– in the generation of various firing motifs responsible for vocal learning in songbirds.

A. Overview on vocal learning in zebra finches

Songbirds are an intriguing model for investigating the neural mechanisms underlying vocal learning. Vocal learning refers to the process by which zebra finches (i.e.,

a class of songbirds) modify their acoustic structures through auditory feedbacks. Acoustic structures consist of syllables which are the units of vocalization, as well as gaps which are the silent intervals between syllables (**Figure 2**). Ensembles of syllables with stereotyped patterns constitute a song motif, and the continuous rendition of several motifs constitutes a song bout.

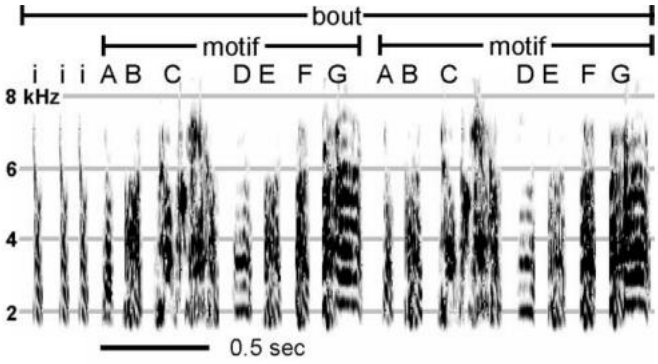

Figure 2: A sonogram of an adult zebra finch song bout plots frequency against time; intensity in each frequency band is indicated by degree of darkness. Different syllables are labeled with different letters; repeated sequence of syllables comprises a motif. Introductory notes ("i") precede the first motif and, together with the multiple motifs, comprise a song bout (Adapted from Solis and Perkel, 2005).

Only male zebra finches have the capacity to learn to sing a song bout due to genetic, neural and hormonal mechanisms controlling the song circuit inside their brains (Agate et al., 2003). Their vocal learning consists of two stages: the sensory stage (25–65 days post-hatch) and sensorimotor stage (30–90 days post-hatch) (**Figure 3**) (Brainard and Doupe 2002; Derégnaucourt et al. 2004; Doupe and Kuhl 1999; Konishi 1985; Margoliash and Schmidt 2010; Tchernichovski et al. 2001; Halle, Gahr, and Kreutzer 2003). During sensory stage, juvenile males (tutee) do not attempt to sing, they only listen to their tutor (often their father) song and store an internal template of the song elements inside their brain. The sensorimotor stage starts with juveniles attempting to sing, they start to gradually modify the

song to match their tutor song via auditory feedbacks. The sensorimotor stage of learning can be divided into three categories based on the features of the vocal outputs: 1) Subsong in which juveniles produce highly unstructured vocalizations that are similar to the babbling of a human baby. 2) Plastic Song in which unstructured vocalizations gradually differentiate into a set of acoustic elements and starts to resemble tutor song via the mechanism of auditory feedbacks. 3) Adult song in which the bird produces an invariant crystallized birdsong. This will be the only song that they would have ever learn throughout their lifespans.

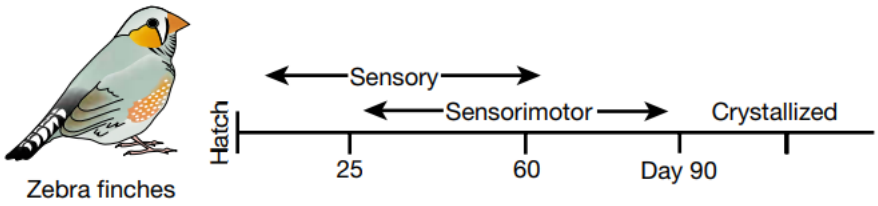

Figure 3: Timelines for song learning in zebra finches. The sensory learning phase ranges between 25 and 65 days, while the sensorimotor learning phase ranges between 30 and 90 days (Retrieved from (Brainard & Doupe, 2002))

B. The anatomy of the song system

In songbirds, vocal learning is mediated by an interconnected circuit of brain nuclei called the song system. It comprises two pathways which are respectively essential for song production and song learning: the vocal motor pathway (VMP) and the anterior forebrain pathway (AFP) (**Figure 4**).

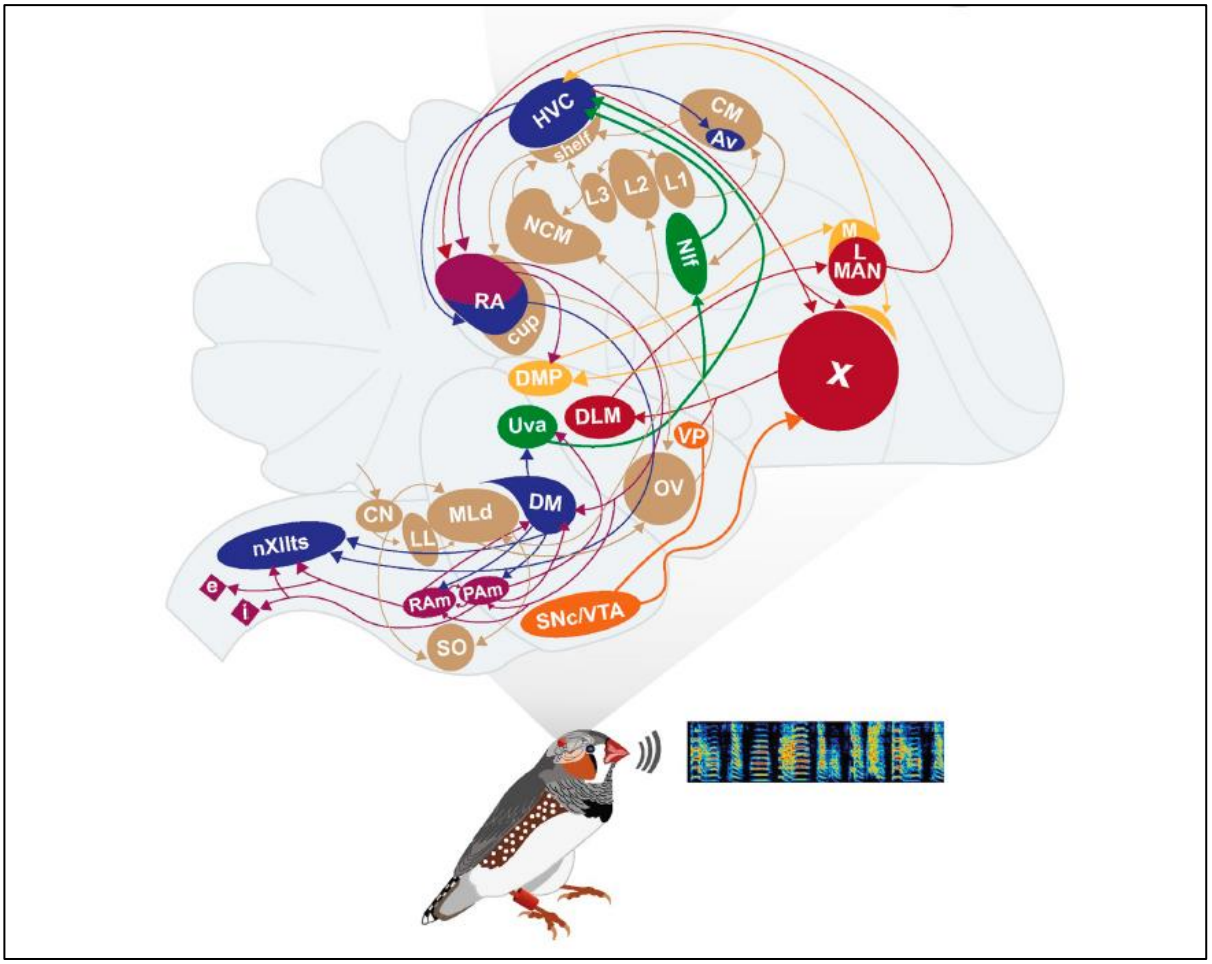

Figure 4: Schematic of a male zebra finch along with a sample spectrogram of a song showing frequency of sound versus time are shown in the lower panel. Reasonably complete song system and auditory system pathways are shown in the middle panel VMP (blue) contains circuits that directly pattern song output. Incoming sensory information is processed by HVC (proper name) and NIf (green), and HVC and RA shape motor sequences that project out to the peripheral vocal organs, the syrinx and respiratory muscles, via the hindbrain nucleus nXIIts and brainstem respiratory nuclei RAm and Pam (purple). In particular, the dorsal part of RA (purple) sends its afferent axons to nuclei DMP, DM, RAm and PAm, while the ventral part of RA (blue) send its axons down to nXIIts. AFP (red) pathway contains circuits that are important for song learning and song variability. HVC sends projections to a basal ganglia loop (striatal-thalamic-cortical-striatal) which has an important output projection to the song motor pathway at nucleus RA. The auditory pathway (light brown color) contains circuits that process sounds, including feedback during singing. Auditory signals enter the brain at CN eventually reaching forebrain nuclei such as NCM and CM. Two nuclei that are known to be connected to the song system but are not well understood are medial MAN, which sends its output to HVC, and VTA (orange color). VTA sends dopaminergic inputs to area X. Abbreviations: AFP: anterior forebrain pathway ,CN: cochlear nucleus ,DM: dorsomedial nucleus of the midbrain nucleus intercollicularis, DMP: ,MAN: magnocellular nucleus of the anterior nidopallium ,Nlf: nucleus interface of the nidopallium, nXIItss: nucleus of the XII cranial nerve ,RA: robust nucleus of arcopallium, Ram: nucleus retroambigualis ,VMP: vocal motor pathway, (Retrieved from (Daou & Margoliash, 2020)).

VMP connects ascending auditory inputs to respiratory nuclei and hindbrain areas (nXIIts) that control motor outputs through syrinx (i.e., a vocal organ). It also includes the robust nucleus of archopallium (RA) and HVc (proper name) nucleus which receives inputs from thalamic nucleus uvaeformis (Uva) and nucleus interfacialis of the nidopallium (NIf). Lesions in the VMP often result in lowering the quality of singing in songbirds (Halle et al., 2003) or in disrupting their singing and uttering song syllables (Nottebohm, Stokes, & Leonard, 1976).

On the other hand, AFP connects HVC nucleus to Area X (in the basal ganglia) which projects to the medial nucleus of the dorsolateral thalamus (DLM). DLM in its turn innervates the lateral magnocellular nucleus of the anterior nidopallium (LMAN). LMAN forms two loops in the AFP by sending connections to both the Area X and RA nucleus. The latter loop that feeds back to RA nucleus affects VMP pathways, and thus modulates song production. Lesions in the AFP of juvenile birds reduce their ability to mimic the tutor's song, however no apparent effects are noted in case of adult birds (Doupe, Perkel, Reiner, & Stern, 2005). This is because at adult stage, song learning stage is over and hence AFP is no longer needed to mimic tutor's song.

C. The avian forebrain HVC nucleus

The avian forebrain HVC (proper name) is reportedly a principal site for auditory learning (Gentner & Margoliash, 2003), song production (Long & Fee, 2008) and perception (Brenowitz, 1991) as it intersects both AFP and VMP pathways. Its anatomical composition is quite complex and includes at the macroscale two categorical classes: : inhibitory local

interneurons (HVC_{INT}) and excitatory projecting neurons (PN). The population of PNs consists of HVC neurons whose axon terminals project into RA (HVC_{RA}) and HVC neurons whose axon terminals project to Area-X (HVC_{X}) They also include $HVC_{RA/X}$ neurons that project to both Area-X and RA (Benezra, Narayanan, Egger, Oberlaender, & Long, 2018), and HVC_{AV} neurons that send long projections to the auditory region avalanche (Av)(Roberts et al., 2017), but the functional roles of these neurons are yet to be determined. HVC_{INT}, HVC_{RA}, HVC_{X} neurons differ in their electrophysiological properties, morphology, anatomy, expression of calcium-binding proteins *in-vitro* (Benezra et al., 2018; Daou, Ross, Johnson, Hyson, & Bertram, 2013; Dutar, Vu, & Perkel, 1998; Michinori Kubota & Taniguchi, 1998; Mooney, 2000; Mooney & Prather, 2005; Oberti, Kirschmann, & Hahnloser, 2010; Ross, Flores, Bertram, Johnson, & Hyson, 2017; Wild, Williams, Howie, & Mooney, 2005) and *in-vivo* (Mooney, 2000; Peng et al., 2012; Roberts, Tschida, Klein, & Mooney, 2010; Solis & Perkel, 2005). They all form interconnected circuits within HVC via excitatory and inhibitory synaptic connections. For instance, a single HVC_{RA} neuron receives an average input of 1,930 synapses with 59% being inhibitory (or symmetric) synapses and 41 % being excitatory (or asymmetric) synapses (Kornfeld et al., 2017). The latter synaptic connections shape the synaptic network architecture that underlies the stable sequential activity of HVC_{RA} neurons.

D. Sequential activity reported in HVC_{RA} neurons

HVR_{RA} neurons produce a sparse sequence of bursts of APs (3-4 spikes) at a precise timing during each song motif rendition in singing and sleeping zebra finches (**Figure 5**)

(Fee, Kozhevnikov, & Hahnloser, 2004; Hahnloser, Kozhevnikov, & Fee, 2003; Okubo, Mackevicius, Payne, Lynch, & Fee, 2015). In particular, every single HVC_{RA} neuron inside the nucleus fires at the same exact time during each rendition of conspecific song. The total contribution of that neuron to the song motif is referred to as ultra-sparse coding. In a total population of approximately 40,000-50,000 HVC_{RA} neurons, it is estimated that only 50-200 HVC_{RA} neurons of 12,500-20,000 song-related HVC_{RA} neurons are co-active each moment in the song motif (Fee et al., 2004; Gibb et al., 2009a). This temporal activity of HVC_{RA} neurons remains nearly stable over the span of several weeks to months (Katlowitz, Picardo, & Long, 2018) and occur independently of onsets or offsets of song syllables (Picardo et al., 2016). These sparse patterns of precisely locked bursts in HVC_{RA} neurons drive a brief burst of sequences in RA neurons, which in turn converge through motor neurons to produce motor control signals. In parallel, HVC_X neurons are also reported to elicit precise time-locked sequential firing during song vocalization (**Figure 6**) (Fujimoto, Hasegawa, & Watanabe, 2011; Kozhevnikov & Fee, 2007; Prather, Peters, Nowicki, & Mooney, 2008). Consequently, these data can be interpreted as if the synaptic interaction between HVC neurons forms the basic unit for encoding song motor and vocal plasticity. In other words, correspondence between sensory and motor codes are being established at the level of HVC projecting neurons to set up neural mechanisms responsible for vocal outputting.

Similar sequences of neural activities underlying well-learned skilled behavior had been observed in hippocampal time cells and gustatory cortex neurons of rats (Jones, Fontanini, Sadacca, Miller, & Katz, 2007; MacDonald, Lepage, Eden, & Eichenbaum, 2011), hippocampal neurons of mice (Harvey, Coen, & Tank, 2012), premotor cortex and amygdala

neurons of monkeys (**Figure 7**) (Crowe, Zarco, Bartolo, & Merchant, 2014; Reitich-Stolero & Paz, 2019).

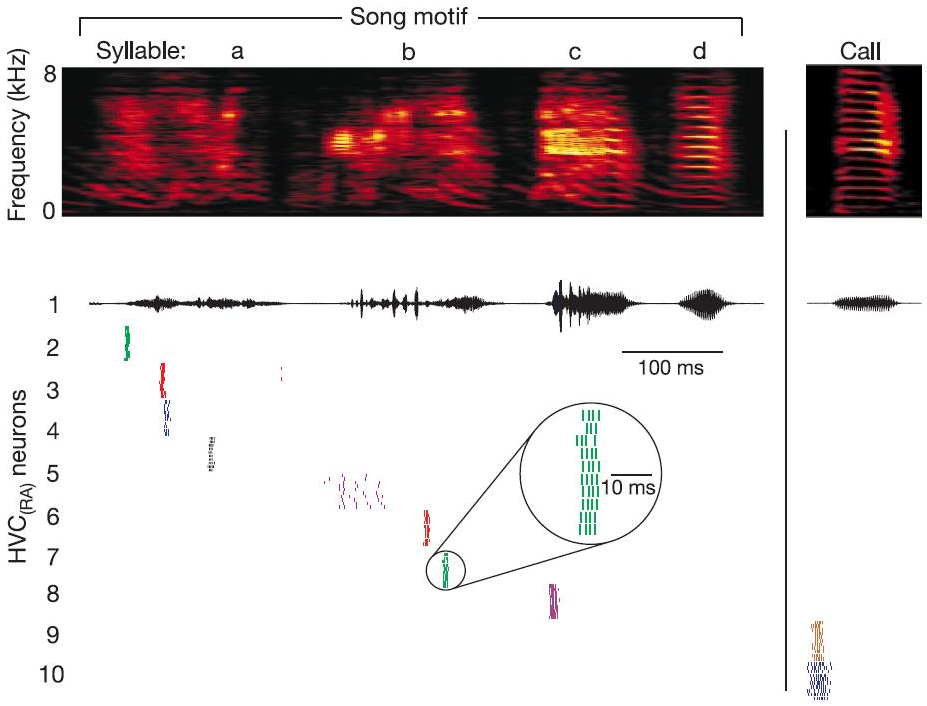

Figure 5: Spike raster plot of ten HVC_{RA} neurons and two HVC interneurons recorded in one bird during singing (left) and call vocalizations (right). Each row of tick marks shows spikes generated during one rendition of the song or call; roughly ten renditions are shown for each neuron. Neural activity is aligned by the acoustic onset of the nearest syllable. HVCRA neurons burst reliably at a single precise time in the song or call; however, HVC interneurons spike or burst densely throughout the vocalizations (Retrieved from (Hahnloser et al., 2003)).

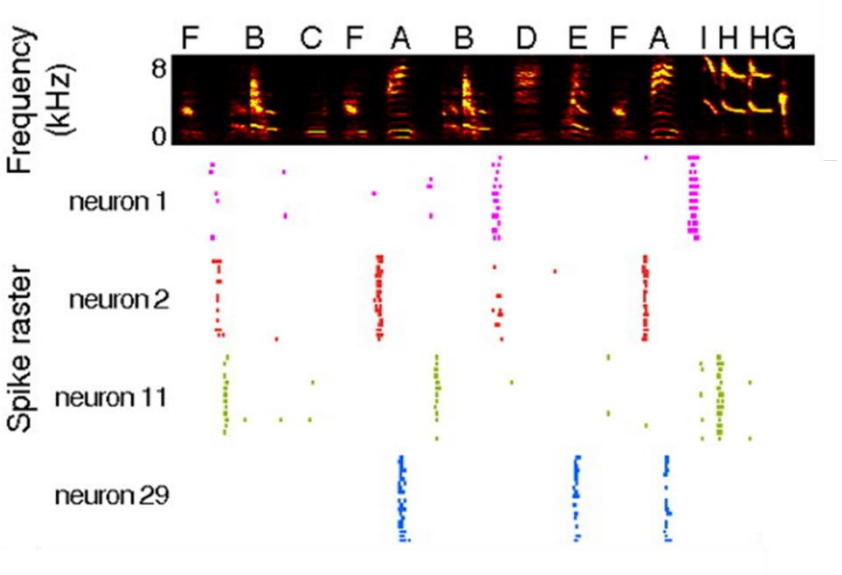

Figure 6: HVCX neural activity recorded from a bird while vocalizing song sequences based on its own syntax. Top, Time-frequency spectrogram of the song segments. Letters above the spectrogram indicate syllable types. Bottom, Spike raster plots of four HVCX neurons (Retrieved from (Fujimoto et al., 2011)).

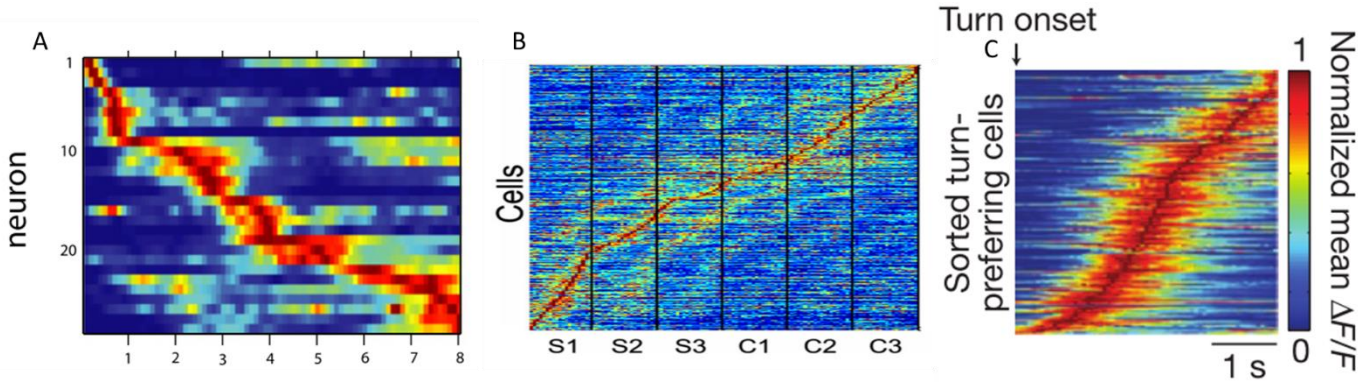

Figure 7: Sequential activities of neurons observed in hippocampal time cells of rats **(A)** retrieved from (MacDonald et al., 2011), premotor cortical neurons of monkeys **(B)** retrieved from (Crowe et al., 2014), and parietal cortical neurons of mice **(C)**. Retrieved from (Harvey et al., 2012).

The sequential activity in HVC neurons is not a spur-of-the-moment phenomenon; the latter activity is the result of progressive plasticity that builds up throughout song development of the songbird (Okubo et al., 2015). However, it should be clarified that the origin of sequential activity seen in HVC neurons is not completely understood as multiple

computational modeling studies are conducted to explain the mechanism behind this topographical pattern of electric activity. One possible model that could explain the time code propagation in HVC neurons is the feedforward model. This is one of the most simplistic mechanistic approaches that considers each HVC_{RA} neuron to be connected to one another through excitatory synaptic connections. These connections could then form a synfire chain spanning over the time duration of the song motif. This model for activity propagation is robust to synaptic variations only if HVC_{RA} neurons are assumed to be intrinsic bursters with regenerative calcium spikes being initiated at the dendrites, being propagated along the neuron to trigger in their turn somatic spikes (Jin, Ramazanoğlu, & Seung, 2007; Long, Jin, & Fee, 2010). However, this modeling approach is not biophysically plausible as it ignores the central role of inhibitory HVC_{INT} neurons and their interaction with HVC projecting neurons in shaping sequence generation in HVC nucleus (Chammas & Daou, 2020; Fiete et al., 2010; Gibb, Gentner, & Abarbanel, 2009b; Kosche, Vallentin, & Long, 2015; Mooney & Prather, 2005). Another emerging modeling approach to explain sequence generation is gesture trajectory extrema (GTE) model which are associated with syringeal tension. It considers bursts recorded in HVC neurons to be synchronized with respiratory gesture movements. Although no coupling was found between the bursts and GTEs (Lynch, Okubo, Hanuschkin, Hahnloser, & Fee, 2016; Picardo et al., 2016), Amador et al. (2013) reported that bursts in HVC_{RA} neurons are perfectly aligned with a near zero latency. Consequently, this would indicate the absence of any functional premotor role for HVC in controlling vocal gestures and thus contradicting the previous notions of HVC nucleus as an integral site for premotor activities.

E. Biophysics governing AP generation: Hodgkin-Huxley model

Understanding the biophysical basis and computational principles of spike generation is central in studying the electrophysiology of HVC_{RA} neurons. Modeling spike generation is brought abought by linear and nonlinear computational mechanisms which are translating incoming inputs into APs. HODGKIN and HUXLEY (1952) set the framework of modeling and developed the first neuron model of giant squid axon using gating variables to explain how an APl is generated. In other words, the work of Hodgkin and Huxley consists of modeling the dynamics of ion channels responsible for the temporality and shape of an AP. These ion channels change their conformation to gate the movement of ions across the plasma membrane by opening or closing the membrane pore, this process is called gating. To build their model, they considered the cell membrane as an RC circuit with total membrane current being divided into capacitive current and ohmic current. The equation of the membrane circuit is given below:

$$C_m \frac{dV}{dt} + I_{ionic} = 0 \qquad \textbf{Equation 1}$$

Where V is the membrane potential, C_m is the membrane capacitance, V is the membrane potential, I_{ionic} is the total ionic currents forming the circuit.

The ionic currents in the model consist only of three component currents: a sodium current (I_{Na}), a potassium current (I_K) and a leak current (I_{leak}).

$$I_{ionic} = I_{Na} + I_K + I_{leak} \qquad \textbf{Equation 2}$$

1. Sodium Current

The Hodgkin-Huxley analysis bases the gating variables of Na^+ current on two kinetic mechanisms: fast activation (the process that opens Na channels during depolarization) and slow inactivation (the process that closes Na channels during depolarization). The equation of Na current is given below

$$I_{Na} = g_{Na} m^3 h (V - V_{Na}) \qquad \textbf{Equation 3}$$

where g_{Na} is the maximal conductance of Na current, m is the activation gating variable, h is the inactivation gating variable, V is the membrane potential, V_{Na} is the reverse potential of Na current.

At rest, the cell membrane is hyperpolarized, the Na^+ channels are completely deactivated (or closed) with gating variables $m \approx 0$ and $h \approx 1$ (**Figure 8**). If an excitatory input current pulse depolarizes the cell membrane, m rises very quickly, and h falls slowly causing the Na^+ channels to open which causes further increase in membrane potential. As the membrane potential depolarizes, the inactivating variable h slowly moves toward zero. This shuts off the sodium channels (complete inactivation) and prevents the membrane potential from becoming too depolarized. At this stage, Na^+ channels are completely closed or inactivated with $m \approx 1$ and $h \approx 0$. To remove inactivation, membrane potential should undergo repolarization/hyperpolarization.

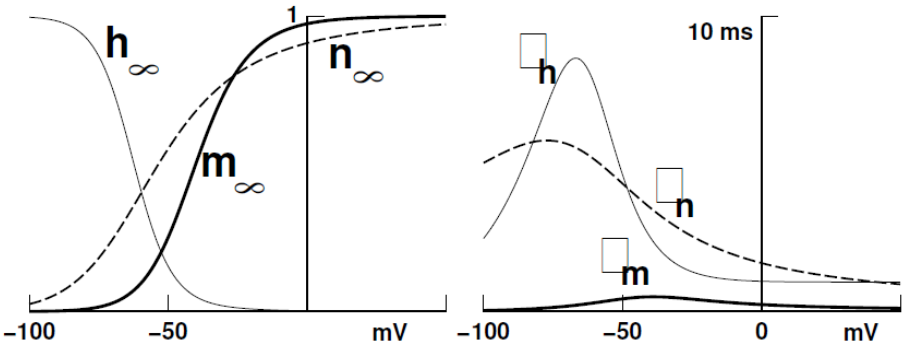

Figure 8: The voltage-dependent functions of the Hodgkin-Huxley model. The left panel shows $m_\infty(V)$, $h_\infty(V)$, and $n_\infty(V)$, the steady-state levels of activation and inactivation of the Na+ conductance, and activation of the K^+ conductance. The right panel shows the voltage-dependent time constants that control the rates at which these steady-state levels are approached for the three gating variables. The 'infinity function' for the Na^+ activation (m_∞) is an increasing function of voltage, and the time constant for Na^+ activation (τ_m) is very small. Therefore, Na^+ channels open quickly in response to depolarizing currents and further depolarize the cell. The infinity function for Na+ inactivation (h_∞) is a decreasing function of voltage, and its time constant (τ_h) is larger. This results in Na^+ channels closing slowly in response to depolarizing currents, after the initial upstroke of the AP. The infinity function for activation of K^+ (n_∞) is also an increasing function of voltage, but its time constant is also large (τ_n). Therefore, K^+ channels open in response to depolarizing currents and repolarize the cell.

2. Potassium Current

The potassium current is based on one activation gating variable, its equation is given by the equation below:

$$I_K = g_K n\,(V - V_K) \qquad \textbf{Equation 4}$$

where g_K is the maximal conductance of K^+ current, n is the activation gating variable, V is the membrane potential, V_K is the reverse potential of K^+ current.

At rest, the K^+ channels are mostly closed with n = 0. Upon depolarization, n activates causing an efflux of K^+ ions out of the membrane and repolarization of membrane potential. The variable n slowly activates when membrane potential is depolarized resulting in an efflux of K^+ ions out of the cell and repolarization of the cell. As the membrane potential repolarizes, K^+ channels start to close slowly such that membrane potential hyperpolarizes beyond its normal resting potential for a short duration.

3. Leak current

Leak current is a voltage-independent current that represents the flow of chloride ions and other ions. Unlike the other ionic currents, the leak conductance is constant indicating that the flow of ions is maximal. Its equation (I_{leak}) is given below:

$$I_{leak} = g_{leak}(V - V_{leak}) \quad \textbf{Equation 5}$$

where g_{leak} is the maximal conductance of leak current, V is the membrane potential, V_{leak} is the reverse potential of Na^+ current.

F. Different types of ion channels

Understanding the roles of various ion channels in shaping the intrinsic properties of neurons is a key objective in biophysical modeling. These ion channels change their conformation in response to changes in electric field (i.e., voltage-gated ion channels) or in response to ligand binding (i.e., ligand-gated ion channels) to gate the movement of ions across the plasma membrane. In this work, we highlight the roles of potassium and calcium channels that were tested pharmacologically in HVC neurons (Daou et al., in preparation). In particular, preliminary electrophysiological and pharmacological manipulations have shown the existence of the D-type and M-type potassium currents that we will talk about next (Daou et al., in preparation).

1. Potassium Channels

Potassium (K^+) channels are considered to have wider range of diversification compared to sodium and calcium channels. They play a critical role in modulating the excitability of a neuron. Out models incorporate voltage-gated K^+ channels (often referred to as Kv channels): delayed-rectifiers, A-type, D-type, M-type potassium channels, in addition to the ligand-gated small-conductance Ca^{2+} activated potassium (SK) channels, all that had been tested pharmacologically (Daou et al. 2013; Daou et al., in preparation). It should be noted that these genes encoding for the different subunits (Kv1-12) forming these classes of K^+ channels were previously identified among the genes of HVC neurons of zebra finches (Lovell, Carleton, & Mello, 2013).

2. Delayed rectifiers K^+ Channels

Delayed-rectifiers K^+ channels (I_{Kdr}) are slowly activating K^+ channels mediated by Kv 3 channels (Kv3.1 – Kv3.4). They get activated with a delay upon membrane depolarization allowing the exit of K^+ ions, it is responsible for the repolarization of AP. Pharmacological experiments and in-silico neuron models show that the blockade of Kv3 currents with tetraethylammonium (TEA) or 4-aminopyridine (4-AP) impairs high-frequency firing by broadening the spike widths of APs (**Figure 9A**) (Martina, Schultz, Ehmke, Monyer, & Jonas, 1998; Rosato-Siri et al., 2015; RUDY et al., 1999). Similar impairments of fast AP firing can be reproduced by reducing the conductances of Kv3- like

channels in in-silico neuronal models (Akemann & Knöpfel, 2006; Lien & Jonas, 2003; Olah et al., 2022).

3. A-type K^+ channels

A-type K^+ current (I_A) is a fast-activating and fast-inactivating outward current, it is constituted mainly of Kv4 subunits. It is reported that I_A limits non desirable excitation by clamping small amplitude APs (Jagger & Housley, 2002). I_A is also attributed to cause a slow ramp trajectory prior to the first spike onset in cortical neurons (Daou et al., 2013; Molineux, Fernandez, Mehaffey, & Turner, 2005). Blocking this current using 4-aminopyridine (millimolar level) can ease the firing of AP by reducing the onset latency of the first spike and increasing the firing frequency in the case of dorsal root ganglion neurons (**Figure 9B**) (Shibata et al., 2000; Vydyanathan, Wu, Chen, & Pan, 2005).

4. D-type K^+ channels

D-type K^+ current (I_D) was first described by Stansfeld et al. (1986), it has fast activation and slow inactivation kinetics. It activates at subthreshold range before AP onset and between individual AP spikes. I_D dynamical components often belongs to Kv1 family in mammalian neurons, they are usually blocked using either (<100 μM) 4-AP or dendrotoxin (DTX). I_D is reported to cause a prolonged delay (>~100ms) prior the onset of neuronal firing in response to depolarizing stimuli compared to I_A (**Figure 9C1)** (Storm, 1988) . This is due to the rapid activation of I_D upon depolarization which keeps the cell membrane from depolarizing further. It is up until I_D gets slowly inactivated that the membrane potential

would get to reach the threshold so the neuron could fire APs. It could be postulated that the interaction between I_D and I_A regulates the time to spike in HVC_{RA} neurons. Furthermore, I_D is reported to reduce the excitability of the cell by limiting AP firing like in the case of phasic firing (**Figure 9C2)**. This is accompanied with a slow ramp following the first spikes of APs (Shu, Yu, Yang, & McCormick, 2007). Blocking these channels using 4-AP transform the shape of APs of the caudal mesopallium neurons into tonic firing (Chen & Meliza, 2018). Additionally, I_D is reportedly associated with stuttering firing behavior of neurons (**Figure 9C3)** (Goldberg et al., 2008) which could help to decipher the ionic mechanism responsible for stuttering firing observed in the electrophysiological recordings of HVC_{RA} neurons (discussed later – in the section of "HVC_{RA} stutterers: add-on to traditional classes").

5. M-type K^+ channels

M-type K^+ current (often referred to as I_M or Kv7/M channel) is a muscarine-sensitive outward current governed by a single voltage-sensitive gating particle due to its non-activating kinetics. I_M is known to dampen the excitability of neuron by decreasing spike frequency. It is responsible for inducing spike frequency adaptation in the membrane potential and for regulating the amplitude of medium AHP which precedes a single spike or a spike burst (**Figure 9D)** (Gu, Vervaeke, Hu, & Storm, 2005). I_M contributes to the dampening of excitability seen in HVC_{RA} along with an active role from small-conductance current (Ross et al., 2017). Recent pharmacological manipulations have seen that this ionic

current is largely expressed in the phasic class of HVC_{RA} neurons (Daou et al., in preparation).

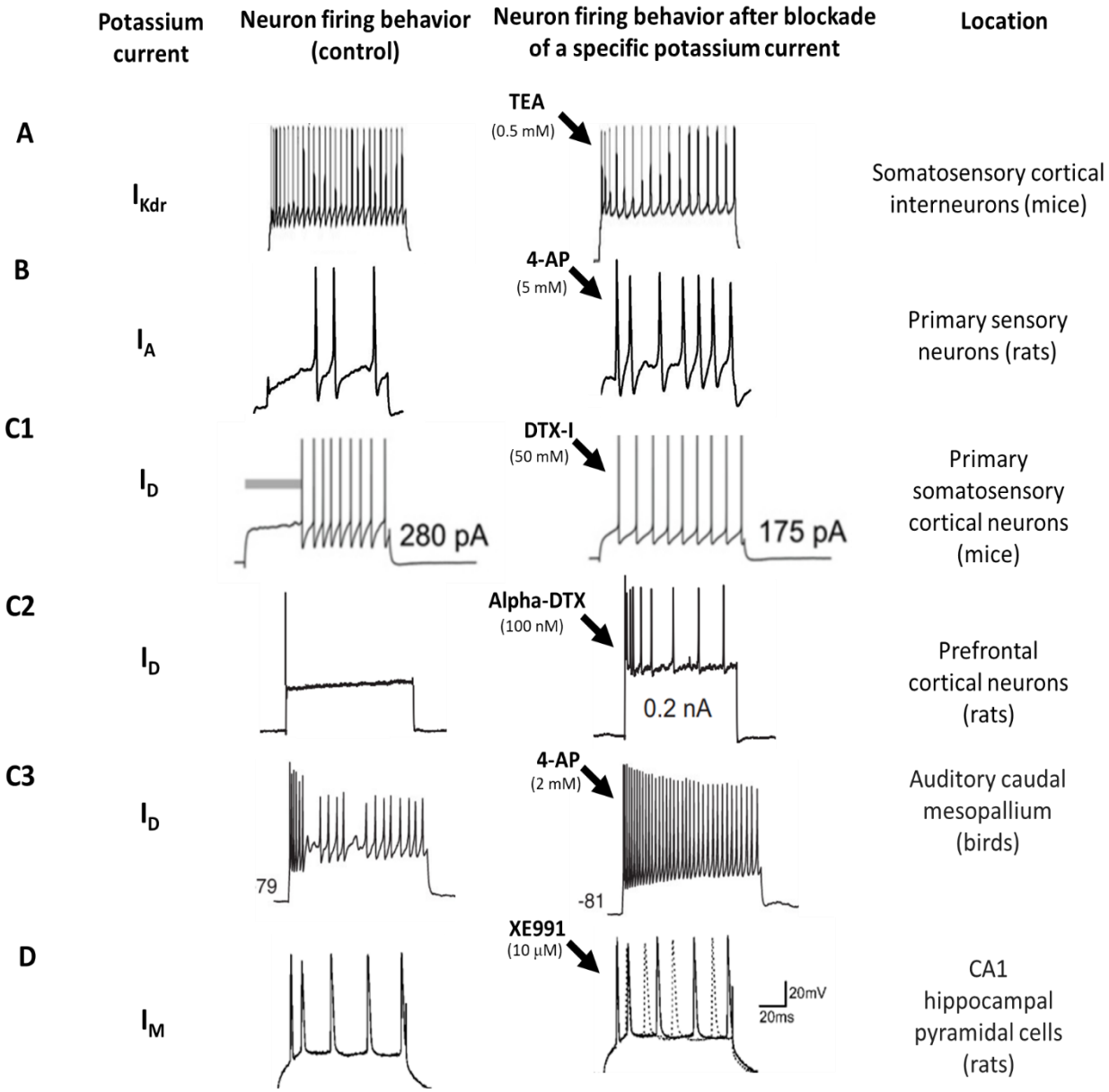

Figure 9: Volage traces of different neurons with unique firing behaviors Each neuron exhibits a unique firing behavior that is primarily dictated by a certain potassium channel. A, the delayed rectifier potassium current is mainly responsible for increasing the frequency of firing action potentials (Retrieved from Rosato-Siri et al. (2015)). B, the fast activated and fast inactivated potassium current is mainly responsible for onset delay (Retrieved from Vydyanathan et al. (2005)). The fast activated and slow inactivated potassium current is mainly responsible for the phasic firing behavior which is often followed by a ramp (C1) (Retrieved from Shu et al. (2007)) and stuttering firing (Retrieved from Chen and Meliza (2018)). The inactivating potassium current is mainly responsible for downregulating the cell excitability and causing spike frequency adaptation (Retrieved from Gu et al. (2005)).

6. Calcium-dependent K^+ Channels

Small-conductance channel (I_{SK}) is Ca^{2+} dependent – voltage-independent – K^+ channels. It is activated by increasing the intracellular Ca^{2+} concentration during repolarization phase of AP. As I_{SK} gets activated, it extrudes potassium ions out of the cell. The outward flow of K^+ shifts membrane potential to a more negative potential (i.e., hyperpolarization), which negatively affects the excitability of a cell. I_{SK} is also noted to contribute to afterhyperpolarization and to the late phase of spike frequency adaptation (Pedarzani et al., 2005). The I_{SK} blocker, Apamin, confirmed the role of I_{SK} in diminishing the excitability of HVC_{RA} neuron and hyperpolarizing its resting membrane potential (Daou et al., 2013).

7. Na^+-dependent K^+ channels

Na^+ -dependent K^+ channels (I_{Kna}) are responsible for an outward K^+ current. They get activated due to increase in intracellular Na^+ concentrations. It was reported that I_{Kna} induces a long-lasting slow afterhyperpolarization after repetitive tetanic stimulation of HVC neurons (Kubota and Saito 1991; Schmidt and Perkel 1998).

8. Calcium channels

Here we consider only two types of calcium channels: L-type and T-type Ca^{2+} channels. In parallel with Na^+ and K^+ channels, the genes encoding the formation of the

building blocks of these calcium channels (CACNA1s) are identified among the list of genes present in HVC neurons of zebra finches (Friedrich, Lovell, Kaser, & Mello, 2019).

9. L-type Ca^{2+} channels

L-type Ca^{2+} current (I_{CaL}, or Ca_v1) is a high voltage-activated inward current with activation threshold above -10 mV. It is responsible for initiating calcium spikes in the dendrites of HVC_{RA} neurons (Long et al., 2010). A calcium spike is an indicative of the presence of Ca^{2+} channels in the dendrites of a neuron. It refers to an AP generated by voltage-gated Ca^{2+} channels present in the dendrites of a neuron. It is generated in response to external depolarizing dendritic stimulation or strong synaptic input. Once initiated inside the dendrites, APs propagate down the soma and the axons – a process called forward propagation. Forward propagation of APs down the axon produces in its turn APs in the soma.

The presence of I_{CaL} in HVC_{RA} was unmasked by blocking sodium and potassium currents using Qx-314 blockers (Long et al., 2010). The intracellular recordings intercepted depolarization events following the application of a current pulse. And the latter depolarization events remained intact after the application of Nickel (i.e., I_{CaT} antagonist), this acknowledges the absence of any interference from low threshold Ca^{2+} currents. The application of BAY K 8644 (I_{CaL} agonist) and Nifedipine (I_{CaL} antagonist) modulated the burst duration and burst incidence. Thus, I_{CaL} contributes to the generation and initiation of calcium spikes.

10. T-type Ca^{2+} channels

T-type Ca^{2+} current (I_{CaT}, or Ca_v3) is a low voltage-activated and fast inactivating current that starts activating at membrane potential above −70 mV. I_{CaT} is reported to be implicated in post-inhibitory rebound firing elicited by HVC_{INT} and HVC_X neurons at the offset of a negative current pulse (Daou et al., 2013).

11. Other currents: H-current

H-current (I_h) is a non-inactivating inward current (permeable to both K^+ and Na^+) that gets activated by hyperpolarizing beyond -80 mV. It was demonstrated that I_h is mainly responsible for the slow inward rectification (also known as a sag) observed in HVC neurons (HVC_X and HVC_{INT}) (Daou et al., 2013).

G. Characterizing the electrophysiological properties of HVC_{RA} neurons

Characterizing the electrophysiological properties of HVC_{RA} neurons is fundamental for breaking down the mechanisms followed by ion channels to orchestrate the intrinsic properties. The latter essentially shape the neural circuitry inside the HVC nucleus at different levels. This section revises the different firing pattern of HVC_{RA} *in-vivo* and *in-vitro*.

1. Characterizing HVC_{RA} firing patterns in-vivo

Several intracellular recordings of HVC_{RA} neurons studied the suprathreshold and subthreshold responses of HVC_{RA} neurons *in-vivo* (Hahnloser, Kozhevnikov, and Fee 2003;

Long, Jin, and Fee 2010; Mooney 2000; Peng et al. 2012; Roberts et al. 2010; Daou et al. (in preparation)). As described earlier, this class of projection neurons tend to elicit a single burst of APs at one particular instance of time during song, which is highly stereotyped from one rendition of song to another (Hahnloser et al., 2003; Long et al., 2010). Moreover, intracellular current injections to HVC_{RA} neurons showed that these neurons exhibit a sluggish firing behavior characterized by a highly variable latency of spike onset (Table 1) as response to a DC-evoked positive current pulses (Long et al., 2010; Mooney, 2000). They also show irregular firing behaviors with a highly variable instantaneous firing frequency along the spike time interval due to the interaction of spontaneous synaptic activities and current injections (**Figure 10**) (Mooney, 2000; Peng et al., 2012).

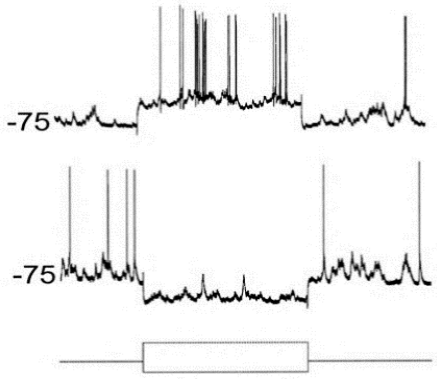

Figure 10: Membrane potential responses of HVC_{RA} neuron to hyperpolarizing (−400 pA) and depolarizing (+600 pA) current pulses (bottom trace; 1 sec duration) applied via the recording electrode. Note the highly irregular firing of the RA-projecting cell (Retrieved from (Mooney, 2000)).

2. Characterizing intrinsic properties of HVC_{RA} in-vitro

Many studies examined the intracellular activity of HVC population in brain slices (Daou et al. 2013; Daou and Margoliash 2020; Kubota and Saito 1991; Mooney, Hoese, and Nowicki 2001; Mooney and Prather 2005; Schmidt and Perkel 1998) and characterized the

electrophysiological properties that distinguish HVC_{RA} neuron from other HVC neurons (Daou et al., 2013; Dutar et al., 1998; Michinori Kubota & Taniguchi, 1998; Ross et al., 2017; Shea, Koch, Baleckaitis, Ramirez, & Margoliash, 2010). Table 1 shows different quantitative electrophysiological features of HVC_{RA} reported *in-vivo* and in brain slices of zebra finches. In response to somatic current stimulation, an HVC_{RA} neuron is mainly characterized by (1) its low excitability compared to other HVC neurons as response to depolarizing current pulse; In other words, the firing behavior of HVC_{RA} presents only one or a few APs followed by a large afterhyperpolarization (AHP) in response to relatively large depolarizing current. (2) the absence of time-dependent inward rectification (also known as a sag) as response to hyperpolarizing current pulse. (3) a hyperpolarized resting membrane potential (approximately ~-80 mV) (**Figure 11**).

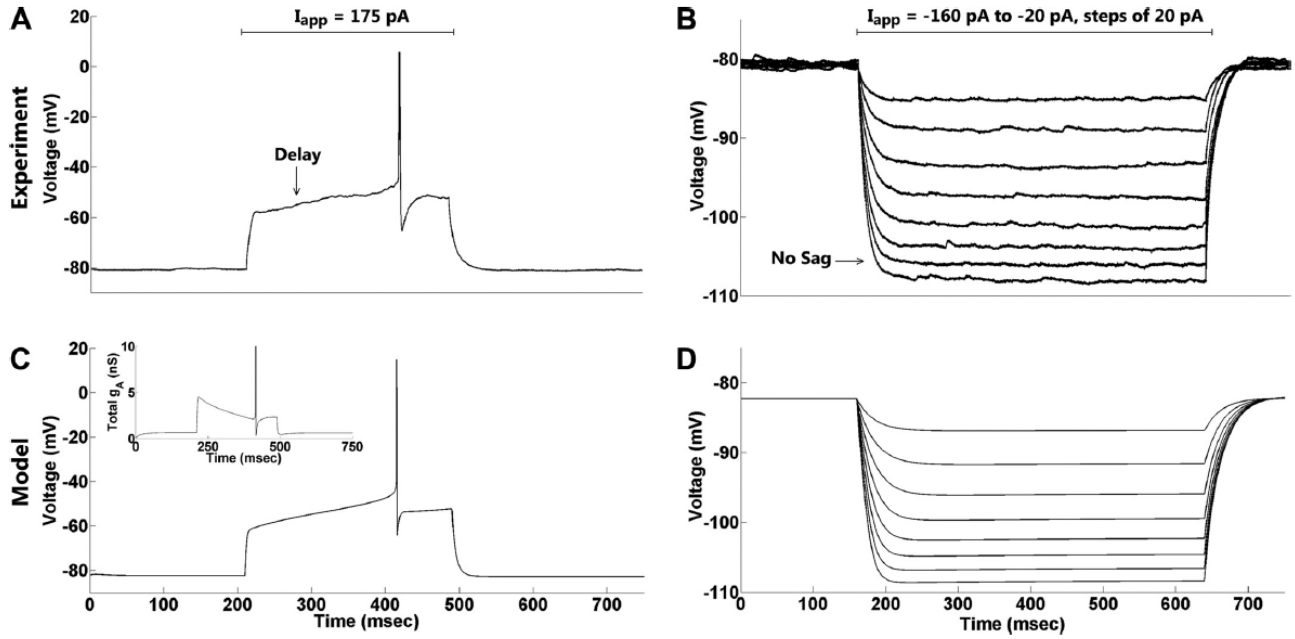

Figure 11: Firing properties of an RA-projecting neuron. A: an RA-projecting neuron fires a single action potential, often with a long delay, in response to a relatively large depolarizing pulse (175 pA). B: no sag is present in response to

hyperpolarizing current pulses (-160 to -20 pA, in steps of 20 pA). C: HVCRA model neuron parameters were calibrated to match the experimental recording (Iapp =150 pA). The long delay to spiking is due to the A-type K^+ current (IA). Inset shows the total I_A conductance (gA) during the current pulse. D: for the same parameter values used in C, the HVCRA

References	HVC_{RA} Subclasses	Passive membrane properties	Active membrane properties			
		Resting membrane potential (mV)	Sag Ratio (SR)	Spikes amplitude (mV)	Afterhyper-polarization (mV)	Spike Onset Delay (ms)
In-vivo						
Mooney 2000	Not specified	-78 +/- 3	––	––	13.4 +/- 1.9	172 +/- 67
In-vitro						
Dutar et al. 1998	Not specified	-80.9 +/- 1.5	––	––	12.8 +/- 1.5	2.6 +/- 0.3
Kubota and Taniguchi 1998	Type Iia HVC neuron	-83.0 +/- 1.2	1.6 +/- 0.3	––	21.8 +/- 0.7	––
	Type IV HVC neuron	-71.9 +/- 1.4	1.6 +/- 0.5	––	13.7 +/- 1.1	––
Shea et al. 2010	Phasic HVR_{RA} neuron	-74.1 +/- 5.3	1.34 +/- 3.0	9.03 +/- 3.7	––	28.9 +/- 14.1
	Tonic HVR_{RA} neuron	-71.9 +/- 8.3	2.08 +/- 3.9	14.2 +/- 3.7	––	73.8 +/- 6. 47
Daou et al. 2013	Not Specified	-85.0 +/- 6.0	0.9 +/- 0.3	––	16 +/- 0.8	13 +/- 1.2
Ross et al. 2017	HVR_{RA} neuron at subsong	-61.0 +/- 2.05	1.00 +/- 0.41	50 +/- 6.39	––	15 +/- 8.07
	HVR_{RA} neuron at plastic song	-66 +/- 0.94	2.00 +/- 0.36	64 +/- 3.29	––	92 +/- 40.53
	HVR_{RA} neuron at adult song	-77 +/-0.57	1.0 +/- 0.09	77 +/- 3.59	––	17 +/- 5.72

model neuron has no sag but exhibits inward rectification in the spacing between voltage traces, as in B (Retrieved from Daou et al., 2013).

Table 1: Quantitative features of HVC_{RA} firing reported experimentally *in-vivo* and in brain slices of zebra finches. The table shows the different types of HVC_{RA} neurons reported in literature.

Other electrophysiological features of HVC_{RA} that were observed experimentally include spike frequency adaptation (i.e., the interspike interval increases with time) in their firing, presence of fast-activated inward rectification and delay in spiking in response to depolarizing pulses (Daou et al., 2013; Michinori Kubota & Taniguchi, 1998).

In terms of classification, HVC_{RA} neurons have been classified in literature into tonic and phasic firing with responses eliciting respectively sustained firing of AP in case of tonic firing and one or few APfiring at onset in case of phasic firing (**Figure 12**) (Daou et al. 2013; Michinori Kubota and Taniguchi 1998; Shea et al. 2010). It should be noted that HVC_{RA} with phasic firing are referred to as class I HVC_{RA} neuron, while HVC_{RA} with tonic firing are referred to as class II HVC_{RA} neurons (Daou et al., in preparation). These electrophysiological properties of HVC_{RA} neurons may vary throughout the vocal development stages of songbirds due to changes in intrinsic properties (Ross et al., 2017). These changes are highly apparent especially at the level of resting membrane potential and spike amplitudes (**Table 1**).

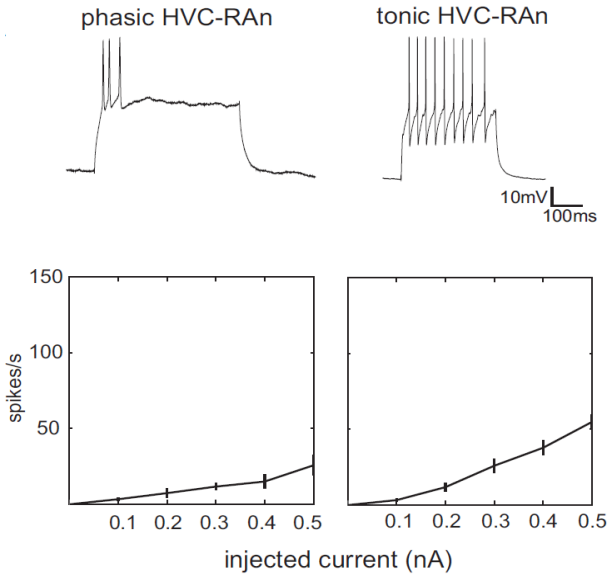

Figure 12: Responses of 2 HVC cells to near-threshold depolarizing current injection (tonic HVC-Ran at 0.4 nA, phasic at: 0.2 nA), show features characteristic (TOP) and the average firing frequency of HVC_{RA} neurons at different current intensities (BOTTOM) (Retrieved from Shea at al. (2010)).

H. HVC_{RA} stutterers: add-on to traditional classes

HVC_{RA} stuttering neurons are a new add-on class of HVC_{RA} neurons in terms of electrophysiological classification. The work conducted by Arij Daou at the University of Chicago has identified a novel class of HVC_{RA} neurons based on their electrophysiological responses: type III (stutterers) HVC_{RA} neurons (**Figure 13**) (Daou et al., in preparation). We will go next over neurons from various systems that exhibit similar firing patterns as class III HVC_{RA} neurons and explain the mechanisms of this irregular firing pattern. The next section goes over stuttering firing patterns of mammalian nerve cells.

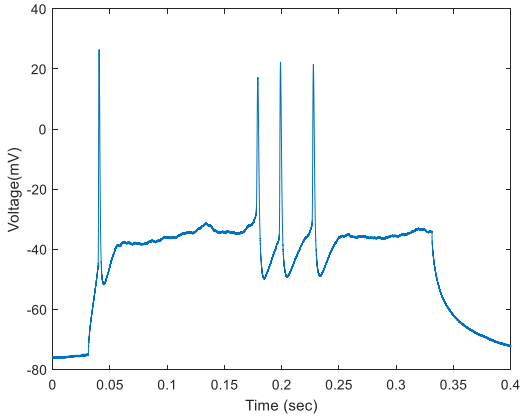

Figure 13: Stuttering firing recorded in (type III) HVC_{RA} neurons in response to somatic current (120 pA) stimulation by Daou et al. at the University of Chicago.

1. Stuttering firing discharges in mammalian neurons

'Stuttering' firing, also known as random bursting, irregular bursting or spike clustering, is a type of AP firing behavior that is being increasingly reported in ng mammalian cells. It is characterized by two or more bursts separated by periods of quiescence which is interspersed by subthreshold membrane potential oscillations. In other words, a stuttering neuron fires bursts (i.e., cluster or AP discharge) of variable number of spikes per burst which the latter is separated by variable inter-burst durations. **Table 2** shows the localization of various mammalian nerve cells that were reportedly exhibiting stuttering firing patterns. The stuttering firing patterns of these neurons is quite diverse; they differ mainly in their number of bursts, number of spikes per each burst and the inter-burst durations. (**Figure 14**). In addition to this classic diversity in stuttering firing patterns, some of these stutterers neurons exhibited a burst of spikes on onset or onset delay prior to spiking (**Figure 14**) (Markram, 2000; Markram et al., 2004).

Specie	Location inside the brain	Class of neurons	References
Rats	Somatosensory cortex	Fast-spiking neurons	La Camera et al. 2006
		GABAergic Interneurons	Markram 2000
		Not specified	Toledo-Rodriguez et al. 2004
		Basket cells	Wang et al. 2002
	Basolateral amygdala	Parvalbumin-positive Interneurons	Rainnie et al. 2006
	Entorthinal cortex	Neurogliaform cells	Price et al. 2005
	Hippocampus	COUP-TFII expressing neurons	Fuentealba et al. 2010
		Parvalbumin/Cholecystokinin-positive CA1 interneurons	Pawelzik, Hughes, and Thomson 2002
		Not specified	Sun et al. 2016
		CA3 pyramidal neurons	Rama et al. 2017
	Cerebral motor cortex	VIPergic interneurons	Porter et al. 1998
	Dentate gyrus	GOT responsive hilar interneurons	Harden and Frazier 2016
	Striatum	Fast-spiking neurons	Bracci et al. 2003
			Sciamanna and Wilson 2011
Mice	Somatosensory cortex	Fast-spiking GABAergic Interneurons	Goldberg et al. 2008
			Okaty et al. 2009
	Striatum	Fast-spiking neurons	Beatty, Song, and Wilson 2015
			Kawaguchi 1993
		Autaptic parvalbumin-positive neurons	Wang et al. 2022
	Visual cortex	Parvalbumin-positive fast-spiking neurons	Helm, Akgul, and Wollmuth 2012
	Hippocampus	Not specified	Szabó, Schlett, and Szücs 2021
Cats	Vestibular cortex of cats	Not specified	Fredrickson, Schwarz, and Kornhuber 1966
Human	Neocortex (epileptic focus)	Pyramidal neurons	Kushner et al. 2022

Table 2: Mammalian nerve cells reported to elicit stuttering firing patterns. Stuttering firing patterns were observed at different hierarchical levels inside the brain of rats, mice, cats, and human species.

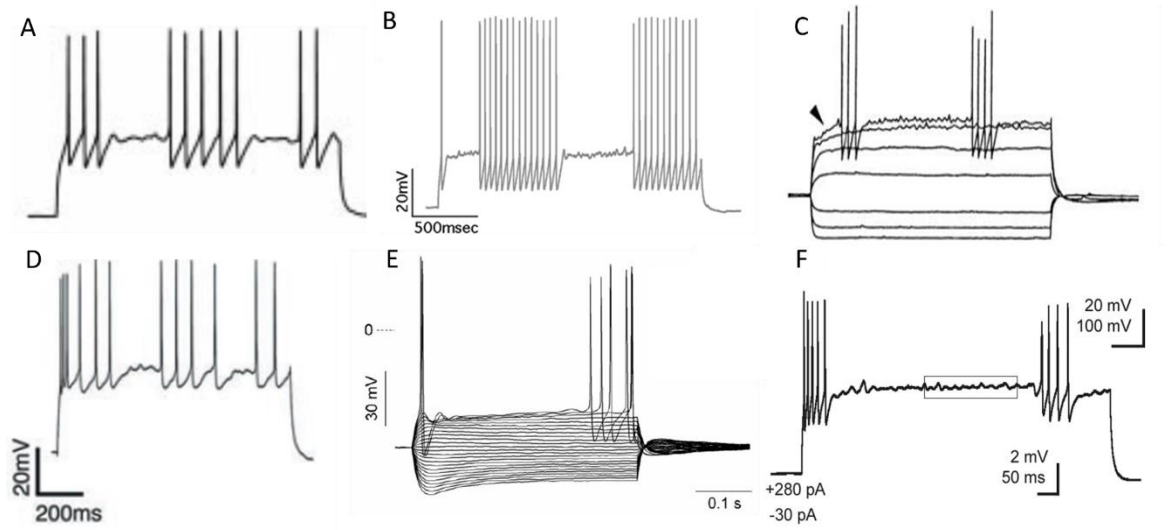

Figure 14: Voltage traces of mammalian neurons eliciting distinctive stuttering firing patterns. A, a classic stuttering discharges reported in the somatosensory cortex of rats (Adapted from Markram(2000)). B) a stuttering firing discharges with one onset spike reported in neocortical neurons located in layers 2–6 of the somatosensory cortex of rats (Adapted from Toledo-Rodriguez et al. (2004)) . C, a delayed stuttering firing discharged recorded in the hippocampal cultured neurons of mice (Adapted from Kawaguchi 1993)). D, a stuttering firing pattern expressing bursting at the onset recorded in the basket cells of the somatosensory cortex of rats (Adapted from Y. Wang et al. (2002)). E, a stuttering firing pattern with spikes near offset recorded in the hippocampal cultured neurons of mice (Adapted from Szabó, Schlett, and Szücs (2021)). F, a stuttering firing pattern with prolonged inter-burst duration recorded in GABAergic neuronal populations in the adult rat hippocampus (Retrieved from Fuentealba et al. (2010)).

2. Mechanisms behind stuttering firing patterns

Despite having frequently being reported, little is known about the intrinsic cellular mechanism underlying the stuttering firing pattern of APs in these neurons. It has been suggested that stuttering firing is the result of the interaction between fast outward dynamics and slow inactivated inward current. Per our knowledge, two driving mechanisms have been suggested to explain the stuttering firing. One proposed mechanism suggests that stochastic stuttering (i.e., arbitrary number of APs per burst) can occur on the condition that is preceded by subthreshold oscillations that is Na^+ dependent (Bracci, Centonze, Bernardi, & Calabresi, 2003; Fuentealba et al., 2010; Golomb et al., 2007). Another deterministic mechanism suggests that phase stuttering firing is the result of temporarily blocking AP firing due to

slowly inactivating K^+ channels (Balu, Larimer, & Strowbridge, 2004; Goldberg et al., 2008; Stiefel, Englitz, & Sejnowski, 2013). In this case, K^+ current within the cell membrane would increase as result of fast recovery from inactivation between spikes and eventually cease the firing. If depolarization of the neuronal membrane potential remains, these K^+ channels partly inactivate driving the potential to depolarize and to eventually fire APs. Both 4-aminopyridine (4-AP, a blocker for the D current at the millimolar level) and alpha-dendrotoxin (DTx-K, a blocker for Kv1 channel containing Kv1.1,Kv 1.2 and/or Kv1.6 subunits) are capable to halt the stuttering form of firing and transform it into a tonic (i.e., sustained) firing (Goldberg et al., 2008; Povysheva et al., 2008; Sciamanna & Wilson, 2011; Toledo-Rodriguez et al., 2004). This is consistent with the study of Okaty et al. (2009) and Toledo-Rodriguez et al. (2004) who reported the upregulation of multiple Kv1-type potassium channel subunit transcripts (e.g., Kcna1, Kcna6, Kcnab1, Kcnab2, and Kcnab3). Hence, it can be concluded in grosso modo that the outward D-current mediated by Kv1 subunits is responsible for modulating the stuttering firing discharge of neurons.

I. HVC_{RA} neuron conductance-based modeling

Voltage-gated and ligand-gated ion channels in the dendritic tree provide the cell with a rich repertoire of electrical behaviors ranging from passive responses to subthreshold active effects, dendritic spike initiation, diminishing somatic excitability. However, little is known about the properties of the ion channels that are responsible for these behaviors in HVC_{RA} neurons with no clear idea about their densities and spatial distribution. This section reviews

what we know so far about ion channels regulation of somatic electrophysiological properties in the past one- and two- compartment models of HVC_{RA} neuron.

While many studies in HVC neuron modeling centered on estimating the values of fixed variables in the one- and two- compartment HVC neurons models using data assimilation approaches (Kadakia et al., 2016; Meliza et al., 2014; Nogaret, Meliza, Margoliash, & Abarbanel, 2016), recent efforts are working on understanding how ion channels orchestrate the intrinsic properties of HVC neurons via biophysical modeling approaches (Daou et al., 2013; Long et al., 2010; Ross et al., 2017) in order to set a realistic framework for neural networks in the avian song system.

1. One-compartment models of HVC_{RA} neuron

Daou et al. (2013) developed the first biophysically realistic models of HVC neurons (e.g., HVC_{INT}, HVC_X, HVC_{RA}) based on pharmacologically identified voltage-gated and ligand-gated ion channels: I_{Na}, I_{Nap} I_{Kdr}, $I_{Ca\text{-}L}$, I_A, I_{SK}, I_h and I_{KNa} currents. One exception of this list of currents is the persistent sodium current (I_{Nap}) which was not identified pharmacologically, however it was inferred from the plateau potential (also known as depolarization block) exhibited by HVC_{RA} neurons. The model captured the key features of HVC_{RA} response to somatic current injections exemplified by (1) lack of excitability in response to depolarizing somatic current pulses, (2) the absence of a sag and post inhibitory rebound firing in response to a hyperpolarizing current, (3) a hyperpolarized resting membrane potential. The delay of first spike onset observed in the experiments was explained

to be caused by the decreased excitability of the neuron resulted from I_A in addition to the activities of I_{SK} and I_{KNa}. However, the model did not replicate wisely the voltage traces of HVC_{RA} neuron in presence of Apamin (i.e., an SK channel blocker agent), and spike frequency adaptation persisted due to the activity of I_{KNa} current in the model (**Figure 15**). Hence, this suggest that the contribution of I_{KNa} current in drawing the firing behavior of HVC_{RA} is ambiguous.

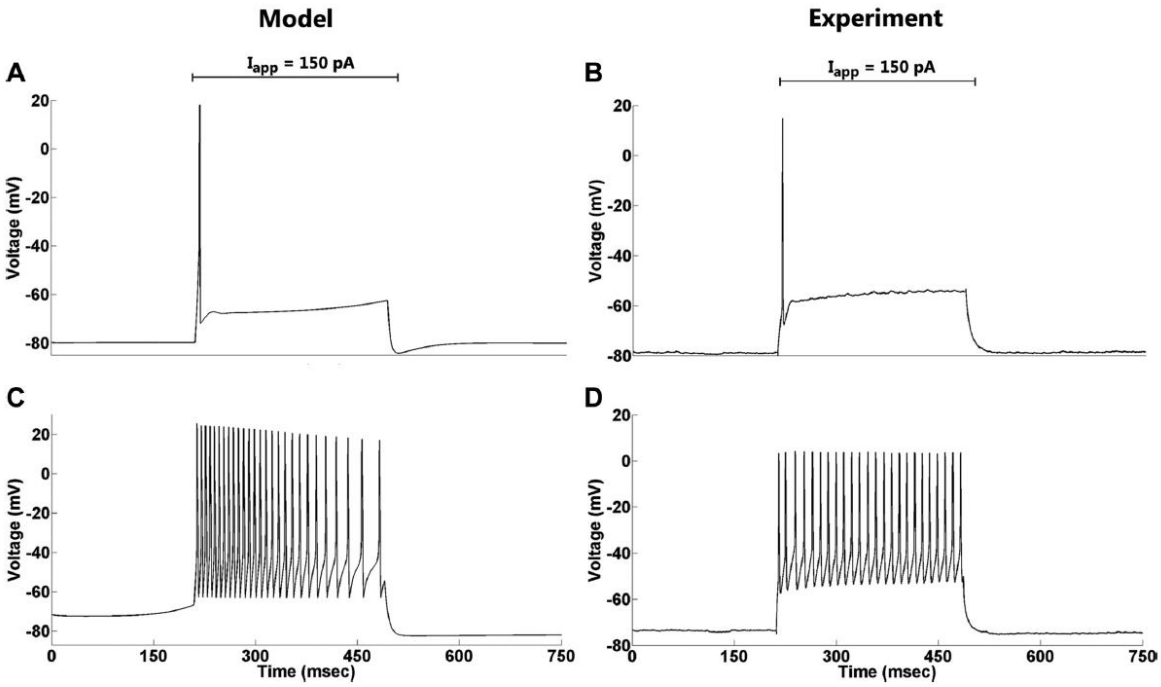

Figure 15: Effect of I_{SK} in HVC_{RA} neurons. A: a model HV_{CRA} neuron with the same parameters. B: an RA-projecting neuron exhibits a single action potential with no delay. C: blocking I_{SK} in the model (g_{SK} = 0) caused a dramatic increase in excitability, decreased the spike amplitude slightly, increased the resting membrane potential by 8 mV, and exhibited adaptation due to I_{KNa}. D: blocking I_{SK} using apamin (150 nM) greatly increased the neuron's excitability, decreased the spike amplitude, and depolarized the resting membrane potential by 5 mV. Unlike the model response, however, no adaptation was seen in this neuron (Retrieved from Daou et al., 2013).

Ross et al. (2017) extended the work of Daou et al. (2013) and used approximately the same ion channels in their one-compartment modeling study to replicate the firing

behavior of HVC PNs at different vocal development stages (e.g., subsong, plastic song, adult song). It should be noted that Ross et al. (2017) decided to introduce M-type current (I_M) and to remove I_{KNa} due to non-selectivity of I_{KNa} blockers. Their model was capable to capture the key electrophysiological features of phasic HVC_{RA} neurons (**Figure 15**) in terms membrane resting potential, spike amplitude, spike width and spike frequency. Spike frequency in the neuron model was regulated using I_{SK} and the interaction of I_{SK} with I_M regulated the phasic firing in these cells by setting the plateau potential. This emphasizes the role of I_{SK} and I_m in shaping the phasic behavior of HVC_{RA} neurons.

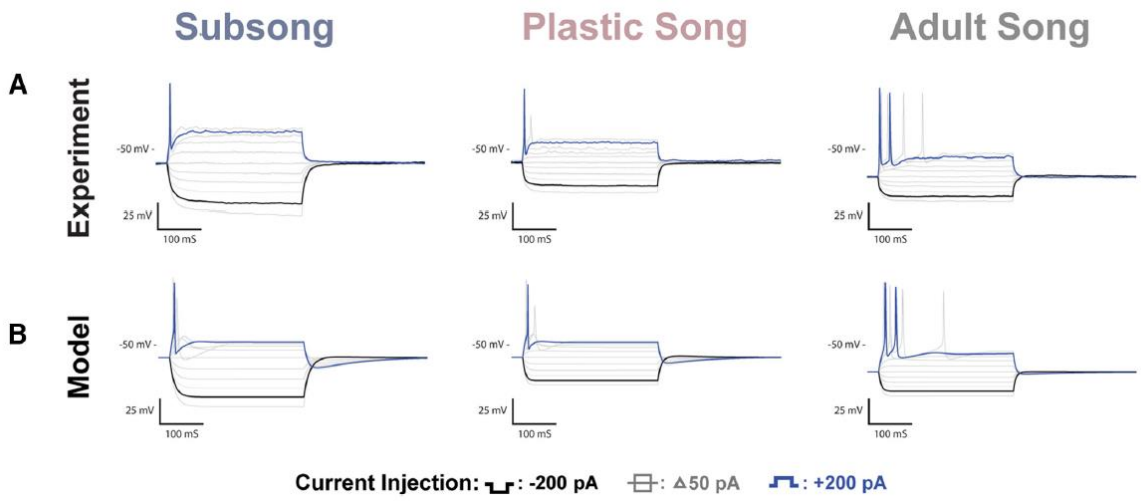

Figure 16: HVC_{RA} recordings and corresponding model traces. A, Voltage traces of HVCRA neurons recorded at subsong, plastic song, or adult stages of development. One of the more prominent changes observed across development was a systematic decrease in the resting potential of HVCRA neurons. B, modeled traces of the three neurons depicted in A. The models attributed the shift in resting potential to the leak current. Retrieved from Ross et al. (2017).

Recently, Daou et al. (in preparation) collected data from a large sample (n>300) of retrogradely labeled HVC_{RA} neurons (labeled with DiI via surgical injections into nucleus RA). Analysis of this large dataset revealed the existence of three classes of RA-projecting

neurons, which are diversified by the cocktail of ion channels that they exhibit. Daou et al. (in preparation) applied various pharmacological and histological manipulations and showed a beautiful interplay between A-type, M-type, D-type and SK channels in orchestrating the firing patterns of these premotor neurons (in preparation). In this work, we give class III neurons a special emphasis in our modeling studies, in an attempt to help unveil the distribution of some of these key channels across the different compartments of the neurons. Given the complexity of the modeling and the lack of knowledge on the distributions of these ion channels, we generated two-compartment models that incorporate a somatic and a dendritic compartment only.

2. Previous attempts at two-compartment modeling of HVC_{RA} neuron

Jin, Ramazanoğlu, and Seung (2007) developed a two-compartment model for HVC_{RA} neuron based on other cortical neurons. The two compartments included one for the soma consisting of I_{Na} and I_K currents which are necessary for spike initiation, and another one for the dendrites comprising high-threshold (I_{KHT}) and low-threshold (I_{KLT}) potassium currents to respectively account for high frequency spiking and spike frequency adaptation (although there was no biophysical evidence of these channels). The model could not replicate the firing patterns with accuracy, most notably the model exhibited higher level of frequency adaptation compared to the electrophysiological features provided by Dutar et al. (1998).

Another two-compartment model was developed by Long, Jin, and Fee (2010), where they constructed a model with I_{Na} and I_K currents located in the soma to account for fast

spiking response in addition to L-type calcium current and calcium activated potassium current which respectively serve for calcium spike initiation and spike termination. The model produced a graded spiking response with gradually increasing number of spikes following increasing the magnitude of current injections. The model was only capable to reproduce the stereotyped HVC_{RA} bursts, but it lacked all necessary ion channels that are able to explain the unique firing patterns of HVC_{RA} neuron.

CHAPTER III

METHODOLOGY

This chapter goes over the experimental setup utilized to record the voltage traces inside HVC_{RA} neurons and the modeling approach that we adopted throughout this study to build the two-compartment models of HVC_{RA} neurons. The thesis work is divided into two major objectives: 1) AIM 1: to investigate the roles of potassium channels in manipulating the features of stuttering firing pattern, 2) AIM 2: to mimic the firing pattern of HVC_{RA} recorded in experimental voltage traces in brain slices. To fulfill these two objectives, conductance-based models are designed to simulate the firing behaviors of HVC_{RA} neurons.

A. Brain slices recording

Voltage recordings of HVC_{RA} neurons that we aim to fit their traces were recorded in brain slices of male zebra finch birds. To capture these traces, whole cell recordings were performed by Arij Daou on brain slices via the patch clamping techniques at the laboratories of University of Chicago. HVC_{RA} neurons were subjected to a series of somatic current injection protocols designed to capture active and passive electric properties. HVC_{RA} neurons are easily identified among the pool of all HVC neurons located in brain slices by their florescence (since they are retrogradely labeled) as well as by their distinctive electrophysiological properties as noted in the previous section (i.e., *Characterizing intrinsic properties of HVC_{RA} in-vitro).*

B. Structuring the two-compartment HVC_{RA} neuron model

In the presence of somatic current injection, ion channels located in the soma interact with one another and with the ones located in the dendritic tree to shape the somatic firing behavior in HVC_{RA} neurons. Consequently, we decided to design two-compartment conductance-based models of HVC_{RA} neurons consisting of a somatic compartment and a dendritic compartment. The models are expansions of the work started by Pinsky and Rinzel (1994), and they extend the modeling work of Daou et al., (2013) and Ross et al. (2017). Hence, all the models consist of the ionic currents: $I_{Na}, I_K,\ I_M, I_{CaL},\ I_M, I_A,\ I_D, I_{SK}$, and I_{leak}. The models are constructed and simulated using MATLAB by solving the charge balance equations of ionic currents in our HVC_{RA} model:

Somatic Compartment: $C_s \frac{dV_s}{dt} = -\sum I_{ionic,\ s} + g_c(V_d - V_s) + I_{app}$ **Equation 6**

Dendritic Compartment: $C_d \frac{dV_d}{dt} = -\sum I_{ionic,\ d} + g_c(V_s - V_d)$ **Equation 7**

Where V_s and V_d are somatic and dendritic membrane potentials, C_s and C_d are respectively the somatic and dendritic membrane capacitance, $\sum I_{ionic,s}$ and $\sum I_{ionic,d}$ are the allocated somatic and dendritic ionic currents, I_{app} is the applied experimental current, g_c is the coupling conductance that connects the two compartments.

The equations of $I_{Na}$and I_K which are necessary for AP generation and propagation are based on Hodgkin and Huxley formalism (Daou et al., 2013):

Equation 8 $I_{Na} = g_{Na}\, m_\infty^3(V)\, h\, (V - V_K)$ and $I_K = g_K\, n^4\, (V)\, (V - V_K)$ **Equation 9**

Other equations of ionic currents (I_A, I_{CaL}, I_{SK}) are also adapted from the work of Daou et al., (2013) given by **Equation 10-12**

$$I_A = g_A a_\infty(V) e(V - V_K) \quad \textbf{Equation 10}$$

$$I_{CaL} = g_{CaL}\, V\, s_\infty^2(V)\left(\frac{Caex}{1 - e^{\frac{2FV}{RT}}}\right) \quad \textbf{Equation 11}$$

$$I_{SK} = g_{SK} k_\infty([Ca^{2+}]_i)\,(V - V_K) \quad \textbf{Equation 12}$$

The equation and kinetics of the non-inactivating I_M are adapted from Ross et al. (2017)

$$I_M = g_M\, y\, (V - V_K) \quad \textbf{Equation 13}$$

The equation and kinetics of fast-inactivating slow-inactivating I_D follows the equations of Shu et al.(2007):

$$I_D = g_D\, w\, z\, (V - V_K) \quad \textbf{Equation 14}$$

The gating variables n, e, y and z are slow and have first order kinetics specified by

$$\frac{dx}{dt} = \frac{x_\infty - x}{\tau_x}\ where\ x = n, s, e, y\ or\ z \quad \textbf{Equation 15}$$

The gating variable at steady state is given by:

$$x(V)_\infty = \frac{1}{1 + e^{\left(\frac{V - \theta_x}{\sigma_x}\right)}}\ where\ x = m, \text{ n, a, e, z a or y} \quad \textbf{Equation 16}$$

where θ_x is the half-activation (or half-inactivation) voltage for gating variable *x* and σ_x is the slope factor for that variable.

The steady state gating variable $w(V)_\infty$ is given by

$$w(V)_\infty = 1 - \frac{1}{1 + e^{(\frac{V-\theta_x}{\sigma_x})}}$$ **Equation 17**

The equation of the $h_\infty(V)$ gating variable is given by:

$$h_\infty(V) = \frac{\alpha_h}{\alpha_h + \beta_h}$$ **Equation 18**

Where $\alpha_h = 0.128\, e^{(\frac{V+15}{-18})}$ and $\beta_h = \frac{4}{1+e^{\frac{V+27}{-5}}}$

The time constant τ_n of n gating variable is given by the equation 17 (Daou et al., 2013):

$$\tau_n = \frac{\tau_{nbar}}{\cosh\,(\frac{V-\theta_n}{\sigma_n})}$$ **Equation 19**

The steady-state activation function of the SK current is solely dependent on the intracellular concentration of Ca^{2+} given by **Equation 20** (Daou et al., 2013)**:**

$$k_\infty([Ca^{2+}]_i) = \frac{[Ca^{2+}]^2}{[Ca^{2+}]^2 + k_s^2}$$ **Equation 20**

The intracellular concentration of free Ca^{2+} ions and is governed by

$$\frac{d[Ca^{2+}]}{dt} = -f\,\{\varepsilon(I_{CaL}) + k_{Ca}([Ca^{2+}] - b_{Ca}\}$$ **Equation 21**

V_{Na}	50		Ca_{ex}	30
σ_m	-5		τ_w	1
τ_h	-1		RT/F	26.7
V_K	-90		θ_s	-20
θ_n	-30		σ_s	-0.05
σ_n	-5		ks	0.5
θ_{aa}	-20		f	0.1
σ_{aa}	-10		ε	0.0015
θ_{ae}	-60		kCa	0.3
σ_{ae}	5		bCa	0.1
τ_{ae}	20		θ_w	-43
θ_y	-45		σ_w	8
σ_y	5		θ_z	-67
V_L	-70		σ_z	7.3

Table 3: The different fixed parameters of the differential equations of ionic currents that are used to build our HVC_{RA} conductance-based neuron models. The values of these fixed parameters are retrieved from (Daou et al., 2013).

C. Distribution of ion channels inside the models

Since there is no exact rule governing the distribution of ion channels inside the cell, we decided to adopt a mammalian distribution of ion channels inside the HVC_{RA} cell (Deardorff, Romer, & Fyffe, 2021; Lai & Jan, 2006). In this case, I_{CaL} and I_{SK}, would be located in both compartments, while I_{Na}, I_{Kdr}, I_A, I_D, I_M, I_{leak} are kept only in the somatic

compartments to ensure AP initiation in the soma (**Figure 17**). In line with experimental patch clamping of HVC slices, traces of experimental current (**Figure 18**) are supplied to the somatic compartment to excite the model HVC_{RA} neurons. Consequently, the HVC_{RA} neuron models obeys the series of equations of the two-compartment model shown in **Equation 22** and **Equation 23**.

Somatic Compartment: **Equation 22**

$$C_s \frac{dV_s}{dt} = -(I_{Na} + I_{Kdr} + \mathrm{I_{CaL,s}} + \mathrm{I_{SK,s}} + \mathrm{I_D} + \mathrm{I_{M,}} + \mathrm{I_{leak,s}}) + g_c(V_d - V_s) + I_{app}$$

Dendritic Compartment: **Equation 23**

$$C_d \frac{dV_d}{dt} = -(\mathrm{I_{CaL,d}} + \mathrm{I_{SK,d}} + \mathrm{I_{A,d}} + \mathrm{I_{leak,d}}) + g_c(V_s - V_d)$$

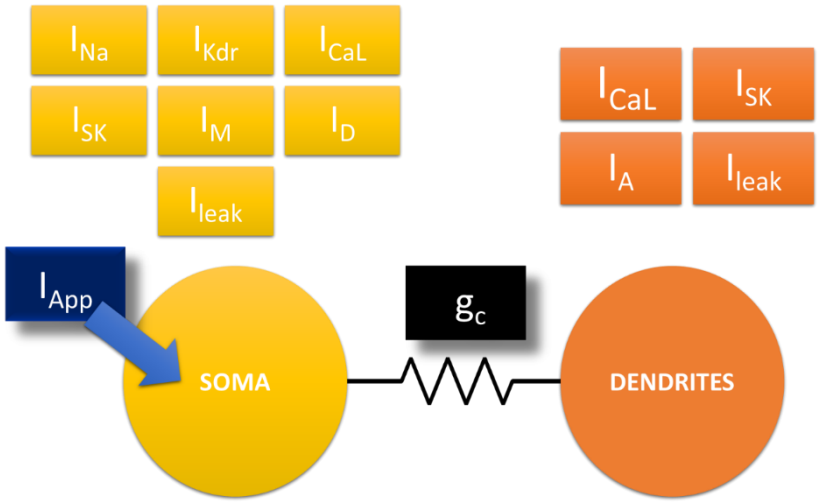

Figure 17: Distribution of ion channels in our models. The adopted distribution follows the one of mammalian neurons. I_{CaL}, I_{SK}, I_A, $I_{leak,}$ are inserted in the dendritic compartment, while I_{Na}, I_{Kdr}, I_{CaL}, I_D, I_M and $I_{leak,,}$. The two compartments are separated by a coupling conductance g_C. Somatic current I_{app} mimicking the experimental current is injected into the somatic current.

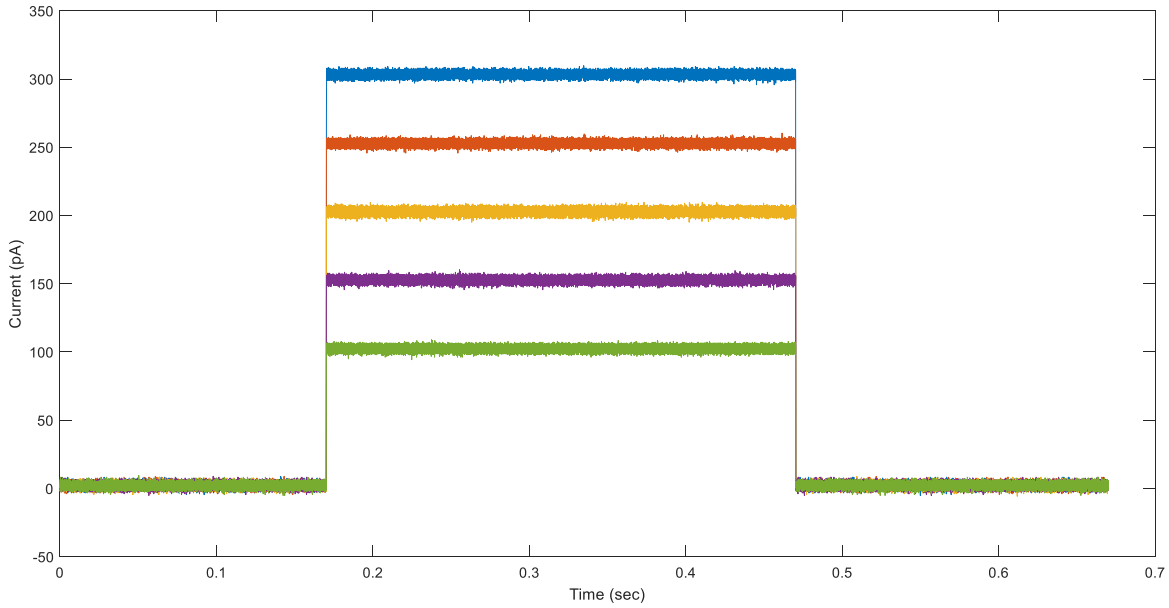

Figure 18: Examples of current traces injected to HVC_{RA} model neurons. These current traces are retrieved from experimental patch clamping experiments of brain slices of zebra finches that were executed at university of Chicago. To mimic experimental work and build our physiological models, experimental current traces are added to the somatic compartment of the models.

D. Flow of work

Since the thesis work concentrate on two aims, we will divide the flow of work into two parts. The first phase will focus on finetuning of the models' parameters to match the voltage traces of the HVC_{RA} models with the ones recorded in experiments. The second phase examines the effects of manipulating the values of different ion channels conductances on the stuttering firing behaviors of our putative HVC_{RA} neuron models. No calibration or manual finetuning of the conductance is performed in this case, only iterative change of the model parameters.

E. Finetuning of model parameters

For AIM 1, hand tuning of the conductances of ions channels is performed to fit the electrophysiological traits of the models with the ones recorded in brain slices. This hand-tuning approach is based on running manually the model with different values of free parameters to check which combination can give the best fit of the electrophysiological properties between the HVC_{RA} modeled neuron and the HVC_{RA} biological neuron. In other words, we manually calibrate the densities of maximal conductances (e.g., g_{Na}, g_{Kdr}, g_D, g_M, g_A, g_{CaL}, g_{SK}, g_{leak}, g_c), capacitance values (e.g., C_S and C_D) and the kinetic parameters (e.g., θ_m, τ_y, τ_z, τ_{nbar}, τ_h) to get a trait match between the electrophysiological traces of the HVC_{RA} model and the ones measured in experiments at different current pulses. Our obtained traces are assessed by matching our designed model with the ones of the experimental voltage traces in terms of number of spikes, the timing of the spikes, depolarization block following the AP spikes, the resting membrane potential elicited by HVC_{RA} cell etc.

F. Conductance manipulation effect on stuttering firing

For AIM 2, no hand tuning of the conductances parameters is executed. Parameter change will be performed iteratively in MATLAB, and the features of the firing behaviors (number of bursts, number of spikes per burst, inter-burst duration and spike-to-offset duration) are quantified and reported. We decided in this course of work to adopt a mammalian neurons distribution of ion channels (**Figure 19**) in parallel with models of AIM 1.

Quantitative features of stuttering firing discharges

To assess the traits of stuttering firings, we extract the electrophysiological features elicited by the putative HVC_{RA} neuron models (**Figure 18**). These features include i) number of bursts: A burst consists of a collection of successive spikes separated by interspike intervals (ISI) ii) number of spikes per burst: the latter are the number of spikes that collectively form a burst, iii) inter-burst durations: these are the occupied time duration that separates two consequential bursts or two consequential clusters of spikes. Onset-to-spike interval: it consist of the time duration that a neuron needs to fire the first AP and iv) spike-to-offset duration: it represents the time duration at which a neuron stops firing AP before shutting down the injection of a stimulating current pulse. These features are manipulated by automatically by varying the values corresponding to conductances of ion channels and solving back again the differential equations noted in **Equation 22** and **Equation 23**.

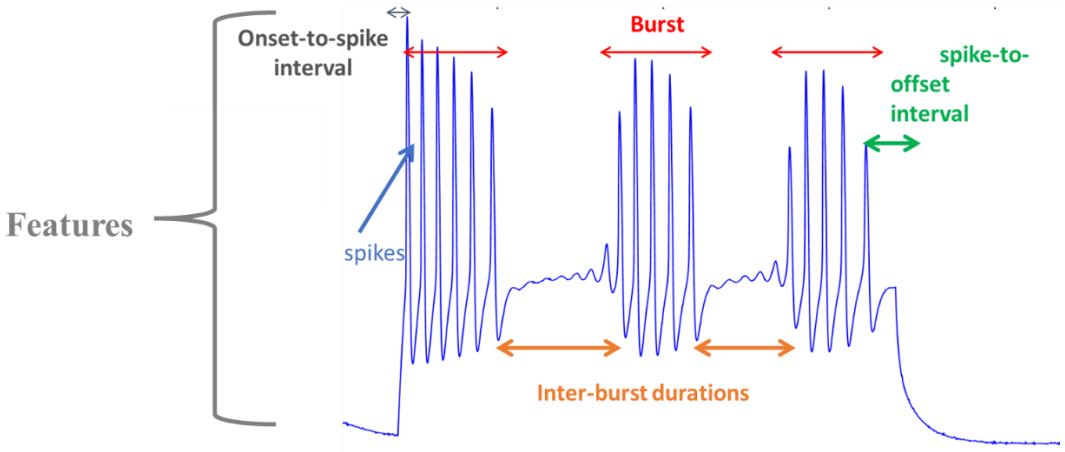

Figure 19: Annotated features of stuttering firing patterns of two generated sample neuron models. The list of features includes number of bursts, number of spikes per burst, inter-burst interval and last-spike-to-offset interval. A burst is a collection of peaks during a certain time window. Spikes per burst are the number of peaks noted during a bursting time window. Interburst interval is the time duration between bursts. Spike-to-offset interval is the duration between the last spike in the last burst and the offset of the current supply.

CHAPTER IV

RESULTS

Dual-compartment conductance-based biophysical models of cells from the HVC_{RA} were developed, based on our current-clamp data. Simulations of these model neurons were performed using Matlab (Mathworks). The source codes containing the models will be available online at our lab's website, as well as at ModelDB website located at http://senselab.med.yale.edu/modeldb/.

We will start by highlighting the different firing patterns recorded in the three classes of HVC_{RA} neurons via patch clamping and the biophysical details that differentiate these classes from each other. The rest of this chapter is divided into two sections that tackles our two main aims: 1- modeling the classes of HVC_{RA} neurons to reproduce the traits of experimental traces exhibited by the biological recordings in brain slices, and 2- understanding the effect of the key parameters of class III HVC_{RA} neurons on their stuttering firing behavior.

A. Different classes of HVC_{RA} neurons

RA projecting neurons are classified into three different classes depending on their electrophysiological responses to injected current. Class I HVC_{RA} neurons are the least excitable among their populational neurons. They are characterized by their phasic firing behavior which exhibits one or few APs following injection of somatic current despite

increasing the magnitude of the injected input current (**Figure 20**, top). Class II HVC_{RA} neurons elicit tonic firing patterns in the presence of somatic current. They fire one or few APs near rheobase, this genre of firing transforms into continuous as the injected current increases in magnitude (**Figure 20**, middle). In other words, what differs class I from class II neurons is the way they respond to current of large magnitude, with class I staying phasic and class II switching to tonic. Class III HVC_{RA} neurons elicit similar firing near rheobase as one or few APs are fired. This phasic firing behavior transforms into stuttering or pausing firing pattern with interrupted firing between the bursts (**Figure 20**, bottom). This class of neurons is an add-on class of HVC_{RA} neurons as no prior study reported this kind of behavior in HVC neurons. It is postulated that all the voltage traces exhibited by HVC_{RA} neurons are the results of intrinsic properties orchestrated by various voltage gated and ligand gated ionic currents. In other words, the ion channels interact with one another to shape the different firing behaviors at the macroscopic neural level.

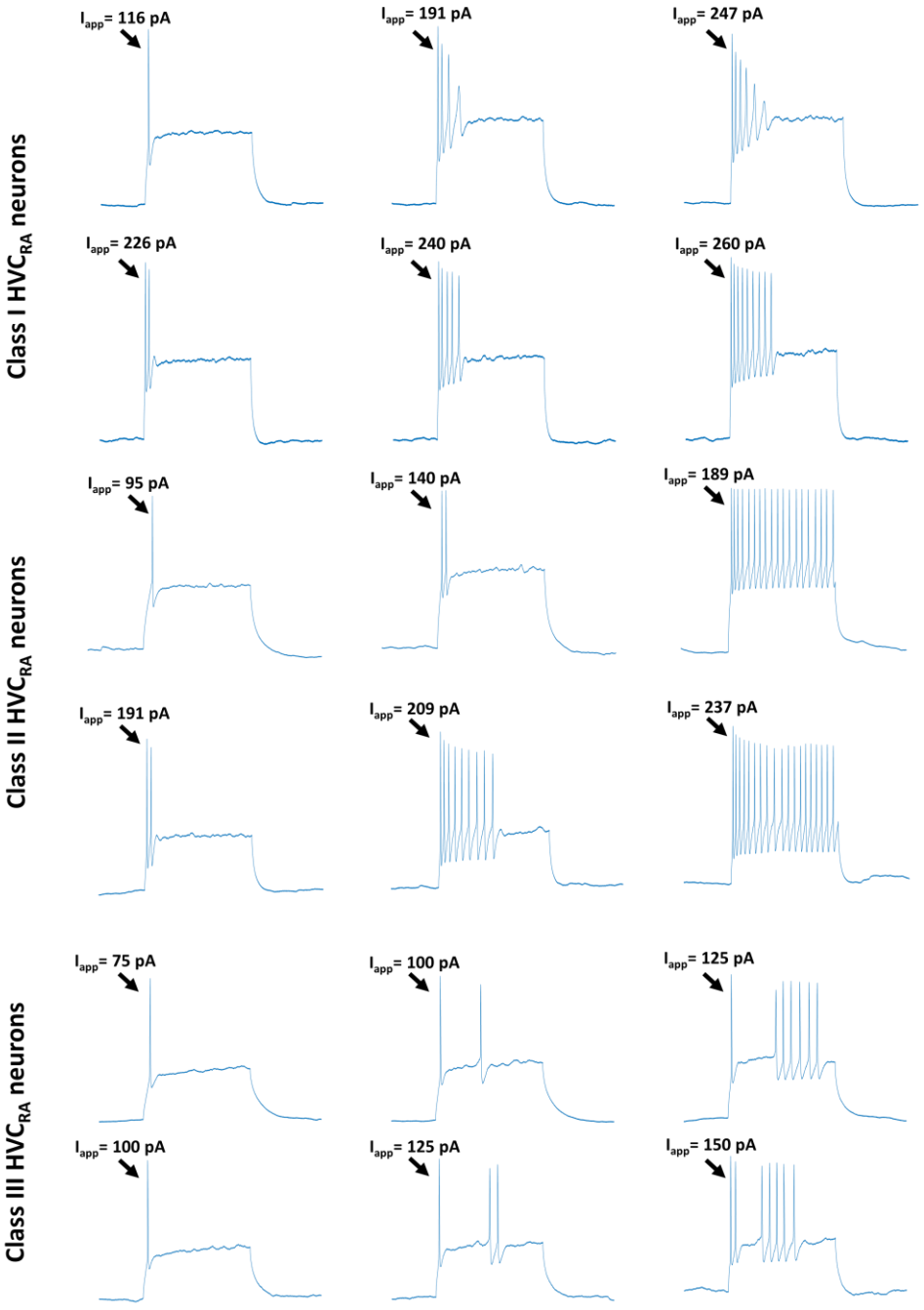

Figure 20: The three classes of HVC_{RA} neurons identified electrophysiologically via patch clamping techniques practiced in the laboratories of University of Chicago. Class 1 HVC_{RA} neurons fire low number of action potential despite increasing the injected input current. Class II HVC_{RA} neuron fire few APs near rheobase current, this for of firing is transformed to tonic as the input current is increased. Class III HVC_{RA} neurons also show one or few APs firing near rheobase current, this phasic firing pattern is transformed to stutter firing pattern with interrupted firing as the provided current is increased.

B. AIM 1: Modeling HVC_{RA} neurons

We have fitted our models to the biological data collected from HVC_{RA} neurons. The calibration of free parameters of our neuron models was performed manually at different experimental current levels (**Figure 21**). The models for HVC_{RA} cells are carefully tuned via hand tuning technique to serve our desired AIM 1. The parameters that were varied were mainly the maximal conductances of the ionic currents incorporated into the somatic and dendritic compartments as well as the capacitances of these neurons, while the rest of the parameters were fixed. The aim here is to have a match in the electrophysiological features between our neuron models and experimental HVC_{RA} traces recorded in brain slices of 7 different zebra finch birds (**Figures 22-23**). **Figures 22-23** show examples of three different biological neurons of class I (blue traces) that have been fit to their corresponding models (red traces). The fits were first conducted for a given current magnitude (upper left traces in each of **Figures 21-23**), and then once a decent fit was obtained, model parameters were used to generated predictions about the behavior of the neuron for different current magnitudes (the rest of the traces in each figure). The results show a close match of the input-outputs between HVC_{RA} models and the actual cell. Class I HVC_{RA} neuron models showed a large decrease in excitability which is mainly due to the somatic I_D and I_M currents. This is clearly visible from the large distribution of their corresponding values (**Figure 24**). The conductance densities of g_{Ad} and g_{Kdr} were either zero or near zero, this means that their roles in determining the intrinsic electrophysiological properties of class I HVC_{RA} neurons are negligible. Dendritic g_{SKd} and g_{CaLd} contribute to the variability in electrophysiology seen in this class of neurons to a larger extinct than the ones located in the somatic compartment:

g_{SKs} and g_{Cals}. This means dendritic intrinsic properties are affiliated in shaping the electrophysiology recorded in the soma. Additionally, the morphology of the dendritic tree (i.e., C_d) plays a determinant role in shaping the intrinsic properties which are unique to this class of neurons (**Figure 25**).

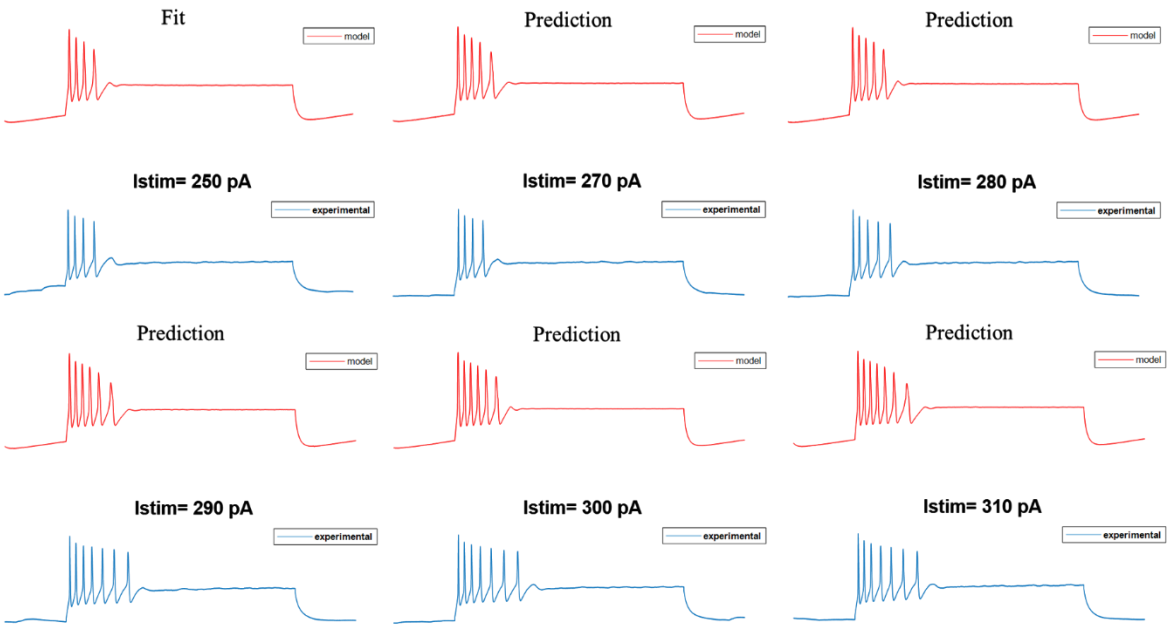

Figure 21: Replicating the voltage traces of one HVC_{RA} neuron recorded in brain slices of the zebra finch (Lilac 135) at various experimental currents with averages ranging from 250 pA to 310 pA. The models are simulated by building conductance based HVC_{RA} neuron models. Red color refers to the voltage traces of the model HVC_{RA} neuron while the blue color refers to the experimental voltage traces of one HVC_{RA} neuron recorded in brain slices via patch clamping techniques in University of Chicago.

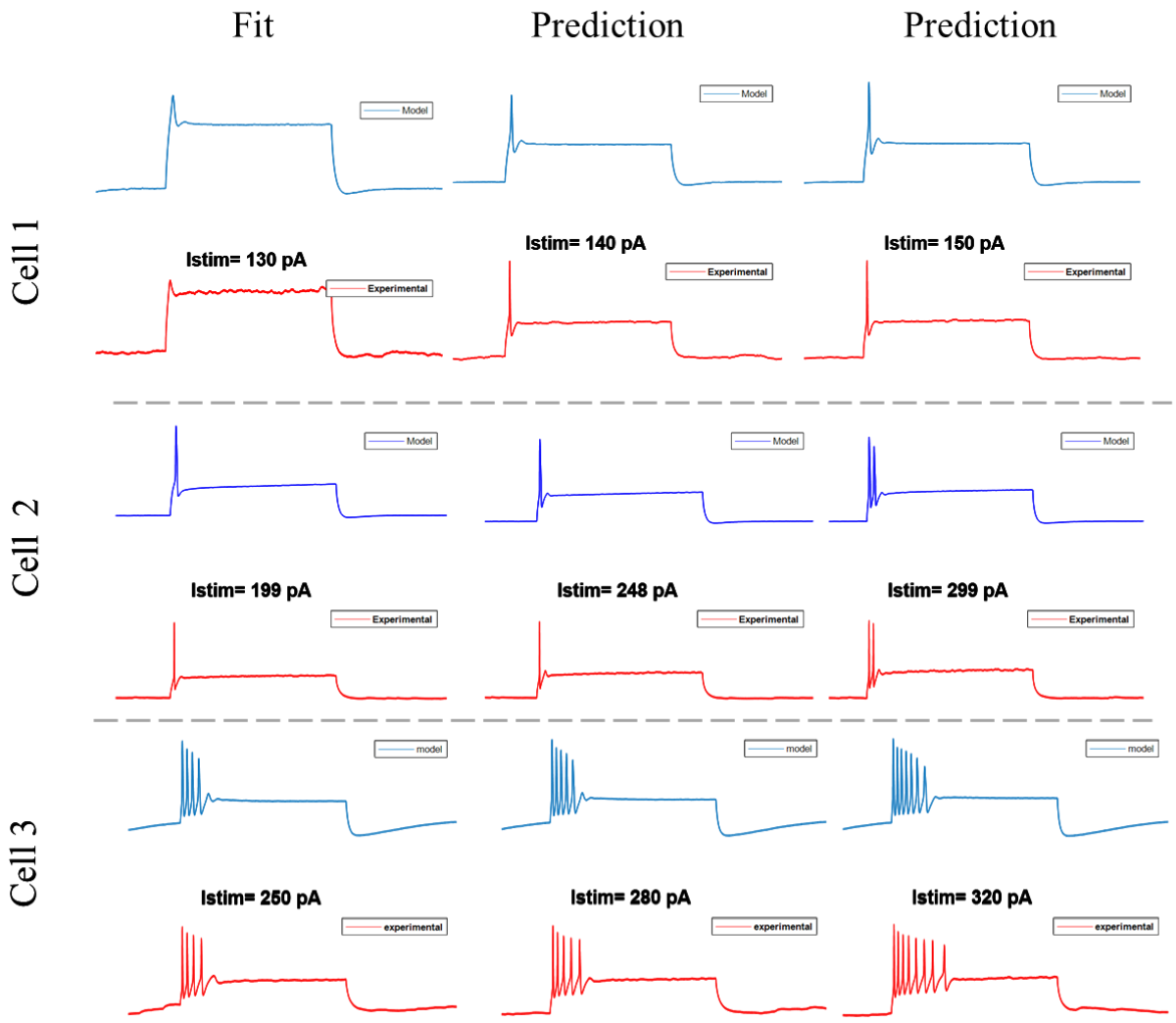

Figure 22: Output of modeling simulations of class I HVC_{RA} neurons (Part 1). HVC_{RA} model neurons are built to replicate the voltage traces of HVC_{RA} neurons recorded via patch clamping techniques. The voltage traces are the result of HVC_{RA} neurons excitations at various experimental currents injected to the soma.

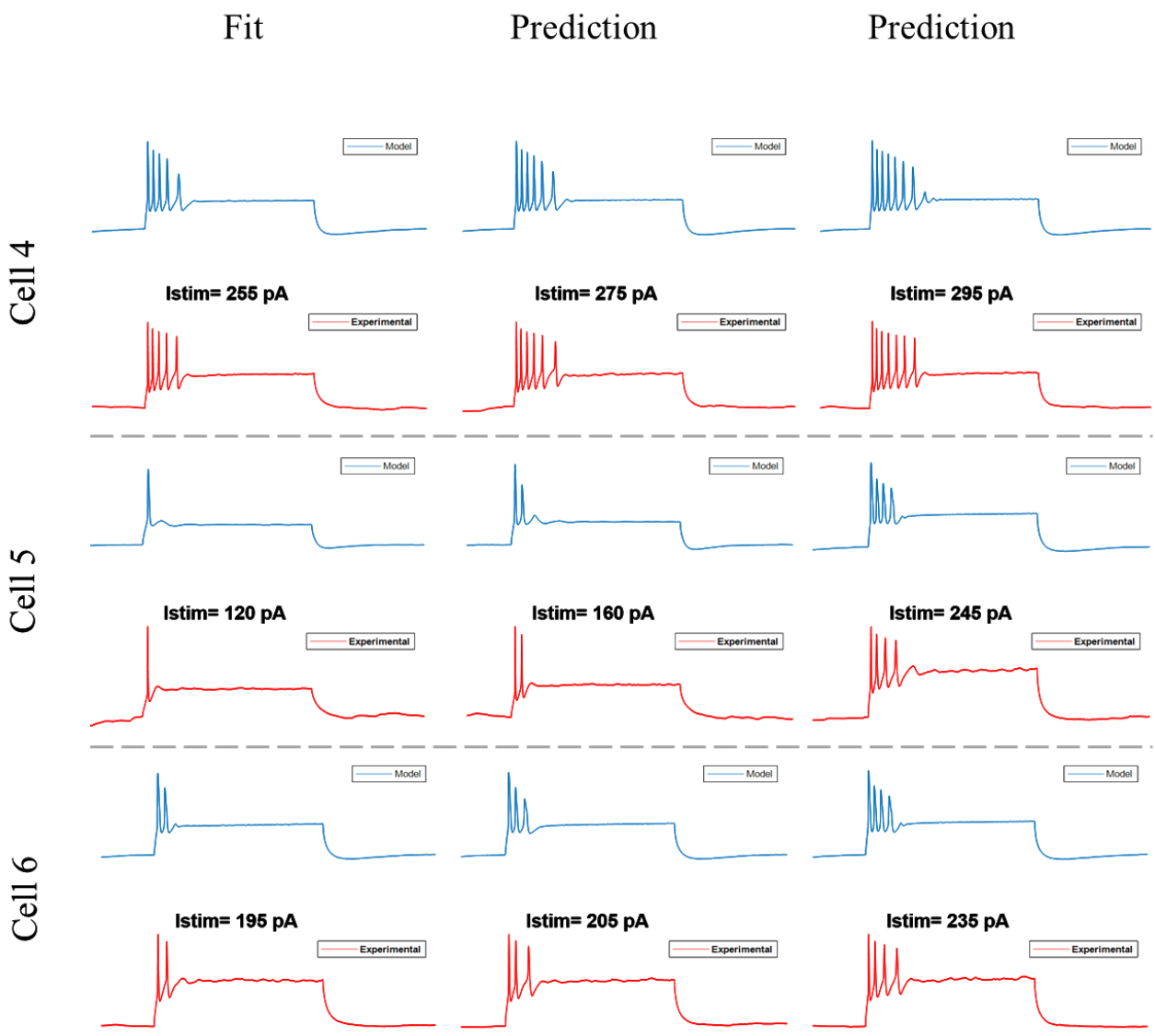

Figure 23: Output of modeling simulations of class I HVC_{RA} neurons (Part 2). HVC_{RA} model neurons are built to replicate the voltage traces of HVC_{RA} neurons recorded via patch clamping techniques. The voltage traces are the result of HVC_{RA} neurons excitations at various experimental currents injected to the soma.

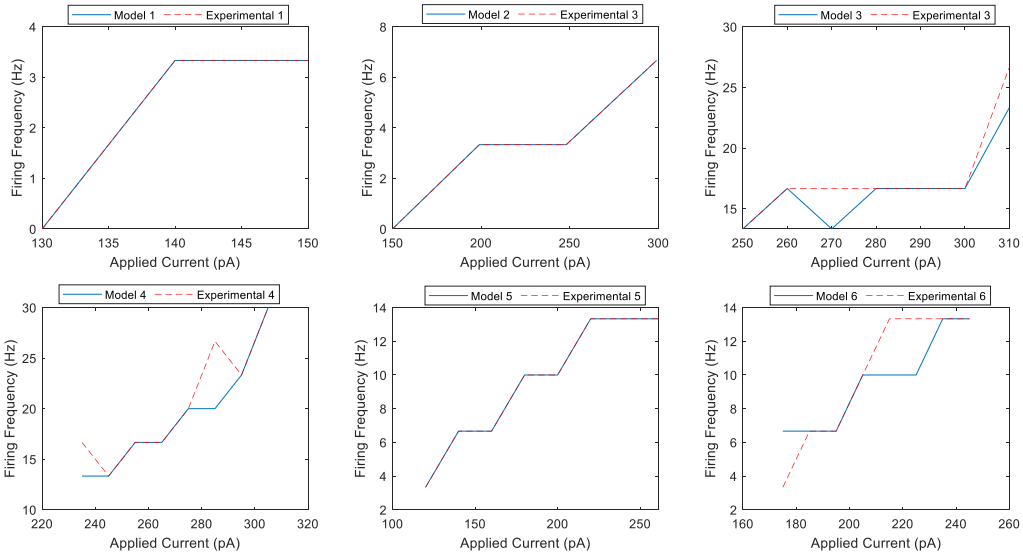

Figure 24: Input-output profiles of the modeled type I HVC_{RA} neurons and physiologically recorded type I HVC_{RA} neurons. Six profiles are shown corresponds to six different HVC_{RA} cells and six calibrated model HVC_{RA} neurons.

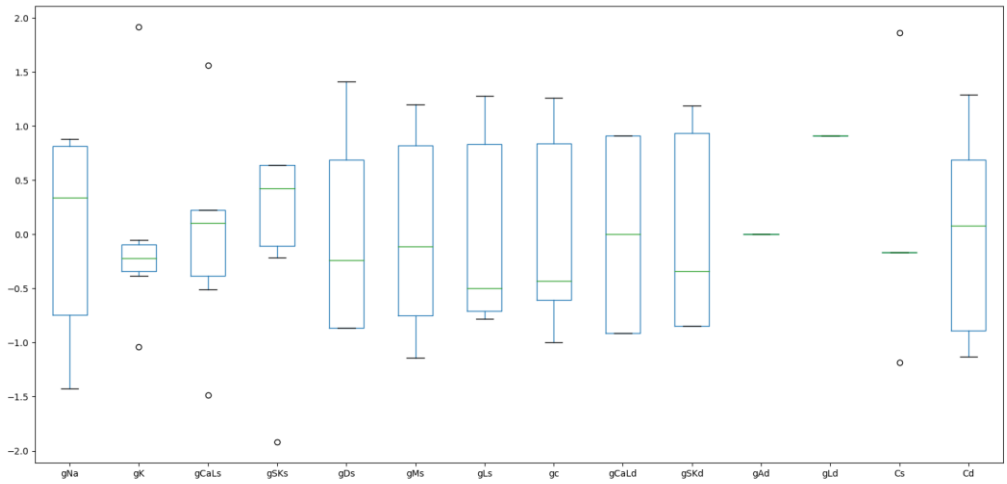

Figure 25: Box plot of normalized maximal conductances and capacitance parameters used in our class I HVC_{RA} models. The normalization is conducted by subtraction with mean of each parameter and divided by the standard deviation of the different values of this parameter

As reported in literature, class II HVC_{RA} neurons fire one or few APs near threshold. This firing behavior turn into tonic as the supplied current increases in magnitude (**Figures 26-27**). In parallel with the simulations of class I HVC_{RA} neurons, the models were closely calibrated to obtain a match between the electrophysiologic properties of the recorded HVC_{RA} neuron and the ones of the built models. This is clearly visible by tracking the close match of the input-output phenotypes between type II HVC_{RA} models and type II HVC_{RA} actual neurons (**Figure 28**). The three somatic parameters, g_{SK}, g_D and g_{Kdr} are shown to have large distributions in terms of density between the different class II HVC_{RA} neuron model (**Figure 29**). This means that the variability in tonic firing recorded in brain slices is primarily controlled by these ion currents. The firing behavior was also determined by the coupling conductance (g_c) which also shows a large variability in our models (**Figure 29**). This indicates that the strength of the coupling between the soma and dendrites is an essential component to form the various tonic firing patterns.

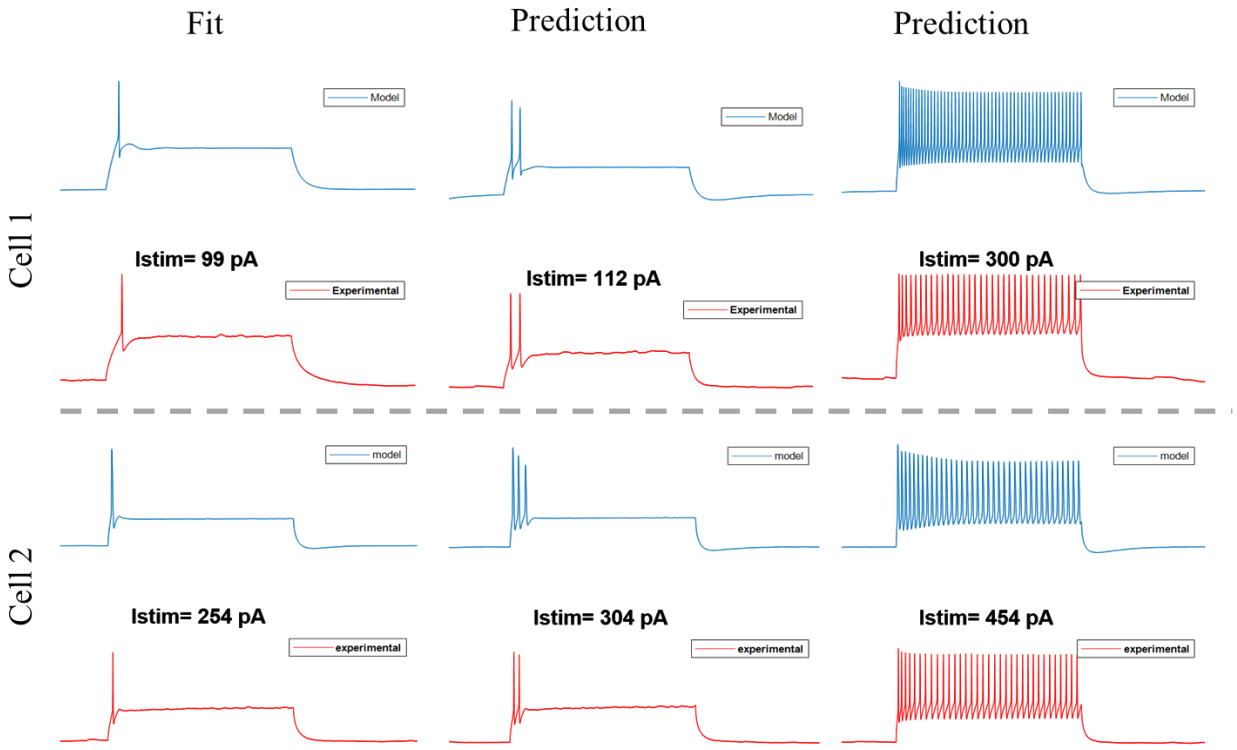

Figure 26: Outputs of modeling simulations of class II HVC_{RA} neurons (Part 1). HVC_{RA} model neurons are built to replicate the voltage traces of HVC_{RA} neurons recorded via patch clamping techniques. The voltage traces are the result of HVC_{RA} neurons excitations at various experimental currents injected to the soma.

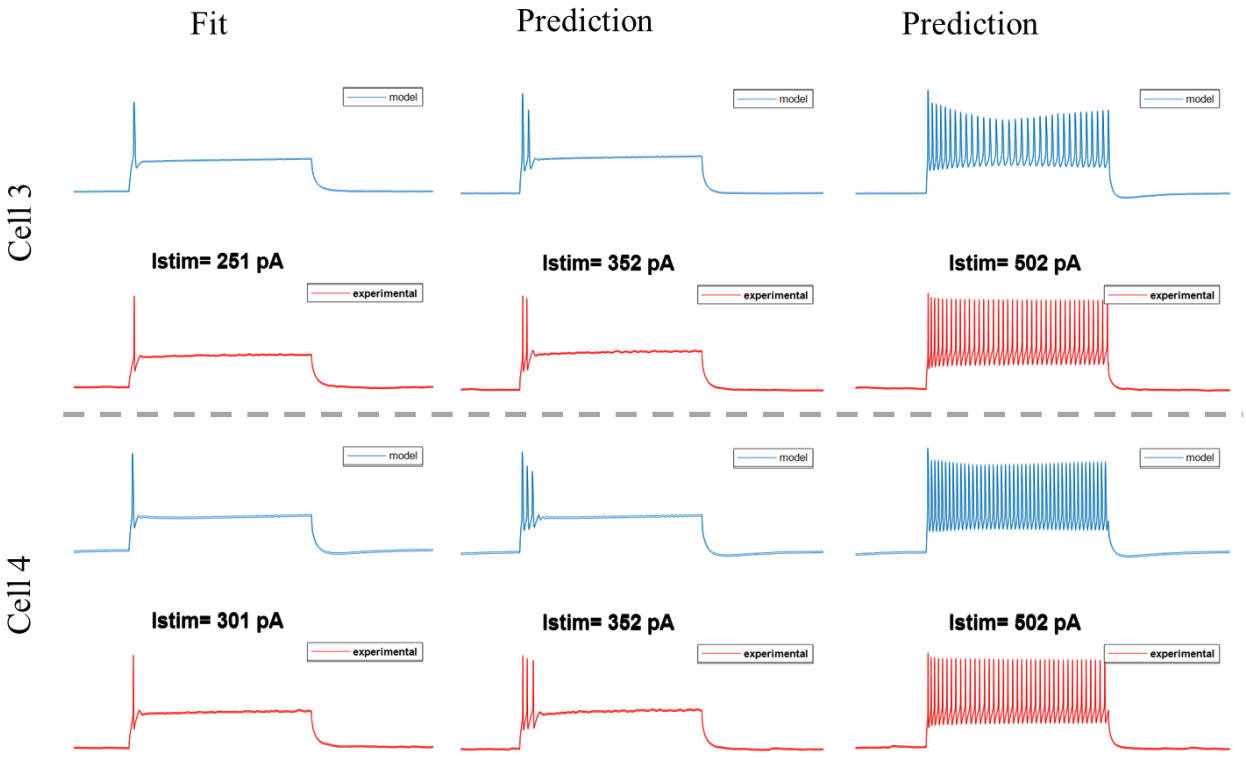

Figure 27: Outputs of modeling simulations of class II HVC_{RA} neurons (Part 2). HVC_{RA} model neurons are built to replicate the voltage traces of HVC_{RA} neurons recorded via patch clamping techniques. The voltage traces are the result of HVC_{RA} neurons excitations at various experimental currents injected to the soma.

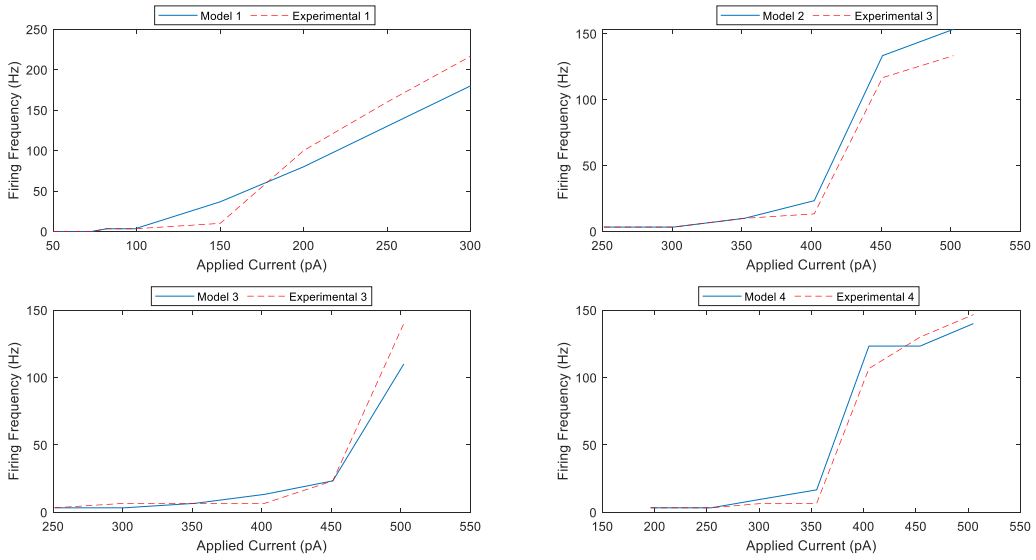

Figure 28: Input-output profiles of the modeled type II HVC_{RA} neurons and physiologically recorded type II HVC_{RA} neurons. Six profiles are shown corresponds to six different HVC_{RA} cells and six calibrated model HVC_{RA} neurons.

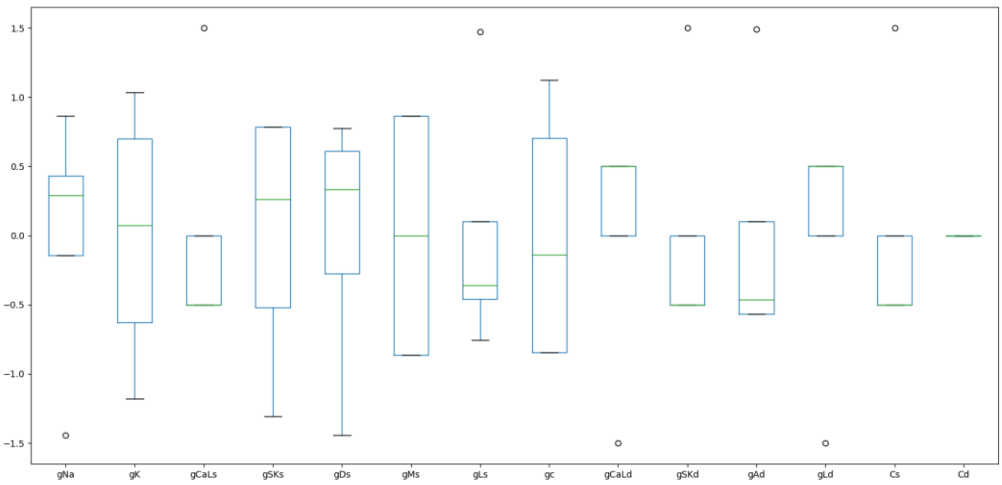

Figure 29: Box plot of normalized maximal conductances and capacitance parameters used in our class I HVC_{RA} models. The normalization is conducted by subtraction with mean of each parameter and divided by the standard deviation of the different values of this parameter.

C. AIM 2: Unveiling key parameters in controlling the stuttering firing behavior of Class III HVC_{RA} neurons.

Since shaping the firing profile by a cell is the result of the interaction between more than one current, we decide to assess the effect of manipulating two parameters at a time and note their corresponding effect on the various features of stuttering firing behavior such as number of bursts, last spike to offset interval, onset to first spike interval, spikes per burst and time durations between bursts. The section includes parameters manipulation of the following series of parameters: $\mathbf{g_M}$ **&** $\mathbf{g_D}$**,** $\mathbf{g_D}$ **&** $\mathbf{g_{SK}}$**,** $\mathbf{g_{Ad}}$ **&** $\mathbf{g_D}$**,** $\boldsymbol{\tau_z}$ **&** $\mathbf{g_D}$**,** $\mathbf{g_{CaL}}$ **&** $\mathbf{g_{SK}}$.

1. Impact of low threshold M-type and D-type potassium currents on stuttering firing patterns

The densities of the conductances – g_M and g_D – were iteratively varied between 0 nS and 20 nS, and the noted stuttering features are quantitatively tracked down. Starting with a tonic firing behavior (i.e., at g_M=0 and g_D=0), calibrating g_M and g_D produces several layers (i.e., clusters) of datapoints with stuttering firings that differentiate in their number of bursts (**Figure 30**). It can be further noted that the densities of g_D was largely maintained along with a low density for g_M to keep eliciting stuttering behavior (**Figures 30-31**). Upregulating g_M was responsible for diminishing the excitability of the putative HVC_{RA} model by lowering the number and amplitude of spikes in each burst. Consequently, this leads to halting the stuttering firing pattern by gradually transitioning the firing into a phasic firing (**Figures 31-32**). Regarding the duration between the last fired spike and offset, no trend was concluded as it can be noted that there are two clusters of datapoints with several intermediate datapoints (**Figure 33**). For the onset delay, an exponential trendline that depends on both g_D and g_M is marked (**Figure 34**). The higher the density of g_M, the more prolonged the delay to spiking becomes.

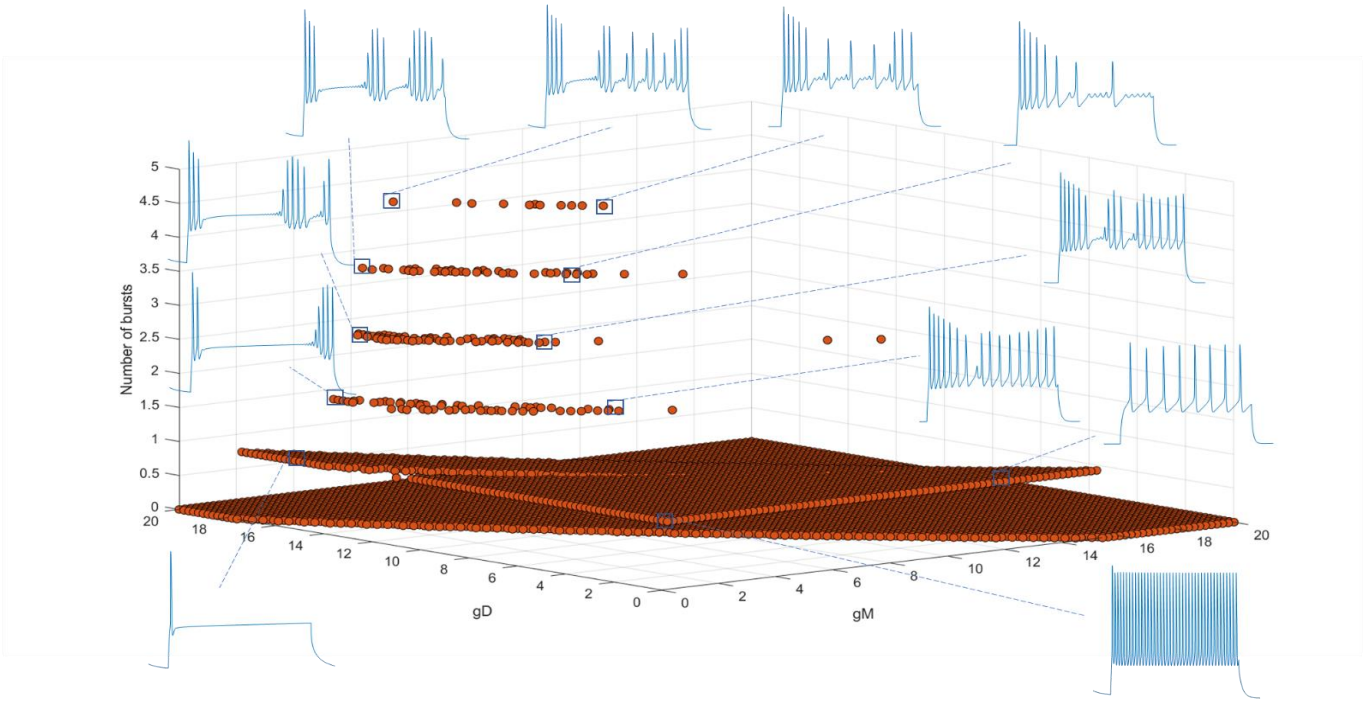

Figure 30: Number of bursts elicited by the putative HVC_{RA} models at different densities of somatic g_M and g_D. The number of bursts drawn by the stuttering models is captured for values of g_M and g_D ranging between 0 and 20 nS.

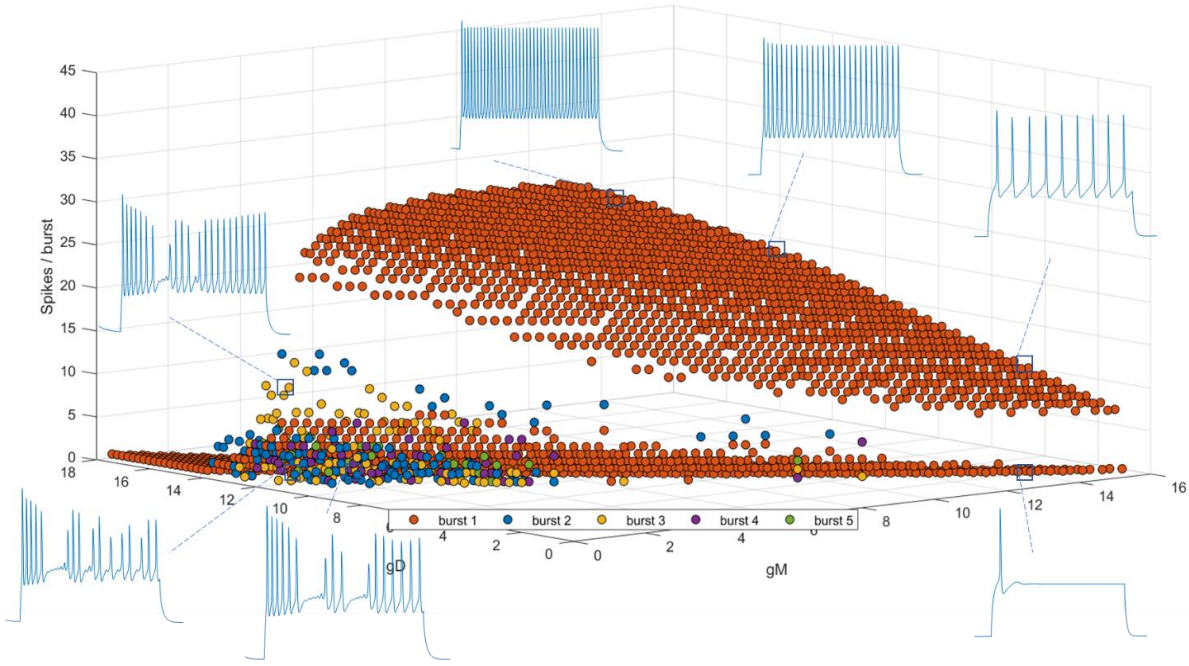

Figure 31: Spikes per burst elicited by the putative HVC_{RA} models at different densities of somatic g_M and g_D. The number of spikes per burst drawn by the stuttering models is captured for values of g_M and g_D ranging between 0 and 20

nS. Color orange corresponds to the values of spikes in the first burst, color blue corresponds to the values of spikes in the second burst, color yellow corresponds to the values of spikes in the third burst, color violet corresponds to the values of spikes in the fourth burst and color green corresponds to the values of spikes in the fifth burst.

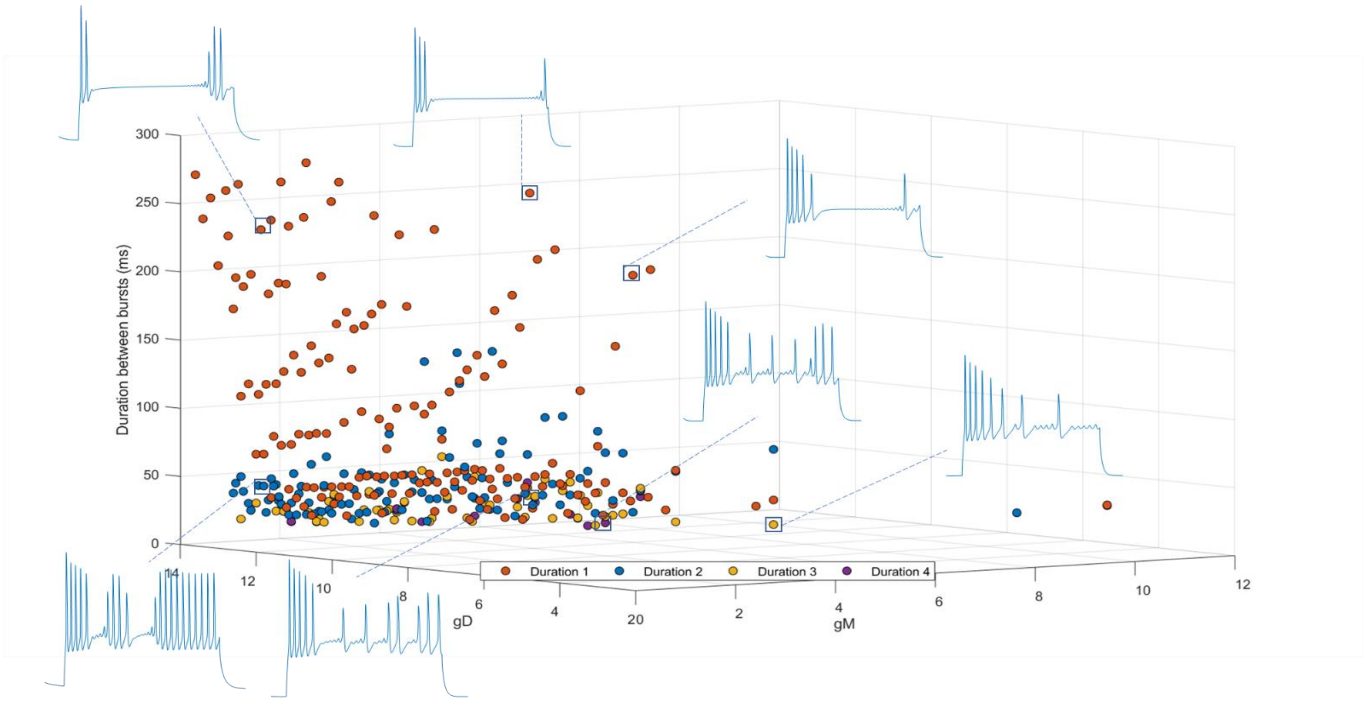

Figure 32: Inter-burst intervals elicited by the putative HVC_{RA} models at different densities of somatic g_M and g_D. Inter-burst intervals drawn by the stuttering models are captured for values of g_M and g_D ranging between 0 and 20 nS. Color orange corresponds to the first time duration between two successive bursts, color blue corresponds to second time duration between two successive bursts, color yellow corresponds to third time duration between two successive bursts, color violet corresponds to the fourth time duration between two successive bursts

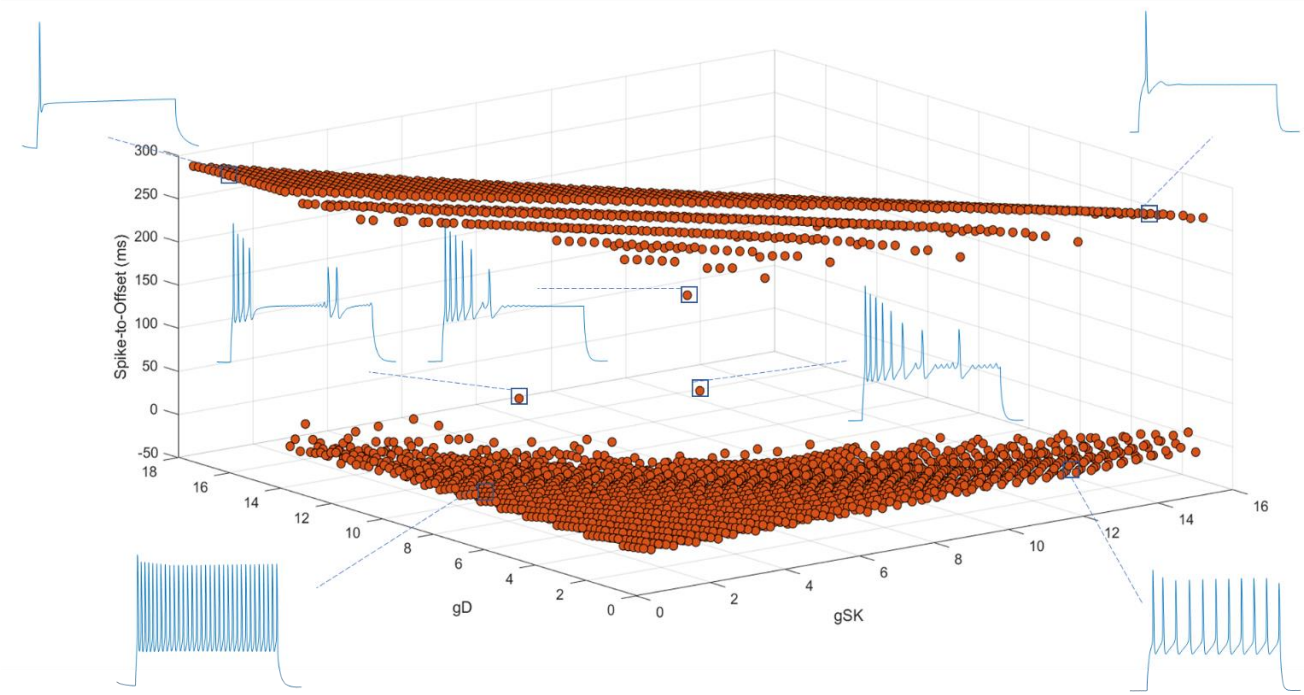

Figure 33: Time duration between last fired action potential and the current offset exhibited by the putative HVC_{RA} models at different densities of somatic g_M and g_D. Inter-burst intervals drawn by the stuttering models are captured for values of g_M and g_D ranging between 0 and 20 nS.

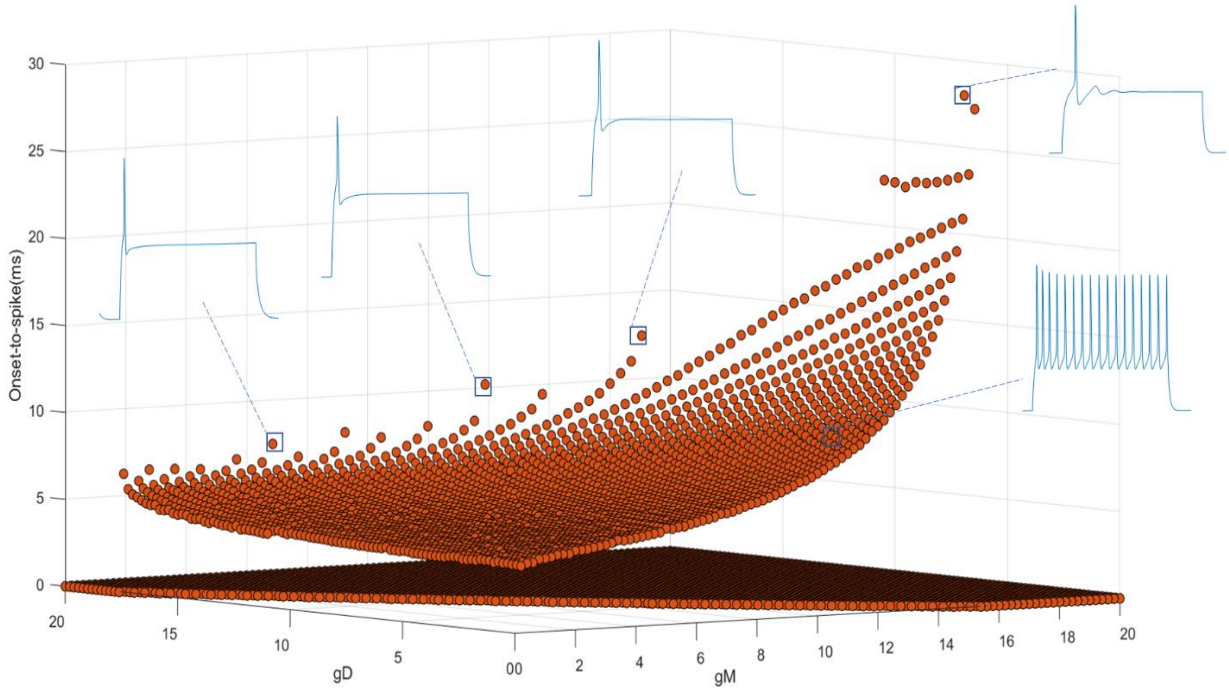

Figure 34: Time duration between current onset and the first fired spike by the putative HVC_{RA} models at different densities of somatic g_M and g_D. Inter-burst intervals drawn by the stuttering models are captured for values of gM and gD ranging between 0 and 20 nS.

2. *Impact of low threshold D-current and calcium activated SK-current on stuttering firing patterns*

The densities of the conductances – g_{SK} and g_D – were iteratively varied respectively between 0 nS and 18 nS, and 0 and 20 nS. Starting with a tonic firing behavior (at g_M=0 and gD=0), calibrating g_{SK} and g_D produce several clusters of stuttering firing behaviors with an alternating number of bursts (**Figure 35**). The number of spikes in each burst can be modulated by varying the densities of both ion channels (**Figure 36**). While regulating the density of g_{SK} is largely dictating the switch between the number of bursts, g_D seems to modulate the time interval between successive bursts (**Figure 37**). The neuron models cease continuous firing and transform into phasic firing as g_D largely increases (**Figure 38**). Regarding the onset-to-spike, a linear trendline is noted that depends on both parameters. As g_D increases and g_M follows a similar track, the delay to spiking increases (**Figure 39**). Consequently, a prolonged delay to the onset spike is obtained, however this delay does not surpass 8 msecs.

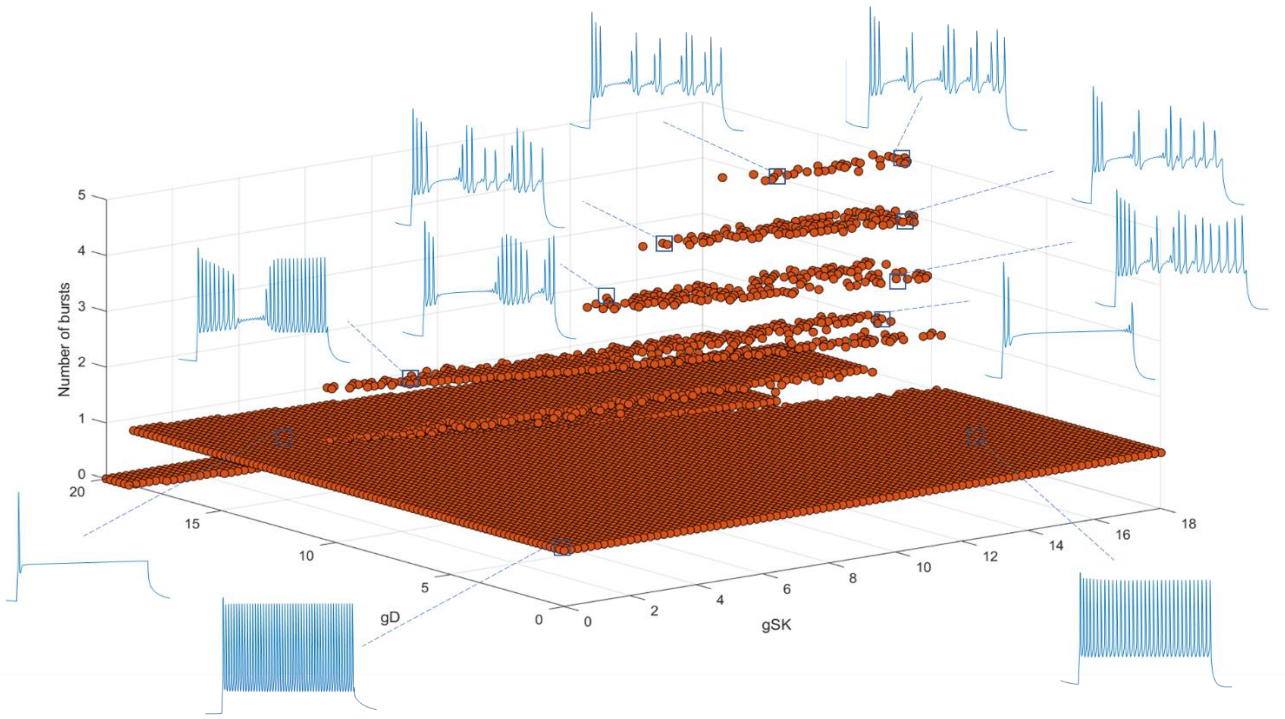

Figure 35: Number of bursts elicited by the putative HVC_{RA} models at different densities of somatic g_{SK} and g_D. The number of bursts drawn by the stuttering models is captured for values of g_{SK} and g_D ranging respectively between 0 and 18 nS, and 0 and 20 nS.

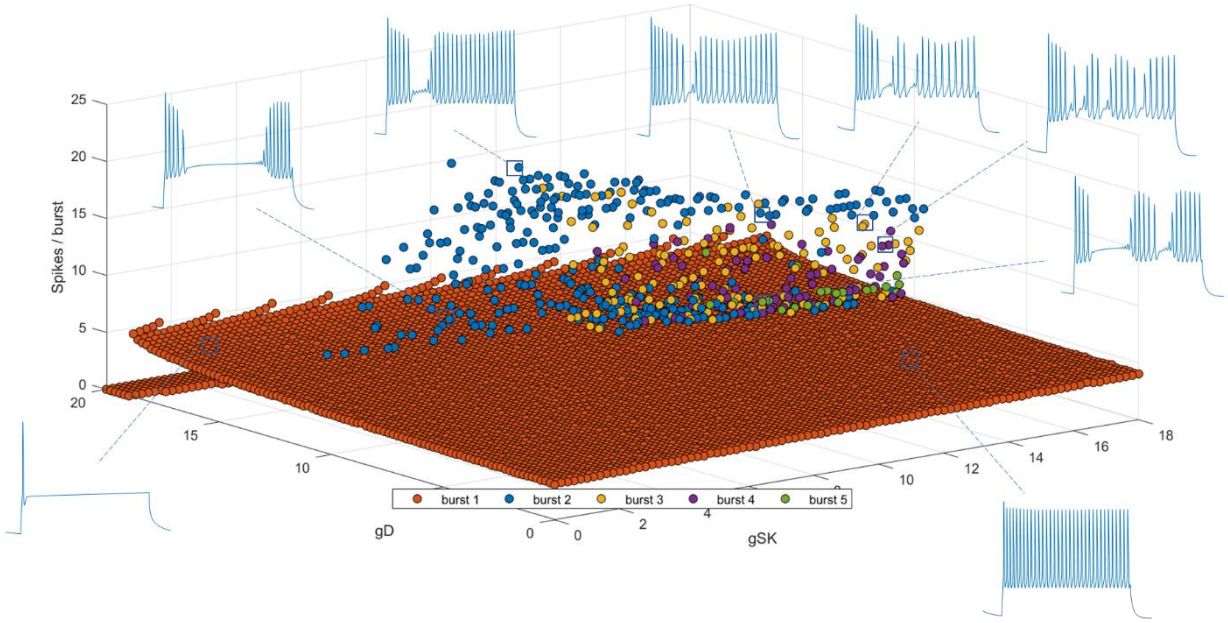

Figure 36: Number of spikes elicited by the putative HVC_{RA} models at different densities of somatic g_{SK} and g_D. The number of spikes per burst drawn by the stuttering models is captured for values of g_{SK} and g_D ranging respectively between 0 and 18 nS, and 0 and 20 nS. Color orange corresponds to the values of spikes in the first burst, color blue corresponds to the values of spikes in the second burst, color yellow corresponds to the values of spikes in the third burst,

color violet corresponds to the values of spikes in the fourth burst and color green corresponds to the values of spikes in the fifth burst.

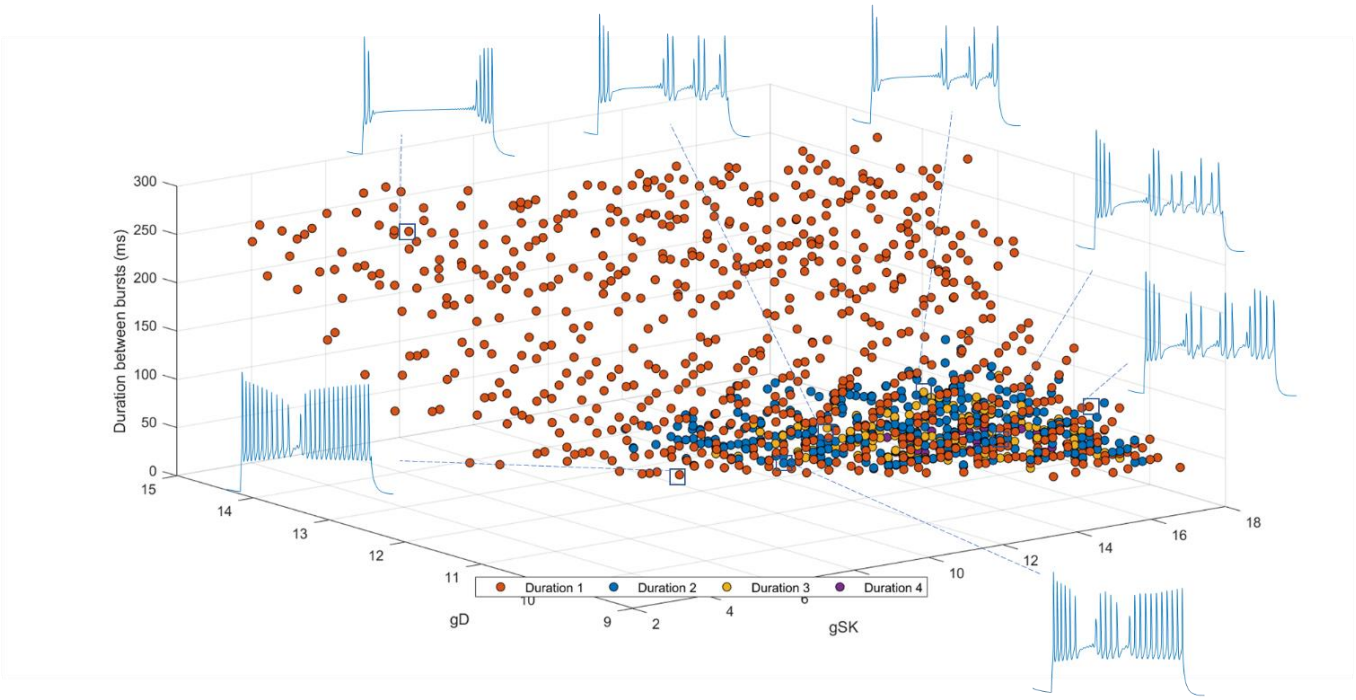

Figure 37: Inter-burst spikes elicited by the putative HVC_{RA} models at different densities of somatic g_{SK} and g_D. Inter-burst intervals shown by the stuttering models is captured for values of g_{SK} and g_D ranging respectively between 0 and 18 nS, and 0 and 20 nS. Color orange corresponds to the first time duration between two successive bursts, color blue corresponds to second time duration between two successive bursts, color yellow corresponds to third time duration between two successive bursts, color violet corresponds to the fourth time duration between two successive bursts.

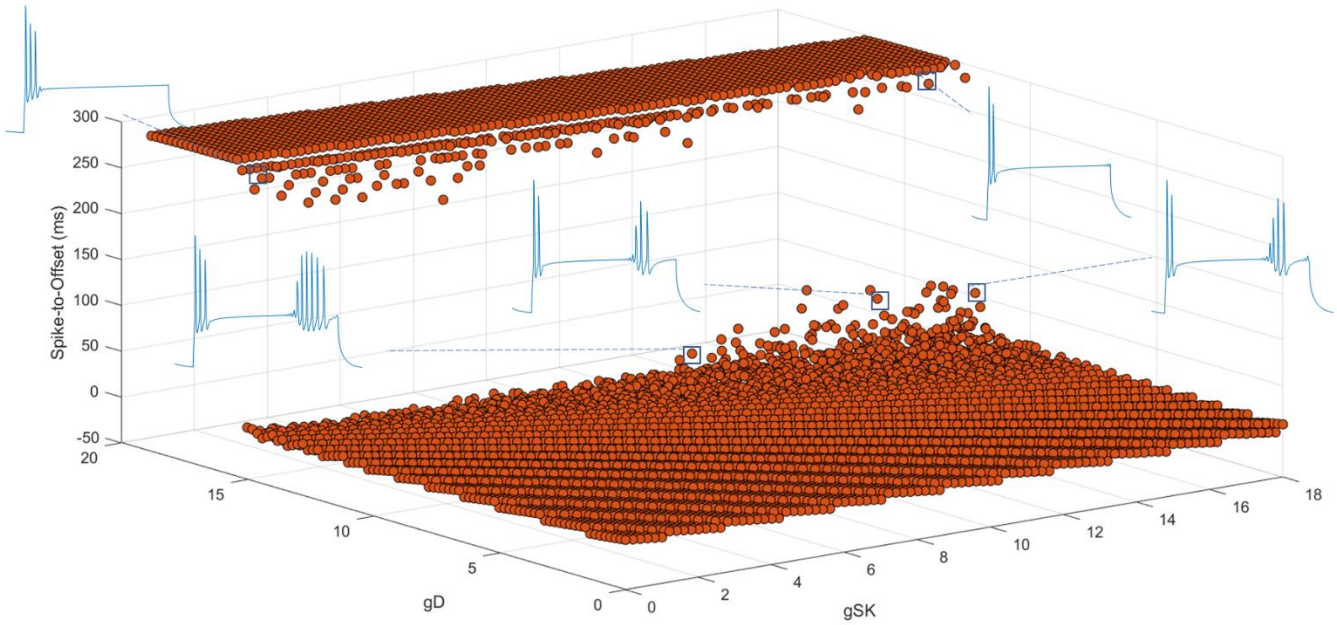

Figure 38: Time duration between last fired action potential and the current offset exhibited by the putative HVC_{RA} models at different densities of somatic g_{SK} and g_D. Inter-burst intervals drawn by the stuttering models are captured for values of g_{SK} and g_D ranging respectively between 0 and 18 nS, and 0 and 20 nS.

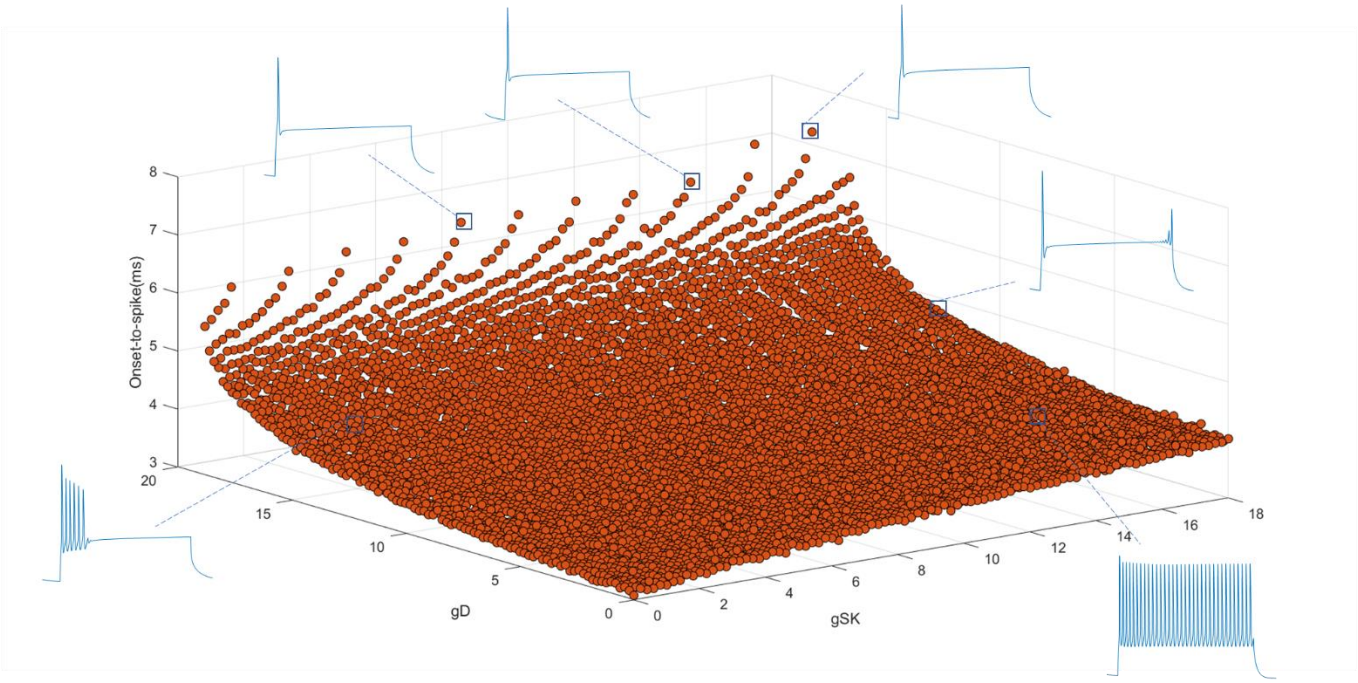

Figure 39: Time duration between last fired action potential and the current offset exhibited by the putative HVCRA models at different densities of somatic g_{SK} and g_D. Inter-burst intervals drawn by the stuttering models are captured for values of g_{SK} and g_D ranging respectively between 0 and 18 nS, and 0 and 20 nS.

3. *Impact of inactivation time constant τ_z and low-threshold D-type current on stuttering firing patterns*

Since I_D is heavily involved in drawing the stutter firing patterns, we sought to explore the role of I_D dynamics in influencing the stutter firing pattern by monitoring the interaction between the conductance g_D and the inactivation time constant τ_z . The latter parameter indicates the time needed for the D-type channel to inactivate during depolarization. In other words, the higher its value, the more time I_D needs to shut down. The corresponding values of τ_z and g_D were iteratively varied respectively between 10 msecs and 400 msecs, and 0 and 20 nS. The interaction between g_D and tau z produce several populations of data points the differentiate in their number of bursts (**Figure 40**). Number of spikes especially the ones of the second burst were dependent on τ_z (τ_z <100 msecs) (**Figure 41**). In other words, as τ_z is upregulated the number of spikes in the second burst decreases. For the same range of τ_z, delayed firing is noted that is proportional to the increase in g_D (**Figure 42**). A τ_z threshold (τ_z > 1000 msecs) is reported that is responsible in inducing the third burst of the stuttering firing pattern (**Figure 43**). No important trend is reported for the time duration between the last spike and current offset as two separate clusters of datapoints are displayed in parallel with previous simulations (**Figure 44**).

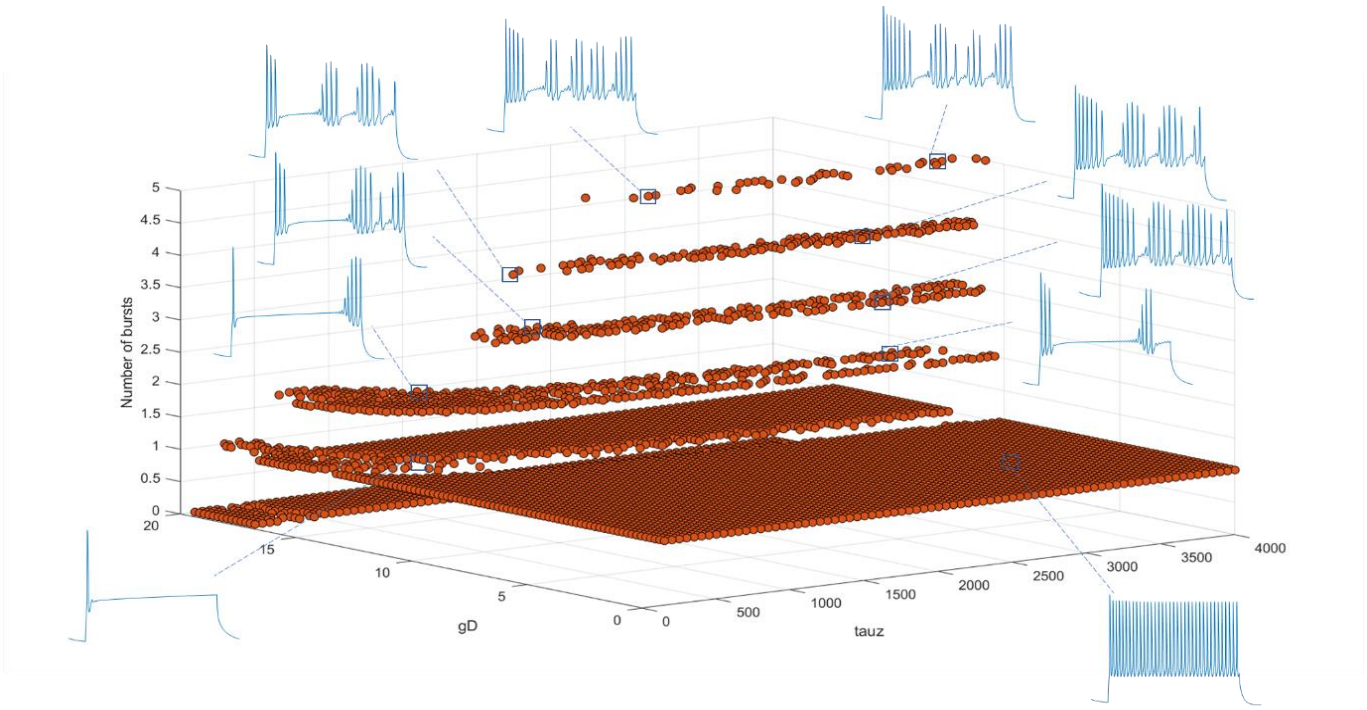

Figure 40: Number of bursts elicited by the putative HVC_{RA} models at different densities of somatic τ_z and g_D. The number of bursts drawn by the stuttering models is captured for values of g_{SK} and g_D ranging respectively between 10 and 4000 msecs, and 0 and 20 nS.

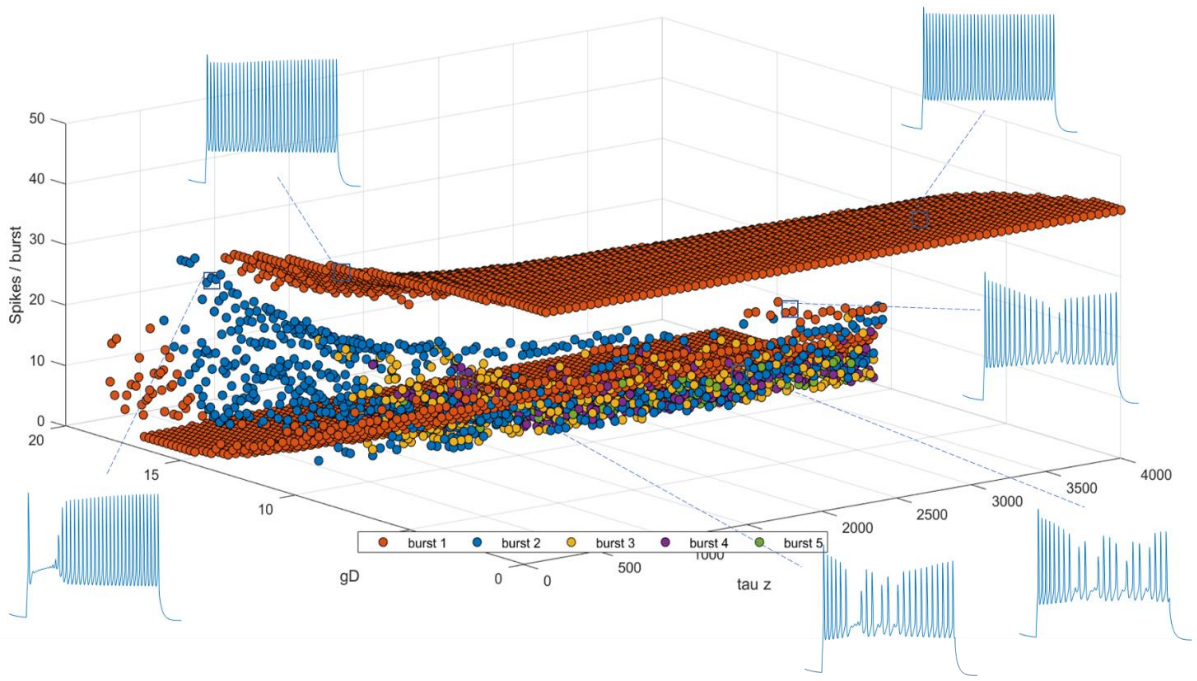

Figure 41: Number of spikes elicited by the putative HVC_{RA} models at different densities of somatic a τ_z and g_D. The number of spikes per burst drawn by the stuttering models is captured for values of τ_z and g_D ranging respectively between 10 and 4000 msecs, and 0 and 20 nS. Color orange corresponds to the values of spikes in the first burst, color blue corresponds to the values of spikes in the second burst, color yellow corresponds to the values of spikes in the third burst, color violet corresponds to the values of spikes in the fourth burst and color green corresponds to the values of spikes in the fifth burst.

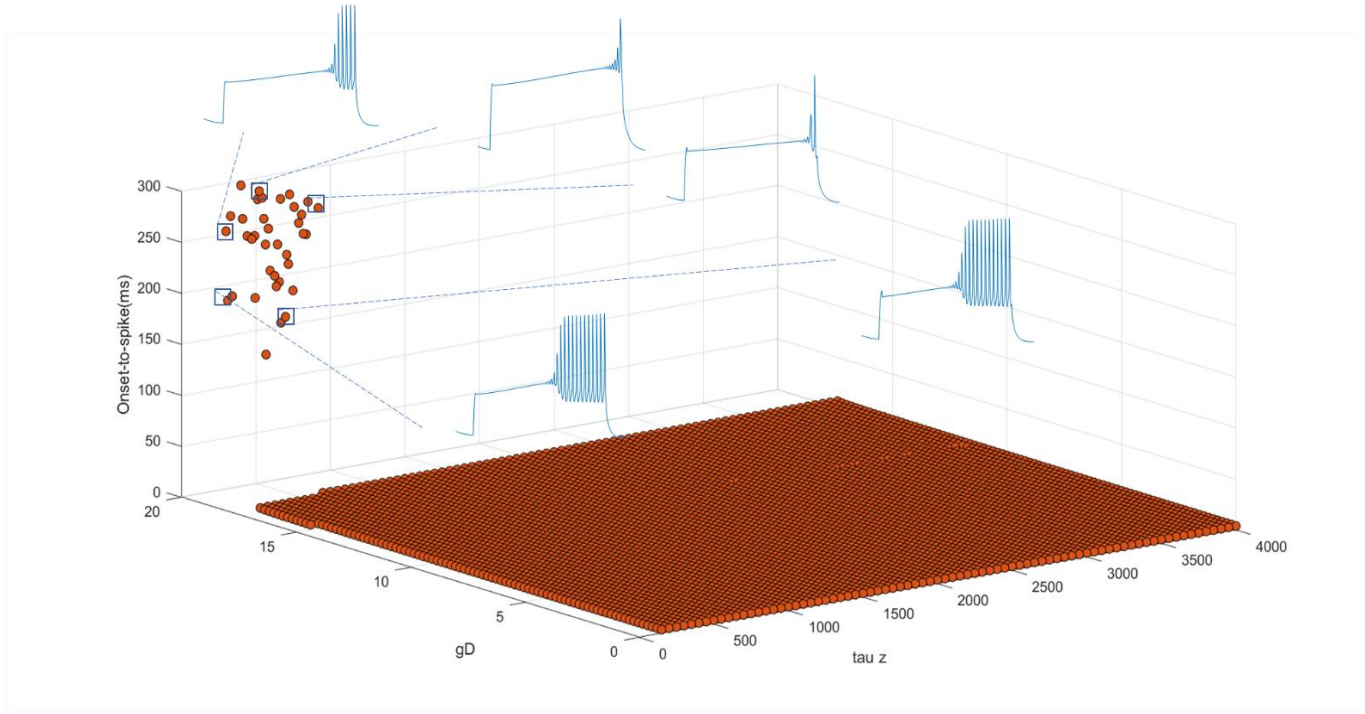

Figure 42: Time duration between current onset and the first fired spike exhibited by the putative HVC_{RA} models at different densities of somatic τ_z and g_D. Inter-burst intervals drawn by the stuttering models are captured for values of τ_z and g_D ranging respectively between 10 and 4000 msecs, and 0 and 20 nS.

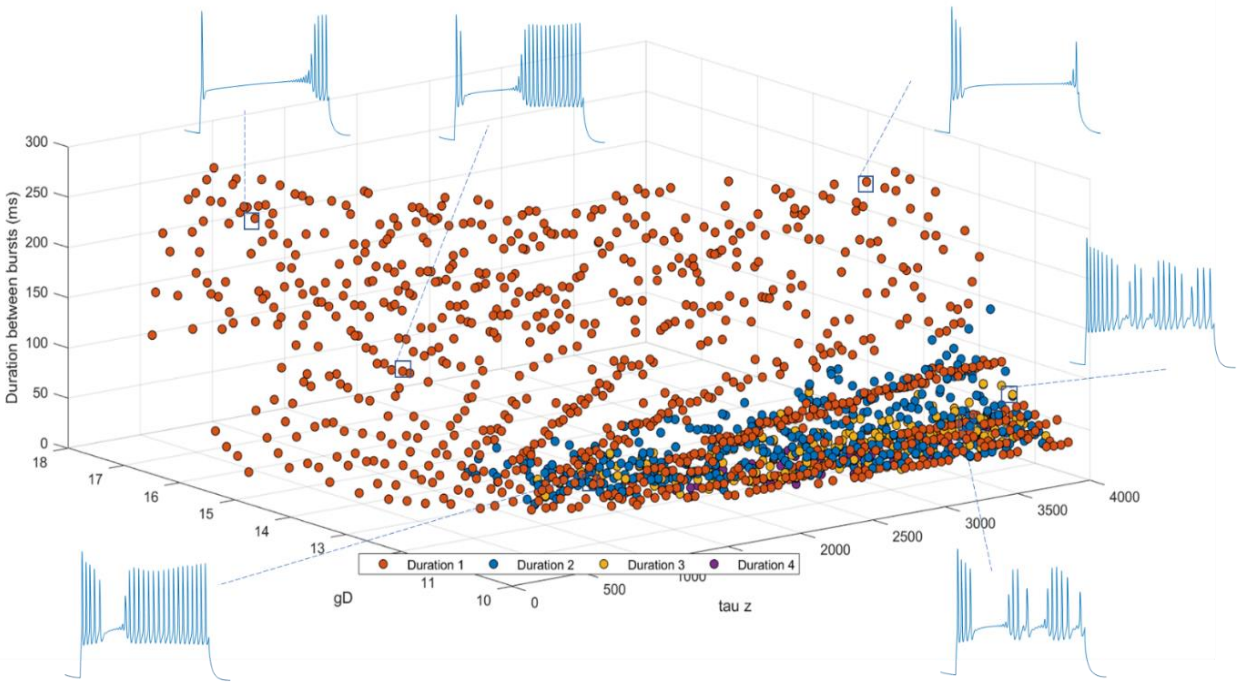

Figure 43: Inter-burst duration elicited by the putative HVC_{RA} models at different densities of somatic τ_z and g_D. Inter-burst intervals shown by the stuttering models is captured for values of τ_z and g_D ranging respectively between 10 and 4000 msecs, and 0 and 20 nS. Color orange corresponds to the first time duration between two successive bursts, color blue corresponds to second time duration between two successive bursts, color yellow corresponds to third time duration between two successive bursts, color violet corresponds to the fourth time duration between two successive bursts.

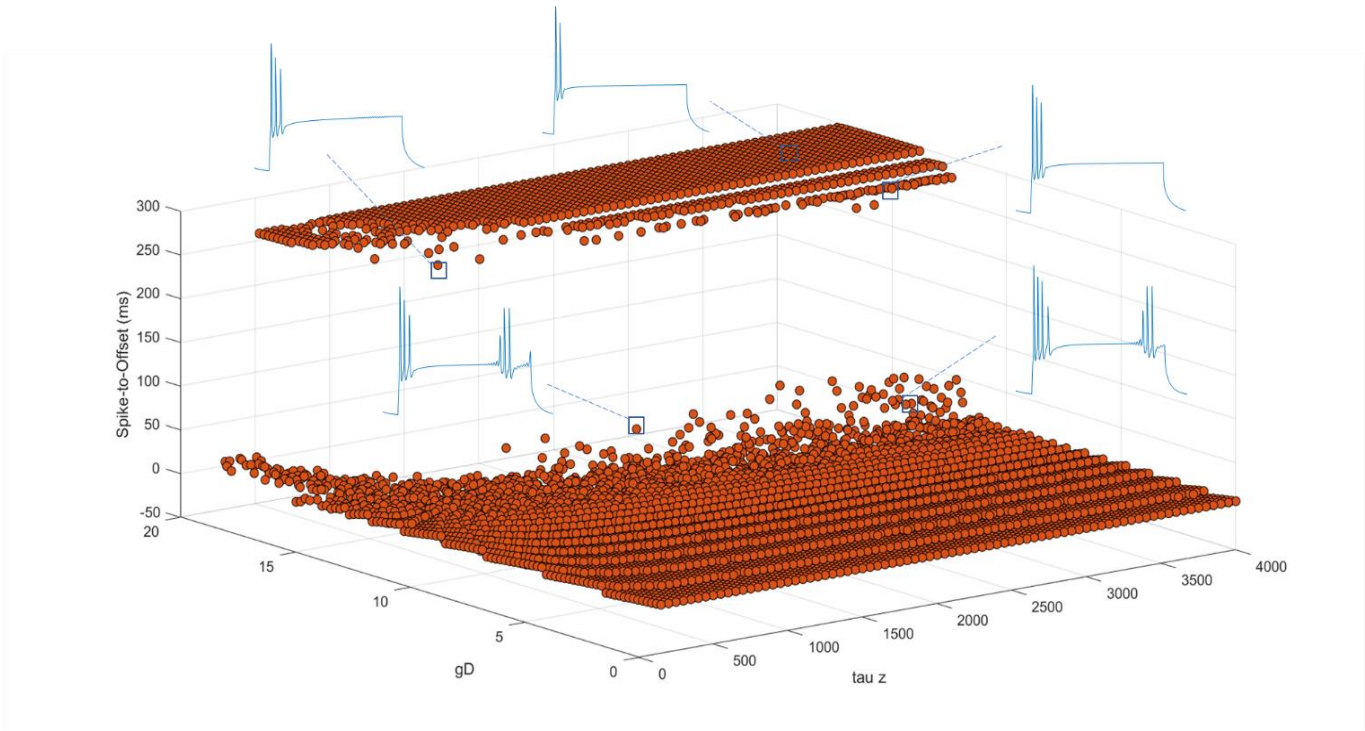

Figure 44: Time duration between last fired action potential and the current offset exhibited by the putative HVC_{RA} models at different densities of somatic τ_z and g_D. Inter-burst intervals drawn by the stuttering models are captured for values of τ_z and g_D ranging respectively between 10 and 4000 msecs, and 0 and 20 nS.

4. Impact of low threshold A-type and D-type potassium currents on stuttering firing patterns

The densities of the conductances – g_{Ad} and g_D – were iteratively varied respectively between 0 nS and 100 nS, and 0 and 20 nS. In parallel with previous simulations, g_{Ad} and g_D generate a datapoints layers with distinct number of bursts. However, this time the first burst holds a low number of spikes (~1 AP) as g_{Ad} increases (**Figures 45-46**). This means that gAd modulates the stuttering firing by dictating the number of spikes in the first burst. Inter-burst intervals are mainly controlled by I_D (**Figure 47**) in parallel with **Figure 37**. While no important trend is reported for the interval between the last spike and offset current (**Figure 48**), a large onset delay was noted for large densities of g_{Ad}. These delays were manipulated by the densities of g_D which triggers a larger prolongment in the duration between the onset and the first spike (**Figure 49**) in parallel with simulations of τ_z (for τ_z <100 msecs) and g_D (**Figure 42**).

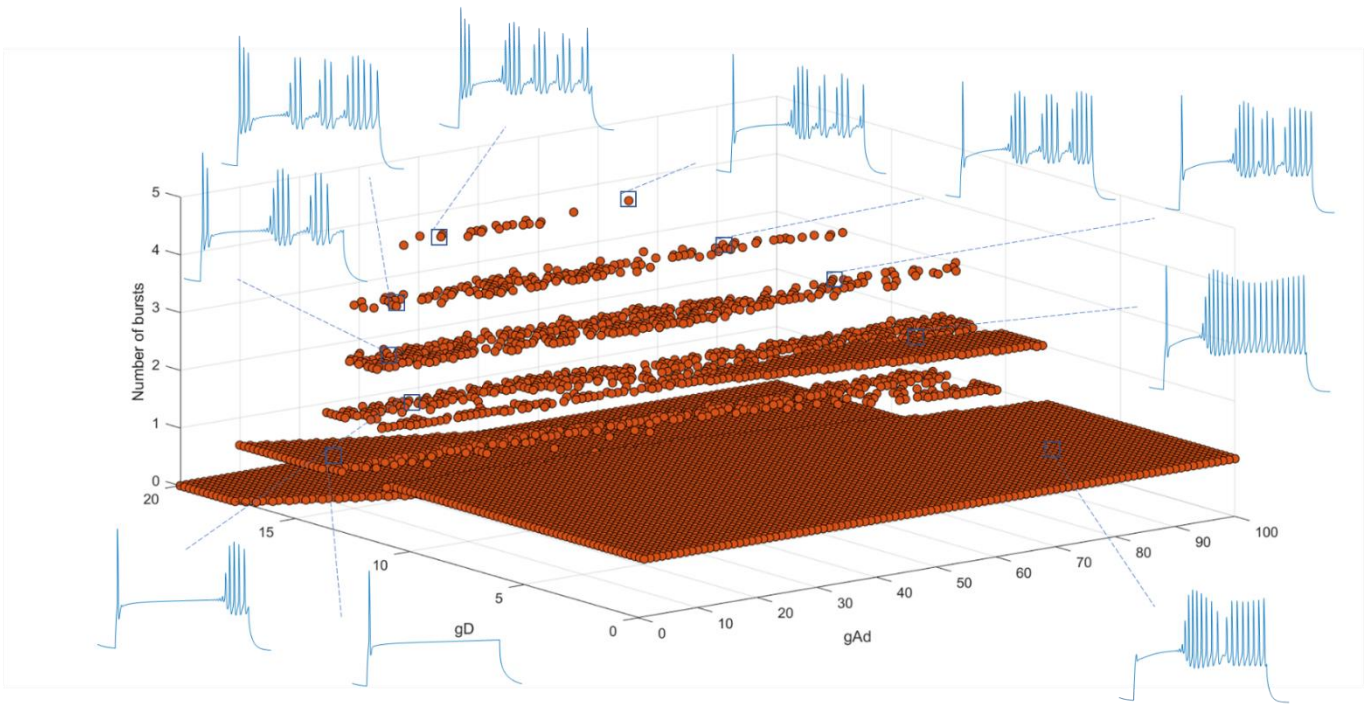

Figure 45: Number of bursts elicited by the putative HVC_{RA} models at different densities of dendritic g_{Ad} and somatic g_D. The number of bursts drawn by the stuttering models is captured for values of g_{Ad} and g_D ranging respectively between 0 and 100 nS, and 0 and 20 nS.

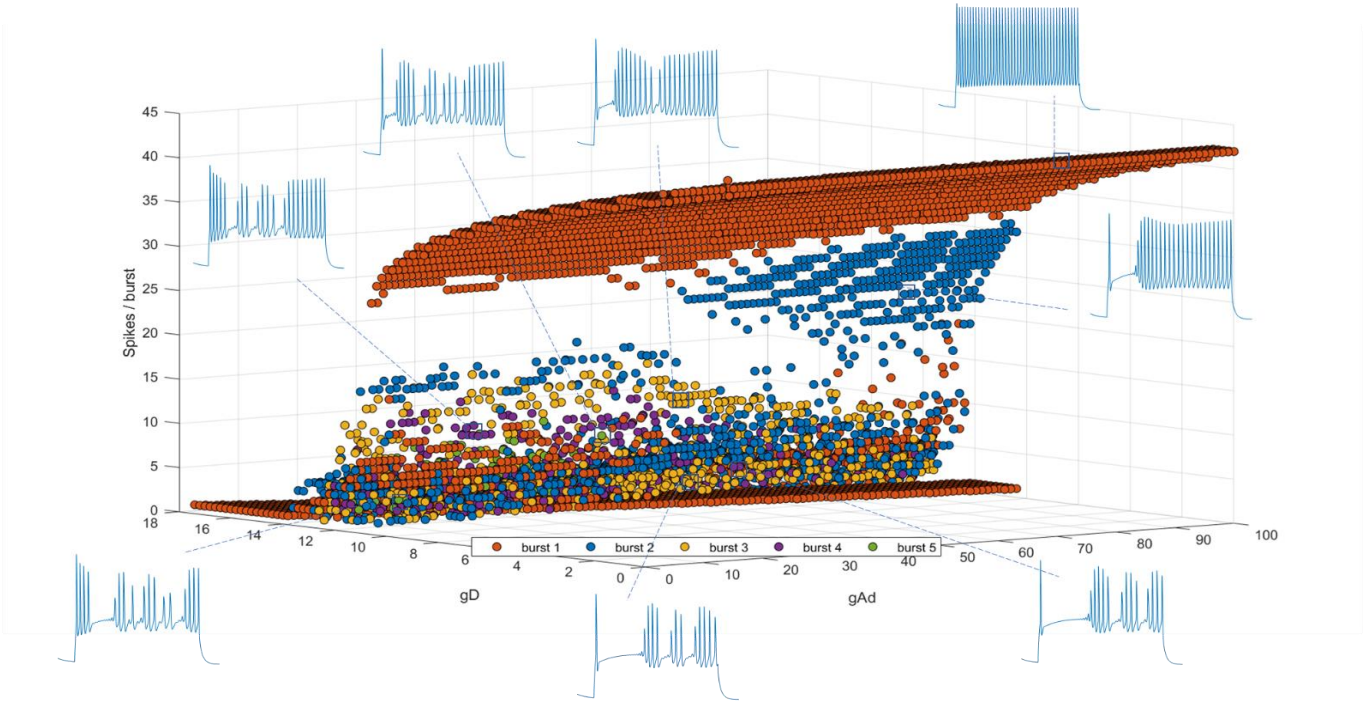

Figure 46: Number of spikes per burst elicited by the putative HVC_{RA} models at different densities of dendritic g_{Ad} and somatic g_D. The number of spikes per burst drawn by the stuttering models is captured for values of g_{Ad} and g_D ranging respectively between 0 and 100 nS, and 0 and 20 nS. Color orange corresponds to the values of spikes in the first burst, color blue corresponds to the values of spikes in the second burst, color yellow corresponds to the values of spikes in the third burst, color violet corresponds to the values of spikes in the fourth burst and color green corresponds to the values of spikes in the fifth burst.

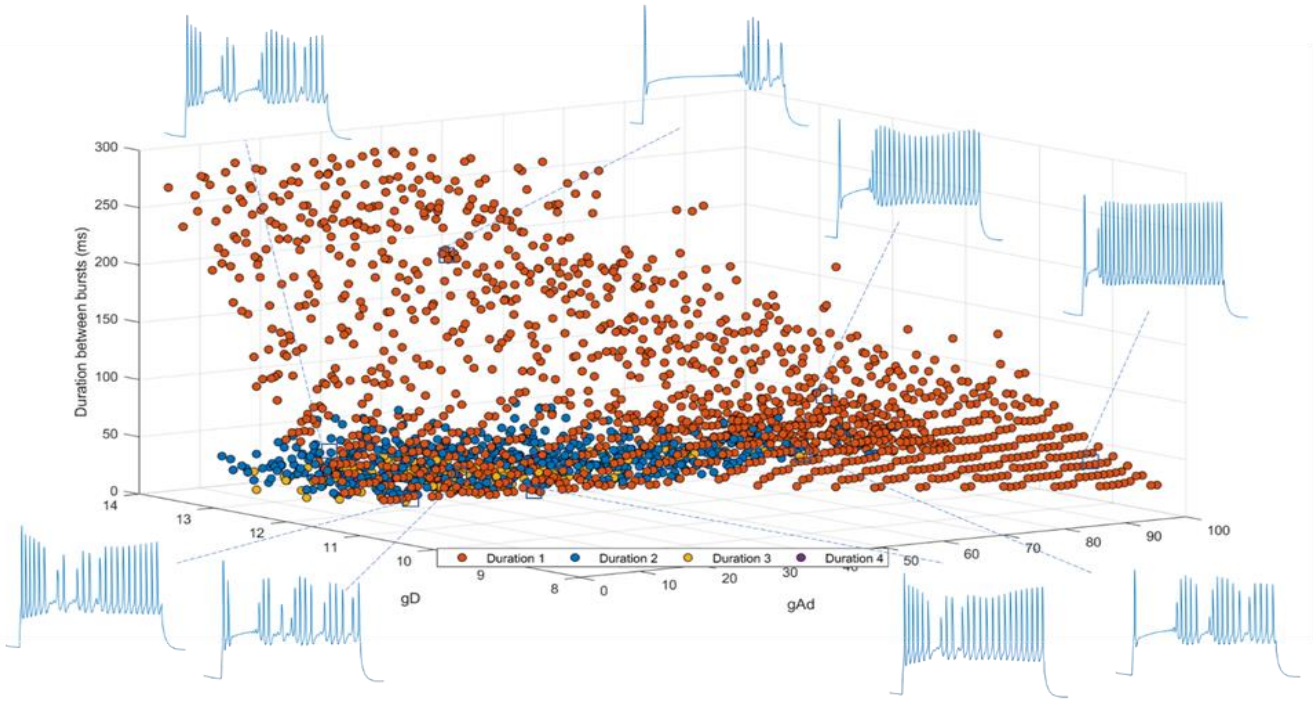

Figure 47: Inter-burst spikes elicited by the putative HVC_{RA} models at different densities of dendritic g_{Ad} and g_D. Inter-burst intervals shown by the stuttering models is captured for values of τ_z and g_D ranging respectively between 10 and 100 nS, and 0 and 20 nS. Color orange corresponds to the first time duration between two successive bursts, color blue corresponds to second time duration between two successive bursts, color yellow corresponds to third time duration between two successive bursts, color violet corresponds to the fourth time duration between two successive bursts.

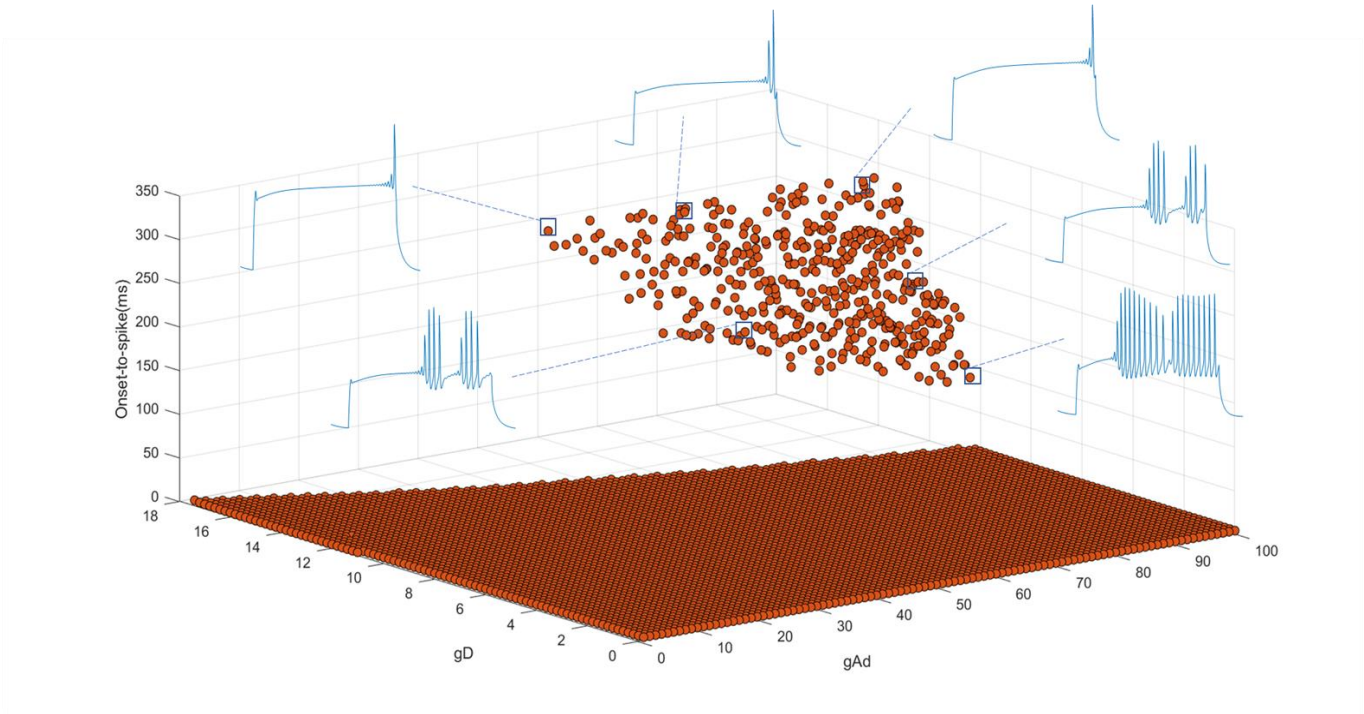

Figure 48: Time duration between last fired action potential and the current offset exhibited by the putative HVC_{RA} models at different densities of dendritic g_{Ad} and somatic g_D. Inter-burst intervals drawn by the stuttering models are captured for values of g_{Ad} and g_D ranging respectively between 0 and 200 nS, and 0 and 20 nS

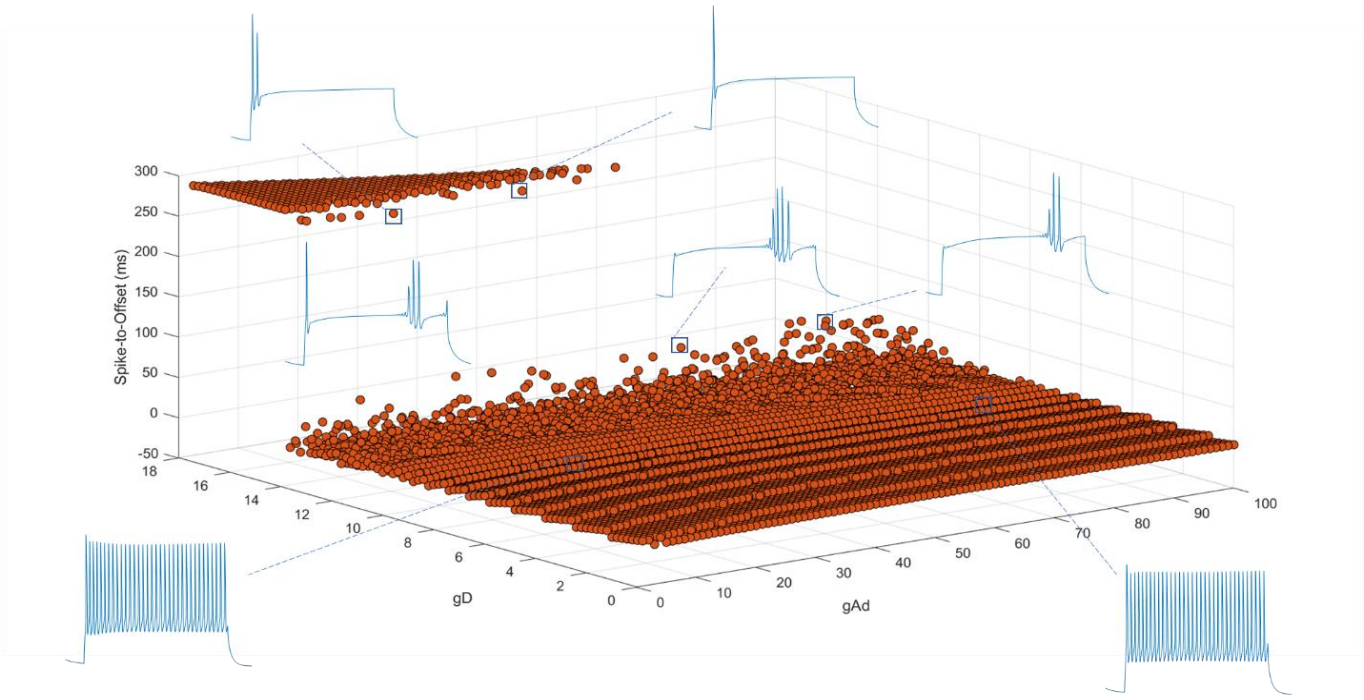

Figure 49: Time duration between the current onset and first fired action potential exhibited by the putative HVC_{RA} models at different densities of dendritic g_{Ad} and somatic g_D. Inter-burst intervals drawn by the stuttering models are captured for values of g_{Ad} and g_D ranging respectively between 0 and 200 nS, and 0 and 20 nS

5. Impact of high threshold calcium L-type current and calcium activated SK current on stuttering firing patterns

The densities of the conductances – g_{CaL} and g_{SK} – were iteratively varied respectively between 0 and 20 nS, and 0 and 18 nS. The interaction between the combinations of these two currents produce semicircle clusters of data points that differ in their number of bursts. It seems as if g_{CaL} coordinate with g_{SK} to conserve the number of bursts (**Figure 50**). In other words, switching the densities of g_{CaL} and g_{SK} provide models with same number of bursts. No notable effect is noted for the fired spikes throughout the bursts as the number of spikes per burst is almost conserved (**Figure 51**). Alternated chaotic datapoints for the inter-burst intervals is produced following the manipulation of g_{CaL} and g_{SK} (**Figure 52**), this suggests the important role of the latter current in controlling time intervals between the bursts. It is worth noting that the interaction between these two currents also determine the offset of firing during depolarization as different contribution of these two parameters result in an alternating timing of offsets (**Figure 53**). Minimal delay on spiking is noted by manipulating the densities of these two conductances (**Figure 54**).

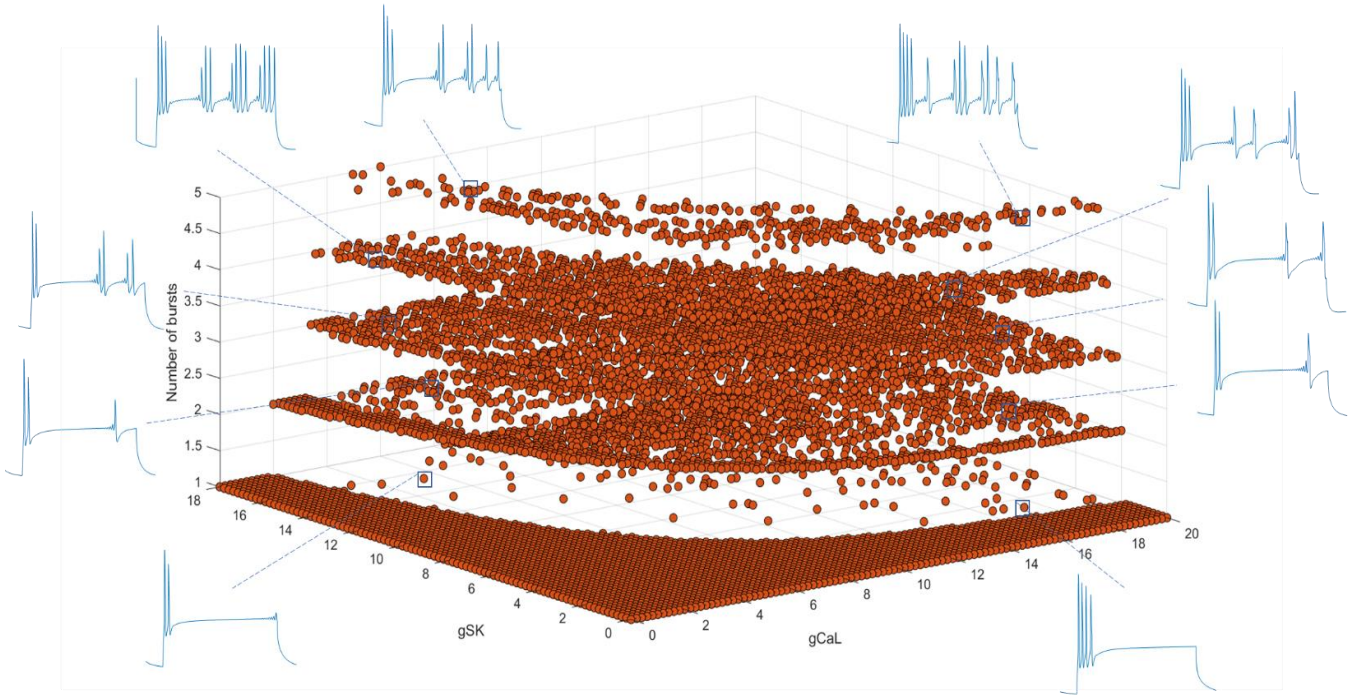

Figure 50: Number of bursts elicited by the putative HVC_{RA} models at different densities of somatic g_{CaL} and g_{SK}. The number of bursts drawn by the stuttering models is captured for values of g_{CaL} and g_{SK} ranging respectively between 0 and 20 nS, and 0 and 18 nS.

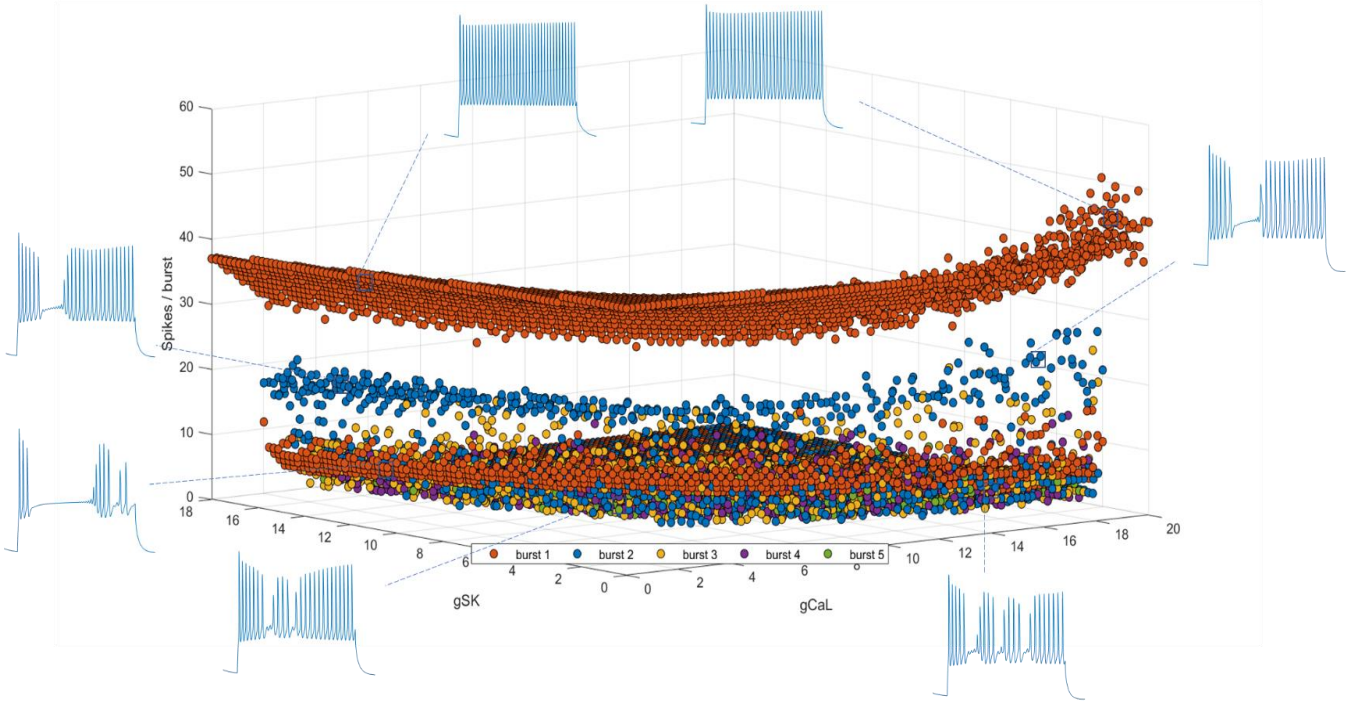

Figure 51: Number of spikes elicited by the putative HVC_{RA} models at different densities of somatic g_{CaL} and g_{SK}. The number of spikes per burst drawn by the stuttering models is captured for values of g_{CaL} and g_{SK} ranging respectively

between 0 and 20 nS, and 0 and 18 nS. Color orange corresponds to the values of spikes in the first burst, color blue corresponds to the values of spikes in the second burst, color yellow corresponds to the values of spikes in the third burst, color violet corresponds to the values of spikes in the fourth burst and color green corresponds to the values of spikes in the fifth burst.

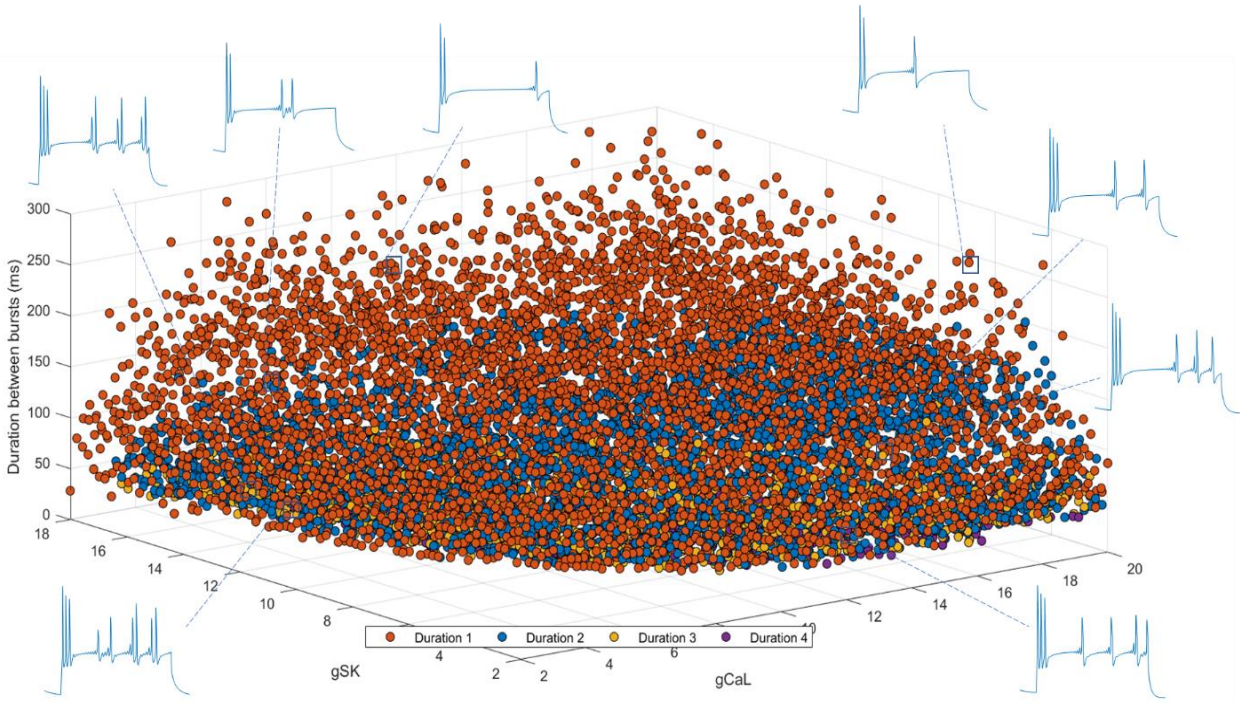

Figure 52: Inter-burst spikes elicited by the putative HVC_{RA} models at different densities of somatic g_{CaL} and g_{SK}. Inter-burst intervals shown by the stuttering models is captured for values of g_{CaL} and g_{SK} ranging respectively between 0 and 20 nS, and 0 and 18 nS. Color orange corresponds to the first time duration between two successive bursts, color blue corresponds to second time duration between two successive bursts, color yellow corresponds to third time duration between two successive bursts, color violet corresponds to the fourth time duration between two successive bursts

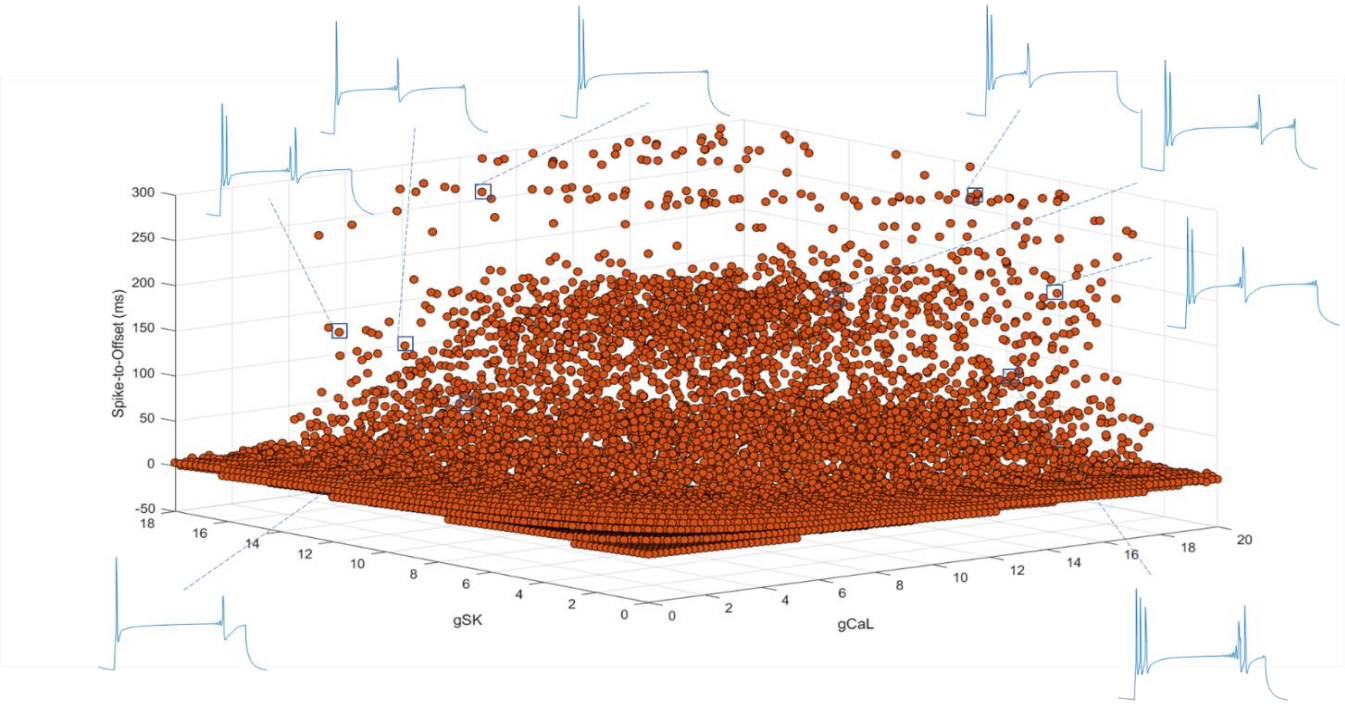

Figure 53: Time duration between last fired action potential and the current offset exhibited by the putative HVC_{RA} models at different densities of somatic g_{CaL} and g_{SK}. Inter-burst intervals drawn by the stuttering models are captured for values of g_{CaL} and g_{SK} ranging respectively between 0 and 20 nS, and 0 and 18 nS

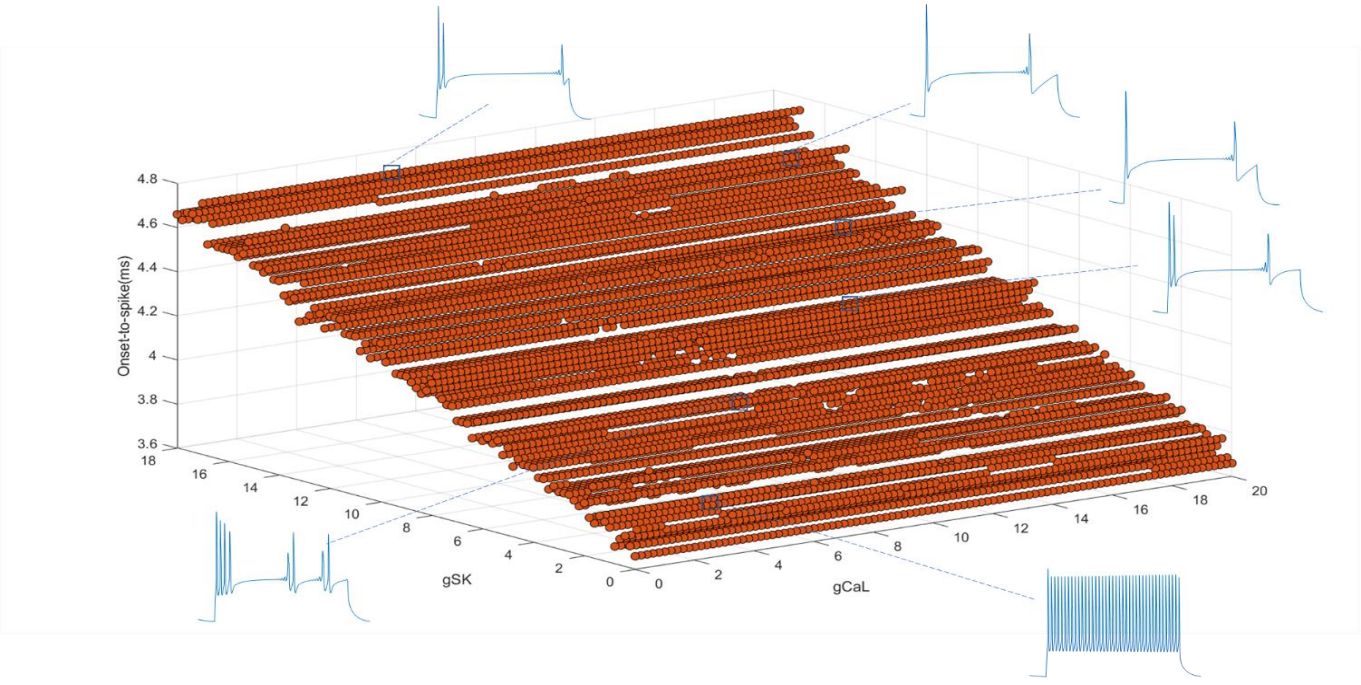

Figure 54: Time duration between current onset and the first fired action potential exhibited by the putative HVC_{RA} models at different densities of somatic g_{CaL} and g_{SK}. Inter-burst intervals drawn by the stuttering models are captured for values of g_{CaL} and g_{SK} ranging respectively between 0 and 20 nS, and 0 and 18 nS

CHAPTER V

DISCUSSION

Throughout this thesis work we aimed to analyze the contribution of different ion channels in shaping the firing patterns of class I, Class II and class III HVC_{RA} neurons. To do that, computational modeling tools were utilized to build HVC_{RA} conductance-based models. These models include a sodium current (I_{Na}), delayed rectifier potassium current (I_{Kdr}), D-type potassium current (I_D), M-type potassium current (I_M), A-type potassium current (I_A), L-type calcium current (I_{CaL}), small-conductance ca current (I_{SK}), leak current (I_{leak}). These currents were distributed inside our two-compartment HVC_{RA} models by following the ion channels distribution in mammalian neurons. In other words, the dendritic compartment includes: I_{CaL}, I_{SK} and I_{leak} , while the somatic compartment consists of I_{Na}, I_{Kdr}, I_D, I_M, I_{CaL}, I_{SK} and $I_{leak.}$

To achieve the aims behind this study, two approaches are adopted. The first aim consists of building HVC_{RA} models that simulates the firing behavior seen in HVC brain slices of zebra finches. The firing behavior of class I and class II HVC_{RA} is reproduced using our biophysical models (**Figures 21-24**, **26-27**). The fitting was assessed using the input-output plots that take into consideration the average input current to our models and the output frequency of AP firing (**Figures 25, 28**). The diminished excitability which characterizes class I HVC_{RA} neurons is predominantly dependent on the contributions of I_M and I_D as outward current and I_{Na} as an inward current (**Figure 26**). Morphology of dendritic tree and dendritic ionic currents like I_{CaL} and I_{SK} are also noted to participate in regulating

the firing is these neurons. For class II HVC_{RA} neurons, somatic potassium ion currents – I_{Kdr}, I_D and I_{SK} – are determinants of the tonic firing behavior recorded experimentally in HVC brain slices (**Figure 29**). Along these ion channels, coupling strength is also an important component to form the various tonic firing patterns.

The second modeling approach explores the roles of different ion channels in drawing the stuttering firing behavior of putative Class III HVC_{RA} neurons. This approach examines the effects of iteratively manipulating the densities of ion channels on the stuttering firing features (number of bursts, number of spikes per burst, interburst intervals, first-spike-to-offset interval, and onset-to-first spike interval). Somatic I_M was responsible for dampening the stuttering activity by reducing number of bursts and the number of spikes fired in each burst (**Figures 30-32**). Dendritic I_A regulates the firing of spikes in the initial burst (**Figure 46**) along with the timing of the start AP firing with the cooperation of I_D (**Figure 48**). In parallel with $I_{A,}$ the latter timing is also controlled by the interaction of I_D with the inactivation time constant tau z (**Figure 42**). This is completely rational since I_D that has low inactivation time constant is no longer slowly inactivating and resemble in its kinetics a fast inactivated $I_{A.}$ Somatic I_{CaL} and I_{SK} interact with one another to control the timing of the last fired spike of an HVC_{RA} model and inter-burst duration in a nonlinear chaotic direction. (**Figure 51**).

Despite the modeling achievements procured in this study, it is worth mentioning that this study is limited to the fitting of somatic recordings of HVC_{RA} neurons. In other words, our study did not consider the fitting of voltage traces recorded in the dendritic tree. Monitoring the fit of dendritic voltage traces ensure a proper biophysical fit of HVC_{RA}

neurons. Another limitation of this study is not expanding the model to include h-type current ($I_{h)}$ knowing that its density is condired low in HVC_{RA} neurons (Daou et al., 2013). The absence of I_h in neurons was reportedly noted to trigger unusual interrupted firing in neocortical neurons of rats (Markram et al., 2004). Concerning the localization of channels, adopting a mammalian neuron distribution of ion channels does not necessarily reflect the true localization of ions channels inside HVC_{RA} neuron. Further histochemical and electrophysiological experimental tests should be performed to ensure the exact locations of the various ion channels. At the computational level, our study lacks the kinetic customization of mathematical equations of sodium, potassium and calcium currents. Customizing the equations of these ionic currents would improve the efficacy of our models and facilitate the fitting procedure of HVC_{RA} voltages traces.

CHAPTER VI

CONCLUSION

Electric properties of neurons are the result of intrinsic and synaptic properties of neurons. In the presence of synaptic blockers, intrinsic properties of a neuron are coordinated by ion channels residing on the membrane of the cell. These ion channels shape electro-physiologically the firing patterns of neurons that could take the shape, for instance, of tonic, phasic and stuttering in case of HVC_{RA} neurons. Our two-compartments HVC_{RA} closely replicate the firing behaviors seen in-vitro. Mammalian distribution of ion channels was demonstrated to be efficacious when dealing with a certain type of neurons with unknown localization of ion channels. Although numerous modeling studies attempted to understand the intrinsic properties behind the firing behavior of HVC_{RA} (Daou et al., 2013; Jin et al., 2007; Long et al., 2010; Ross et al., 2017), this is the first study to examine both the somatic and dendritic repertoires behind the unique HVC_{RA} firings. It brings us one step closer towards comprehending the micro agents that could potentially affect the neural network at the macro level. This study serves as a modeling reference that clarifies the contribution of ion channels in dictating the intrinsic properties of neurons with stuttering firing patterns. It is debatable if intrinsic properties of HVC neurons are dictated only by behavioral plasticity (Daou & Margoliash, 2020) or by developmental maturity (Okaty et al., 2009). Further studies are needed to confirm if intrinsic properties in HVC_{RA} are the result of one of these phenomena or both.

REFERENCES

Agate, R. J., Grisham, W., Wade, J., Mann, S., Wingfield, J., Schanen, C., … Arnold, A. P. (2003). Neural, not gonadal, origin of brain sex differences in a gynandromorphic finch. *Proceedings of the National Academy of Sciences of the United States of America*, *100*(8), 4873–4878. https://doi.org/10.1073/pnas.0636925100

Akemann, W., & Knöpfel, T. (2006). Interaction of Kv3 Potassium Channels and Resurgent Sodium Current Influences the Rate of Spontaneous Firing of Purkinje Neurons. *The Journal of Neuroscience*, *26*(17), 4602 LP-4612. https://doi.org/10.1523/JNEUROSCI.5204-05.2006

Balu, R., Larimer, P., & Strowbridge, B. W. (2004). Phasic Stimuli Evoke Precisely Timed Spikes in Intermittently Discharging Mitral Cells. *Journal of Neurophysiology*, *92*(2), 743–753. https://doi.org/10.1152/jn.00016.2004

Beatty, J. A., Song, S. C., & Wilson, C. J. (2015). Cell-type-specific resonances shape the responses of striatal neurons to synaptic input. *Journal of Neurophysiology*, *113*(3), 688–700.

Benezra, S. E., Narayanan, R. T., Egger, R., Oberlaender, M., & Long, M. A. (2018). Morphological characterization of HVC projection neurons in the zebra finch (Taeniopygia guttata). *Journal of Comparative Neurology*, *526*(10), 1673–1689. https://doi.org/10.1002/cne.24437

Bracci, E., Centonze, D., Bernardi, G., & Calabresi, P. (2003). Voltage-dependent membrane potential oscillations of rat striatal fast-spiking interneurons. *The Journal of Physiology*, *549*(1), 121–130. https://doi.org/https://doi.org/10.1113/jphysiol.2003.040857

Brainard, M. S., & Doupe, A. J. (2002). What songbirds teach us about learning. *Nature*, *417*(6886), 351–358. https://doi.org/10.1038/417351a

Brenowitz, E. A. (1991). Altered perception of species-specific song by female birds after lesions of a forebrain nucleus. *Science*, *251*(4991), 303–305.

Chammas, M., & Daou, A. (2020). UNVEILING THE NEURAL NETWORK UNDERLYING THE GENERATION OF NEURAL SEQUENCES IN THE HVC THROUGH COMPUTATIONAL MODELING.

Chen, A. N., & Meliza, C. D. (2018). Phasic and tonic cell types in the zebra finch auditory caudal mesopallium. *Journal of Neurophysiology*, *119*(3), 1127–1139.

Crowe, D. A., Zarco, W., Bartolo, R., & Merchant, H. (2014). Dynamic representation of the temporal and sequential structure of rhythmic movements in the primate medial premotor cortex. *Journal of Neuroscience*, *34*(36), 11972–11983. https://doi.org/10.1523/JNEUROSCI.2177-14.2014

Daou, A., & Margoliash, D. (2020). Intrinsic neuronal properties represent song and error in zebra finch vocal learning. *Nature Communications*, *11*(1), 1–17. https://doi.org/10.1038/s41467-020-14738-7

Daou, A., Ross, M. T., Johnson, F., Hyson, R. L., & Bertram, R. (2013). Electrophysiological characterization and computational models of HVC neurons in the zebra finch. *Journal of Neurophysiology*, *110*(5), 1227–1245. https://doi.org/10.1152/jn.00162.2013

Deardorff, A. S., Romer, S. H., & Fyffe, R. E. W. (2021). Location, location, location: the organization and roles of potassium channels in mammalian motoneurons. *The Journal of Physiology*, *599*(5), 1391–1420.

Derégnaucourt, S., Mitra, P. P., Fehér, O., Maul, K. K., Lints, T. J., & Tchernichovski, O. (2004). Song development: In search of the error-signal. *Annals of the New York Academy of Sciences*, *1016*, 364–376. https://doi.org/10.1196/annals.1298.036

Doupe, A. J., & Kuhl, P. K. (1999). Birdsong and human speech: Common themes and mechanisms. *Annual Review of Neuroscience*, *22*, 567–631. https://doi.org/10.1146/annurev.neuro.22.1.567

Doupe, A. J., Perkel, D. J., Reiner, A., & Stern, E. A. (2005). Birdbrains could teach basal ganglia research a new song. *Trends in Neurosciences*, *28*(7), 353–363. https://doi.org/10.1016/j.tins.2005.05.005

Dutar, P., Vu, H. M., & Perkel, D. J. (1998). Multiple cell types distinguished by physiological, pharmacological, and anatomic properties in nucleus HVc of the adult zebra finch. *Journal of Neurophysiology*, *80*(4), 1828–1838. https://doi.org/10.1152/jn.1998.80.4.1828

Edelman, G. M., & Gally, J. A. (2001). Degeneracy and complexity in biological systems. *Proceedings of the National Academy of Sciences of the United States of America*, *98*(24), 13763–13768. https://doi.org/10.1073/pnas.231499798

Fee, M. S., Kozhevnikov, A. A., & Hahnloser, R. H. R. (2004). Neural mechanisms of vocal sequence: Generation in the songbird. *Annals of the New York Academy of Sciences*, *1016*, 153–170. https://doi.org/10.1196/annals.1298.022

Fiete, I. R., Senn, W., Wang, C. Z. H., & Hahnloser, R. H. R. (2010). Spike-Time-Dependent Plasticity and Heterosynaptic Competition Organize Networks to Produce Long Scale-Free Sequences of Neural Activity. *Neuron*, *65*(4), 563–576. https://doi.org/10.1016/j.neuron.2010.02.003

Friedrich, S. R., Lovell, P. V., Kaser, T. M., & Mello, C. V. (2019). Exploring the molecular basis of neuronal excitability in a vocal learner. *BMC Genomics*, *20*(1), 1–26. https://doi.org/10.1186/s12864-019-5871-2

Fuentealba, P., Klausberger, T., Karayannis, T., Suen, W. Y., Huck, J., Tomioka, R., … Somogyi, P. (2010). Expression of COUP-TFII Nuclear Receptor in Restricted

GABAergic Neuronal Populations in the Adult Rat Hippocampus. *The Journal of Neuroscience*, *30*(5), 1595 LP-1609. https://doi.org/10.1523/JNEUROSCI.4199-09.2010

Fujimoto, H., Hasegawa, T., & Watanabe, D. (2011). Neural coding of syntactic structure in learned vocalizations in the songbird. *Journal of Neuroscience*, *31*(27), 10023–10033.

Gentner, T. Q., & Margoliash, D. (2003). Neuronal populations and single cells representing learned auditory objects. *Nature*, *424*(6949), 669–674. https://doi.org/10.1038/nature01731

Gibb, L., Gentner, T. Q., & Abarbanel, H. D. I. (2009a). Inhibition and recurrent excitation in a computational model of sparse bursting in song nucleus HVC. *Journal of Neurophysiology*, *102*(3), 1748–1762. https://doi.org/10.1152/jn.00670.2007

Gibb, L., Gentner, T. Q., & Abarbanel, H. D. I. (2009b). Inhibition and recurrent excitation in a computational model of sparse bursting in song nucleus HVC. *Journal of Neurophysiology*, *102*(3), 1748–1762.

Goldberg, E. M., Clark, B. D., Zagha, E., Nahmani, M., Erisir, A., & Rudy, B. (2008). K+ Channels at the Axon Initial Segment Dampen Near-Threshold Excitability of Neocortical Fast-Spiking GABAergic Interneurons. *Neuron*, *58*(3), 387–400. https://doi.org/https://doi.org/10.1016/j.neuron.2008.03.003

Golomb, D., Donner, K., Shacham, L., Shlosberg, D., Amitai, Y., & Hansel, D. (2007). Mechanisms of Firing Patterns in Fast-Spiking Cortical Interneurons. *PLOS Computational Biology*, *3*(8), e156. Retrieved from https://doi.org/10.1371/journal.pcbi.0030156

Gu, N., Vervaeke, K., Hu, H., & Storm, J. F. (2005). Kv7/KCNQ/M and HCN/h, but not KCa2/SK channels, contribute to the somatic medium after-hyperpolarization and excitability control in CA1 hippocampal pyramidal cells. *Journal of Physiology*, *566*(3), 689–715. https://doi.org/10.1113/jphysiol.2005.086835

Hahnloser, R. H. R., Kozhevnikov, A. A., & Fee, M. S. (2003). Erratum: An ultra-sparse code underlies the generation of neural sequences in a songbird (Nature (2022) 419 (65-70)). *Nature*, *421*(6920), 294. https://doi.org/10.1038/nature01221

Halle, F., Gahr, M., & Kreutzer, M. (2003). Effects of unilateral lesions of HVC on song patterns of male domesticated canaries. *Journal of Neurobiology*, *56*(4), 303–314. https://doi.org/10.1002/neu.10230

Harden, S. W., & Frazier, C. J. (2016). Oxytocin depolarizes fast-spiking hilar interneurons and induces GABA release onto mossy cells of the rat dentate gyrus. *Hippocampus*, *26*(9), 1124–1139. https://doi.org/https://doi.org/10.1002/hipo.22595

Harvey, C. D., Coen, P., & Tank, D. W. (2012). Choice-specific sequences in parietal cortex during a virtual-navigation decision task. *Nature*, *484*(7392), 62–68.

https://doi.org/10.1038/nature10918

Helm, J., Akgul, G., & Wollmuth, L. P. (2012). Subgroups of parvalbumin-expressing interneurons in layers 2/3 of the visual cortex. *Journal of Neurophysiology*, *109*(6), 1600–1613. https://doi.org/10.1152/jn.00782.2012

HODGKIN, A. L., & HUXLEY, A. F. (1952). A quantitative description of membrane current and its application to conduction and excitation in nerve. *The Journal of Physiology*, *117*(4), 500–544. https://doi.org/10.1113/jphysiol.1952.sp004764

Huang, Z., Khaled, H. G., Kirschmann, M., Gobes, S. M. H., & Hahnloser, R. H. R. (2018). Excitatory and inhibitory synapse reorganization immediately after critical sensory experience in a vocal learner. *eLife*, *7*, 1–23. https://doi.org/10.7554/eLife.37571

Jagger, D. J., & Housley, G. D. (2002). A-type potassium currents dominate repolarisation of neonatal rat primary auditory neurones in situ. *Neuroscience*, *109*(1), 169–182. https://doi.org/https://doi.org/10.1016/S0306-4522(01)00454-7

Jin, D. Z., Ramazanoğlu, F. M., & Seung, H. S. (2007). Intrinsic bursting enhances the robustness of a neural network model of sequence generation by avian brain area HVC. *Journal of Computational Neuroscience*, *23*(3), 283–299. https://doi.org/10.1007/s10827-007-0032-z

Jones, L. M., Fontanini, A., Sadacca, B. F., Miller, P., & Katz, D. B. (2007). Natural stimuli evoke dynamic sequences of states in sensory cortical ensembles. *Proceedings of the National Academy of Sciences of the United States of America*, *104*(47), 18772–18777. https://doi.org/10.1073/pnas.0705546104

Kadakia, N., Armstrong, E., Breen, D., Morone, U., Daou, A., Margoliash, D., & Abarbanel, H. D. I. (2016). Nonlinear statistical data assimilation for HVC RA neurons in the avian song system. *Biological Cybernetics*, *110*(6), 417–434. https://doi.org/10.1007/s00422-016-0697-3

Katlowitz, K. A., Picardo, M. A., & Long, M. A. (2018). Stable Sequential Activity Underlying the Maintenance of a Precisely Executed Skilled Behavior. *Neuron*, *98*(6), 1133–1140.e3. https://doi.org/10.1016/j.neuron.2018.05.017

Kawaguchi, Y. (1993). Physiological, morphological, and histochemical characterization of three classes of interneurons in rat neostriatum. *Journal of Neuroscience*, *13*(11), 4908–4923.

Konishi, M. (1985). Birdsong: From behavior to neuron. *Annual Review of Neuroscience*, *VOL. 8*, 125–170. https://doi.org/10.1146/annurev.neuro.8.1.125

Kornfeld, J., Benezra, S. E., Narayanan, R. T., Svara, F., Egger, R., Oberlaender, M., … Long, M. A. (2017). EM connectomics reveals axonal target variation in a sequence-generating network. *eLife*, *6*, 1–20. https://doi.org/10.7554/eLife.24364

Kosche, G., Vallentin, D., & Long, M. A. (2015). Interplay of inhibition and excitation shapes a premotor neural sequence. *Journal of Neuroscience*, *35*(3), 1217–1227.

Kozhevnikov, A. A., & Fee, M. S. (2007). Singing-related activity of identified HVC neurons in the zebra finch. *Journal of Neurophysiology*, *97*(6), 4271–4283.

Kubota, M., & Saito, N. (1991). Sodium- and calcium-dependent conductances of neurones in the zebra finch hyperstriatum ventrale pars caudale in vitro. *The Journal of Physiology*, *440*(1), 131–142. https://doi.org/https://doi.org/10.1113/jphysiol.1991.sp018700

Kubota, M., & Taniguchi, I. (1998). Electrophysiological characteristics of classes of neuron in the HVc of the zebra finch. *Journal of Neurophysiology*, *80*(2), 914–923. https://doi.org/10.1152/jn.1998.80.2.914

Kushner, J. K., Hoffman, P. B., Brzezinski, C., Huntsman, M. M., & Alexander, A. L. (2022). Characterizing the diversity of L2/3 human neocortical neurons in epilepsy. *bioRxiv*, 2022.06.13.495678. https://doi.org/10.1101/2022.06.13.495678

La Camera, G., Rauch, A., Thurbon, D., Lüscher, H.-R., Senn, W., & Fusi, S. (2006). Multiple Time Scales of Temporal Response in Pyramidal and Fast Spiking Cortical Neurons. *Journal of Neurophysiology*, *96*(6), 3448–3464. https://doi.org/10.1152/jn.00453.2006

Lai, H. C., & Jan, L. Y. (2006). The distribution and targeting of neuronal voltage-gated ion channels. *Nature Reviews Neuroscience*, *7*(7), 548–562.

Lien, C.-C., & Jonas, P. (2003). Kv3 Potassium Conductance is Necessary and Kinetically Optimized for High-Frequency Action Potential Generation in Hippocampal Interneurons. *The Journal of Neuroscience*, *23*(6), 2058 LP-2068. https://doi.org/10.1523/JNEUROSCI.23-06-02058.2003

Llinás, R. R. (2014). Intrinsic electrical properties of mammalian neurons and CNS function: A historical perspective. *Frontiers in Cellular Neuroscience*, *8*(November), 1–14. https://doi.org/10.3389/fncel.2014.00320

Long, M. A., & Fee, M. S. (2008). Using temperature to analyse temporal dynamics in the songbird motor pathway. *Nature*, *456*(7219), 189–194. https://doi.org/10.1038/nature07448

Long, M. A., Jin, D. Z., & Fee, M. S. (2010). Support for a synaptic chain model of neuronal sequence generation. *Nature*, *468*(7322), 394–399. https://doi.org/10.1038/nature09514

Lovell, P. V., Carleton, J. B., & Mello, C. V. (2013). Genomics analysis of potassium channel genes in songbirds reveals molecular specializations of brain circuits for the maintenance and production of learned vocalizations. *BMC Genomics*, *14*(1). https://doi.org/10.1186/1471-2164-14-470

Lynch, G. F., Okubo, T. S., Hanuschkin, A., Hahnloser, R. H. R., & Fee, M. S. (2016). Rhythmic continuous-time coding in the songbird analog of vocal motor cortex. *Neuron*, *90*(4), 877–892.

MacDonald, C. J., Lepage, K. Q., Eden, U. T., & Eichenbaum, H. (2011). Hippocampal "time cells" bridge the gap in memory for discontiguous events. *Neuron*, *71*(4), 737–749. https://doi.org/10.1016/j.neuron.2011.07.012

Marder, E., & Taylor, A. L. (2011). Multiple models to capture the variability in biological neurons and networks. *Nature Neuroscience*, *14*(2), 133–138. https://doi.org/10.1038/nn.2735

Margoliash, D., & Schmidt, M. F. (2010). Sleep, off-line processing, and vocal learning. *Brain and Language*, *115*(1), 45–58. https://doi.org/10.1016/j.bandl.2009.09.005

Markram, H. (2000). Organizing Principles for a Diversity of GABAergic Interneurons and Synapses in the Neocortex. *Science (American Association for the Advancement of Science)*. WASHINGTON: American Society for the Advancement of Science. https://doi.org/10.1126/science.287.5451.273

Markram, H., Toledo-Rodriguez, M., Wang, Y., Gupta, A., Silberberg, G., & Wu, C. (2004). Interneurons of the neocortical inhibitory system. *Nature Reviews Neuroscience*, *5*(10), 793–807. https://doi.org/10.1038/nrn1519

Martina, M., Schultz, J. H., Ehmke, H., Monyer, H., & Jonas, P. (1998). Functional and Molecular Differences between Voltage-Gated K⁺ Channels of Fast-Spiking Interneurons and Pyramidal Neurons of Rat Hippocampus. *The Journal of Neuroscience*, *18*(20), 8111 LP-8125. https://doi.org/10.1523/JNEUROSCI.18-20-08111.1998

Meliza, C. D., Kostuk, M., Huang, H., Nogaret, A., Margoliash, D., & Abarbanel, H. D. I. (2014). Estimating parameters and predicting membrane voltages with conductance-based neuron models. *Biological Cybernetics*, *108*(4), 495–516. https://doi.org/10.1007/s00422-014-0615-5

Molineux, M. L., Fernandez, F. R., Mehaffey, W. H., & Turner, R. W. (2005). A-type and T-type currents interact to produce a novel spike latency-voltage relationship in cerebellar stellate cells. *Journal of Neuroscience*, *25*(47), 10863–10873.

Mooney, R. (2000). Different subthreshold mechanisms underlie song selectivity in identfile:///C:/Users/Mounir Arab/Desktop/Neuroscience/The HVC Microcircuit The Synaptic Basis for Interactions between song motor and vocal plasticity pathways (Mooney 2005).pdfified HVc neur. *Journal of Neuroscience*, *20*(14), 5420–5436. https://doi.org/10.1523/jneurosci.20-14-05420.2000

Mooney, R., Hoese, W., & Nowicki, S. (2001). Auditory representation of the vocal repertoire in a songbird with multiple song types. *Proceedings of the National Academy of Sciences of the United States of America*, *98*(22), 12778–12783. https://doi.org/10.1073/pnas.221453298

Mooney, R., & Prather, J. F. (2005). The HVC microcircuit: The synaptic basis for interactions between song motor and vocal plasticity pathways. *Journal of Neuroscience*, *25*(8), 1952–1964. https://doi.org/10.1523/JNEUROSCI.3726-04.2005

Nogaret, A., Meliza, C. D., Margoliash, D., & Abarbanel, H. D. I. (2016). Automatic Construction of Predictive Neuron Models through Large Scale Assimilation of Electrophysiological Data. *Scientific Reports*, *6*(September), 1–14. https://doi.org/10.1038/srep32749

Nottebohm, F., Stokes, T. M., & Leonard, C. M. (1976). Central control of song in the canary, Serinus canarius. *Journal of Comparative Neurology*, *165*(4), 457–486. https://doi.org/10.1002/cne.901650405

Oberti, D., Kirschmann, M. A., & Hahnloser, R. H. R. (2010). Correlative microscopy of densely labeled projection neurons using neural tracers. *Frontiers in Neuroanatomy*, *4*(JUNE), 1–7. https://doi.org/10.3389/fnana.2010.00024

Okaty, B. W., Miller, M. N., Sugino, K., Hempel, C. M., & Nelson, S. B. (2009). Transcriptional and electrophysiological maturation of neocortical fast-spiking GABAergic interneurons. *Journal of Neuroscience*, *29*(21), 7040–7052.

Okubo, T. S., Mackevicius, E. L., Payne, H. L., Lynch, G. F., & Fee, M. S. (2015). Growth and splitting of neural sequences in songbird vocal development. *Nature*, *528*(7582), 352–357. https://doi.org/10.1038/nature15741

Olah, V. J., Goettemoeller, A. M., Rayaprolu, S., Dammer, E. B., Seyfried, N. T., Rangaraju, S., … Rowan, M. J. M. (2022). Biophysical Kv3 channel alterations dampen excitability of cortical PV interneurons and contribute to network hyperexcitability in early Alzheimer's. *Elife*, *11*, e75316.

Pawelzik, H., Hughes, D. I., & Thomson, A. M. (2002). Physiological and morphological diversity of immunocytochemically defined parvalbumin- and cholecystokinin-positive interneurones in CA1 of the adult rat hippocampus. *Journal of Comparative Neurology*, *443*(4), 346–367. https://doi.org/https://doi.org/10.1002/cne.10118

Pedarzani, P., McCutcheon, J. E., Rogge, G., Jensen, B. S., Christophersen, P., Hougaard, C., … Stocker, M. (2005). Specific enhancement of SK channel activity selectively potentiates the afterhyperpolarizing current IAHP and modulates the firing properties of hippocampal pyramidal neurons. *Journal of Biological Chemistry*, *280*(50), 41404–41411. https://doi.org/10.1074/jbc.M509610200

Peng, Z., Zhang, X. B., Xi, C., Zeng, S. J., Liu, N., Zuo, M. X., & Zhang, X. W. (2012). Changes in ultra-structures and electrophysiological properties in HVC of untutored and deafened Bengalese finches relation to normally reared birds: Implications for song learning. *Brain Research Bulletin*, *89*(5–6), 211–222. https://doi.org/10.1016/j.brainresbull.2012.09.004

Picardo, M. A., Merel, J., Katlowitz, K. A., Vallentin, D., Okobi, D. E., Benezra, S. E., … Long, M. A. (2016). Population-Level Representation of a Temporal Sequence Underlying Song Production in the Zebra Finch. *Neuron*, *90*(4), 866–876. https://doi.org/10.1016/j.neuron.2016.02.016

Porter, J. T., Cauli, B., Staiger, J. F., Lambolez, B., Rossier, J., & Audinat, E. (1998).

Properties of bipolar VIPergic interneurons and their excitation by pyramidal neurons in the rat neocortex. *European Journal of Neuroscience*, *10*(12), 3617–3628.

Povysheva, N. V, Zaitsev, A. V, Rotaru, D. C., Gonzalez-Burgos, G., Lewis, D. A., & Krimer, L. S. (2008). Parvalbumin-positive basket interneurons in monkey and rat prefrontal cortex. *Journal of Neurophysiology*, *100*(4), 2348–2360.

Prather, J. F., Peters, S., Nowicki, S., & Mooney, R. (2008). Precise auditory–vocal mirroring in neurons for learned vocal communication. *Nature*, *451*(7176), 305–310.

Price, C. J., Cauli, B., Kovacs, E. R., Kulik, A., Lambolez, B., Shigemoto, R., & Capogna, M. (2005). Neurogliaform Neurons Form a Novel Inhibitory Network in the Hippocampal CA1 Area. *The Journal of Neuroscience*, *25*(29), 6775 LP-6786. https://doi.org/10.1523/JNEUROSCI.1135-05.2005

Rainnie, D. G., Mania, I., Mascagni, F., & McDonald, A. J. (2006). Physiological and morphological characterization of parvalbumin-containing interneurons of the rat basolateral amygdala. *Journal of Comparative Neurology*, *498*(1), 142–161. https://doi.org/https://doi.org/10.1002/cne.21049

Rama, S., Zbili, M., Fékété, A., Tapia, M., Benitez, M. J., Boumedine, N., … Debanne, D. (2017). The role of axonal Kv1 channels in CA3 pyramidal cell excitability. *Scientific Reports*, *7*(1), 1–12.

Reitich-Stolero, T., & Paz, R. (2019). Affective memory rehearsal with temporal sequences in amygdala neurons. *Nature Neuroscience*, *22*(12), 2050–2059. https://doi.org/10.1038/s41593-019-0542-9

Roberts, T. F., Hisey, E., Tanaka, M., Kearney, M. G., Chattree, G., Yang, C. F., … Mooney, R. (2017). Identification of a motor-to-auditory pathway important for vocal learning. *Nature Neuroscience*, *20*(7), 978–986. https://doi.org/10.1038/nn.4563

Roberts, T. F., Tschida, K. A., Klein, M. E., & Mooney, R. (2010). Rapid spine stabilization and synaptic enhancement at the onset of behavioural learning. *Nature*, *463*(7283), 948–952. https://doi.org/10.1038/nature08759

Rosato-Siri, M. D., Zambello, E., Mutinelli, C., Garbati, N., Benedetti, R., Aldegheri, L., … Large, C. H. (2015). A novel modulator of Kv3 potassium channels regulates the firing of parvalbumin-positive cortical interneurons. *Journal of Pharmacology and Experimental Therapeutics*, *354*(3), 251–260.

Ross, M. T., Flores, D., Bertram, R., Johnson, F., & Hyson, R. L. (2017). Neuronal intrinsic physiology changes during development of a learned behavior. *eNeuro*, *4*(5), 1–16. https://doi.org/10.1523/ENEURO.0297-17.2017

RUDY, B., CHOW, A., LAU, D., AMARILLO, Y., OZAITA, A., SAGANICH, M., … DE Miera, E. V.-S. (1999). Contributions of Kv3 Channels to Neuronal Excitability. *Annals of the New York Academy of Sciences*, *868*(1), 304–343. https://doi.org/https://doi.org/10.1111/j.1749-6632.1999.tb11295.x

Schmidt, M. F., & Perkel, D. J. (1998). Slow synaptic inhibition in nucleus HVc of the adult zebra finch. *Journal of Neuroscience*, *18*(3), 895–904. https://doi.org/10.1523/jneurosci.18-03-00895.1998

Sciamanna, G., & Wilson, C. J. (2011). The ionic mechanism of gamma resonance in rat striatal fast-spiking neurons. *Journal of Neurophysiology*, *106*(6), 2936–2949. https://doi.org/10.1152/jn.00280.2011

Shea, S. D., Koch, H., Baleckaitis, D., Ramirez, J. M., & Margoliash, D. (2010). Neuron-specific cholinergic modulation of a forebrain song control nucleus. *Journal of Neurophysiology*, *103*(2), 733–745. https://doi.org/10.1152/jn.00803.2009

Shibata, R., Nakahira, K., Shibasaki, K., Wakazono, Y., Imoto, K., & Ikenaka, K. (2000). A-type K+ current mediated by the Kv4 channel regulates the generation of action potential in developing cerebellar granule cells. *Journal of Neuroscience*, *20*(11), 4145–4155.

Shima, K., Isoda, M., Mushiake, H., & Tanji, J. (2007). Categorization of behavioural sequences in the prefrontal cortex. *Nature*, *445*(7125), 315–318. https://doi.org/10.1038/nature05470

Shu, Y., Yu, G., Yang, J., & McCormick, D. A. (2007). Selective control of cortical axonal spikes by a slowly inactivating K + current. *Proceedings of the National Academy of Sciences of the United States of America*, *104*(27), 11453–11458. https://doi.org/10.1073/pnas.0702041104

Solis, M. M., & Perkel, D. J. (2005). Rhythmic activity in a forebrain vocal control nucleus in vitro. *Journal of Neuroscience*, *25*(11), 2811–2822. https://doi.org/10.1523/JNEUROSCI.5285-04.2005

Stansfeld, C. E., Marsh, S. J., Halliwell, J. V, & Brown, D. A. (1986). 4-Aminopyridine and dendrotoxin induce repetitive firing in rat visceral sensory neurones by blocking a slowly inactivating outward current. *Neuroscience Letters*, *64*(3), 299–304. https://doi.org/https://doi.org/10.1016/0304-3940(86)90345-9

Stiefel, K. M., Englitz, B., & Sejnowski, T. J. (2013). Origin of intrinsic irregular firing in cortical interneurons. *Proceedings of the National Academy of Sciences*, *110*(19), 7886–7891.

Storm, J. F. (1988). Temporal integration by a slowly inactivating K+ current in hippocampal neurons. *Nature*, *336*(6197), 379–381. https://doi.org/10.1038/336379a0

Sun, Y., Pașca, S. P., Portmann, T., Goold, C., Worringer, K. A., Guan, W., … Chen, Y.-J. J. (2016). A deleterious Nav1. 1 mutation selectively impairs telencephalic inhibitory neurons derived from Dravet Syndrome patients. *Elife*, *5*, e13073.

Szabó, A., Schlett, K., & Szücs, A. (2021). Conventional measures of intrinsic excitability are poor estimators of neuronal activity under realistic synaptic inputs. *PLOS Computational Biology*, *17*(9), e1009378. Retrieved from

https://doi.org/10.1371/journal.pcbi.1009378

Tchernichovski, O., Mitra, P. P., Lints, T., & Nottebohm, F. (2001). Dynamics of the vocal imitation process: How a zebra finch learns its song. *Science*, *291*(5513), 2564–2569. https://doi.org/10.1126/science.1058522

Toledo-Rodriguez, M., Blumenfeld, B., Wu, C., Luo, J., Attali, B., Goodman, P., & Markram, H. (2004). Correlation Maps Allow Neuronal Electrical Properties to be Predicted from Single-cell Gene Expression Profiles in Rat Neocortex. *Cerebral Cortex*, *14*(12), 1310–1327. https://doi.org/10.1093/cercor/bhh092

Vydyanathan, A., Wu, Z.-Z., Chen, S.-R., & Pan, H.-L. (2005). A-Type Voltage-Gated K+ Currents Influence Firing Properties of Isolectin B4-Positive But Not Isolectin B4-Negative Primary Sensory Neurons. *Journal of Neurophysiology*, *93*(6), 3401–3409. https://doi.org/10.1152/jn.01267.2004

Wang, X., Shu, Z., He, Q., Zhang, X., Li, L., Zhang, X., … Guo, F. (2022). Functional autapses form in striatal parvalbumin interneurons but not medium spiny neurons. *bioRxiv*.

Wang, Y., Gupta, A., Toledo-Rodriguez, M., Wu, C. Z., & Markram, H. (2002). Anatomical, physiological, molecular and circuit properties of nest basket cells in the developing somatosensory cortex. *Cerebral Cortex*, *12*(4), 395–410.

Wild, J. M., Williams, M. N., Howie, G. J., & Mooney, R. (2005). Calcium-binding proteins define interneurons in HVC of the zebra finch (Taeniopygia guttata). *Journal of Comparative Neurology*, *483*(1), 76–90. https://doi.org/10.1002/cne.20403